UNIVERSITÀ
DEGLI STUDI
DI PADOVA

Sede Amministrativa: Università degli Studi di Padova

Dipartimento di *Scienze Chimiche*

SCUOLA DI DOTTORATO DI RICERCA IN: Scienze Molecolari

INDIRIZZO: Scienze Chimiche

CICLO: XVII

Polymer/fullerene OPV materials investigated by unconventional EPR techniques

Direttore della Scuola: Ch.mo Prof. Antonino Polimeno

Coordinatore d'indirizzo: Ch.mo Prof. Antonino Polimeno

Supervisore: Prof. Antonio Toffoletti

Dottorando: Tommaso Margola

Abstract[1]

Il fotovoltaico organico (OPVS) ha guadagnato molto interesse nelle ultime decadi grazie ad alcune caratteristiche migliori rispetto al fotovoltaico inorganico come, flessibilità, facilità di produzione e costi inferiori. Anche se l'efficienza di conversione è ancora molto inferiore rispetto alle celle solari basate su silicio, l'intensa ricerca ha portato ad un netto miglioramento delle performance fino all'ottenimento del 12% di efficienza. Tra tutte le possibili caratteristiche responsabili di una migliore efficienza (morfologia, energetica del sistema, metodo di deposizione ecc), questo lavoro di tesi si concentra sui processi fotofisici di miscele, in stato solido, di polimeri coniugati e fullereni, studiati attraverso spettroscopia EPR. La Risonanza Paramagnetica Elettronica rappresenta uno strumento molto potente nello studio delle miscele organiche grazie alla grande sensibilità che questa tecnica possiede nei confronti della maggioranza delle specie foto-generate che si formano durante il processo fotovoltaico. La distribuzione degli stati energetici all'interno del band gap (o mobility edge) è stata studiata attraverso misure LMEPR, da cui si è in grado di rilevare il tempo di vita apparente delle specie. Questo può essere usato come parametro di paragone tra campioni differenti per individuare qualitativamente il grado di mobilità dei polaroni dopo la dissociazione degli stati CT. Queste osservazioni sono state confermate da misure LEPR in funzione delle lunghezza d'onda di eccitazione in cui l'intensità degli spettri ha mostrato un red-shift rispetto alla banda di assorbimento . Si è quindi confrontato il grado di generazione di polaroni, per dissociazione da stati CT rilassati e hot, con i tempi di vita apparenti ottenuti dalle misure LMEPR.

Spettri LEPR di film sottili di P3HT/Pc_{61}BM, depositati per spin-coating, hanno mostrato un segnale dipendente dall'orientazione del campione. Le simulazioni degli spettri hanno permesso di calcolare il parametro d'ordine S che identifica un ordine macroscopico assegnato unicamente al polimero.

In ultima è stato studiato l'effetto del Diiodoottano (DIO) come additivo in film sottili e di bulk per miscele di PTB7/PC_{61}BM e PTB7/PC_{71}BM. Gli spettri LEPR mostrano che il

[1] Abstract is written in double language: Italian and English

DIO porta ad una scomparsa del segnale di entrambi i fullereni, mentre gli spettri TREPR, nel caso di film sottili in presenza di DIO, mostrano segnali di tripletto dipendendi dall'orientazione del campione per entrambe le fasi. In particolare per il PTB7 è stato individuato un tripletto di ricombinazione mentre per i fullereni un tripletto di ISC.

Abstract

Organic Photovoltaics (OPV)s has gained lot of interest in the last decades thanks to its improved characteristics with respect to inorganic photovoltaic such as, flexibility, easy production processes, cheaper costs etc. Even though power conversion efficiency (PCE) is quite lower than silicon based solar cells, there've been quite an improvement of organic cells characteristics and a 12% PCE was registered. Among all the possible features that are responsible for a better efficiency (morphology, energy levels set-up, method of deposition etc), this work focused on the photophysical processes of solid state blends based on conjugated polymer/fullerene studied by EPR spectroscopy. Electron Paramagnetic Resonance is a useful tool in organic blends investigation thanks to its great sensitivity towards most of the photo-generated species. Distribution of states inside the band gap (or mobility edge) was studied by LMEPR which is able to detect an apparent lifetime that has been used as comparison parameter between different blends in order to find the degree of mobility of polarons after CT states dissociation. Data were supplied by LEPR measurement as a function of wavelength of excitation. LEPR intensity was found not to follow the absorption band profile and maximum LEPR intensity was found to be red-shifted. In the end we compare the possibility of relaxed and hot charge transfer states formation and the global apparent lifetime by LMEPR. P3HT/$PC_{61}BM$ thin film by spin-coating showed an orientation dependent LEPR signal outlining a macroscopic order of polymeric phase. Simulation allowed to determine the parameter of order S which is attributed only to polymeric phase. The effect of Diiodooctane (DIO) on PTB7/$PC_{61}BM$ and PTB7/$PC_{71}BM$ blends on bulk and thin films. LEPR spectra showed that DIO completely shut down the fullerene signals while TREPR spectra displayed, for thin film samples with DIO, oriented recombination triplets for PTB7 and ISC oriented triplets for both fullerenes. Simulation allows to determine the degree of order of about $S = 0.87$ for PTB7 and $S = 0.93$ for fullerenes. In the end we found PTB7 has dipolar Z axis as preferential orientation axis, $PC_{61}BM$ the dipolar Z axis and $PC_{71}BM$ a in XZ plane axis.

Index

Chapter 1 - Introduction

1.1 Organic Photovoltaics (OPV)

Due to limited fossil fuel reserves (1, 2), the possibility to produce electric energy from renewable sources, has been widely developed in the last century. Free sunlight has gained a lot of interest as renewable source for it represents an almost infinity supply for free energy compared to world's energy demand. Inorganic Silicon based solar devices got a dominant role in photovoltaic application and global market. Their Power Conversion Efficiency (PCE) reached over 42.3% for multijunction solar cell (3) anyway their production is generally complex and expensive compared to traditional energy sources as coal, natural gas etc. Moreover, Silicon cells cannot be fabricated industrially in large sizes and their rigidity adds difficulties in solar panels processing. An alternative to inorganic solar cells is given by organic Photovoltaics (OPV) which is based on, oligomeric and polymeric semiconductors, made of conjugated organic molecules coupled with fullerene and fullerene derivatives (4). These materials can be easily processed in bulk heterojunction (BHJ) thin films and can generate electric current by their good ability to undergo electron transfer under illumination (5).

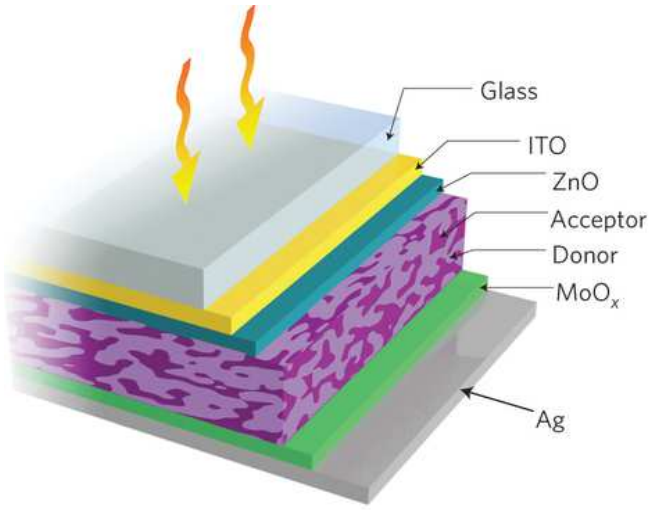

Figure 1.1

Thin films are usually fabricated by simple technique, as spin-coating, spray deposition, and printing (6), they have great flexibility and cheaper cost for their disposal. PCE of these devices is still far from being competitive with silicon solar cells (7), recently a 12% PCE was reached (Heliatek GmbH press release, jan. 2013). This is the principal reason for their almost absence in commerce. In figure 1.1 an example of organic solar cell is shown.

1.1.1 Organic Solar cells

The general mechanism of a solar cell is based on the interaction of an electromagnetic radiation with a semiconductor that is able to promote electron transfer from covalence band to conduction band (figure 1.2) generating and hole-electron quasiparticle called exciton. The latter is considered as formed by weakly interacting particles (25 meV) that can move along the solid matrix as free particles with a reduced mass. Electrons and holes can easily be collected by opportune electrodes and polarize it in order to generate an electrical potential and current flow.

For organic solar cells, the excitons are more strongly bound (0.5 eV) and have lower degree of mobility along the semiconductor. High electron affinity materials are then necessary for exciton dissociation into free charges.

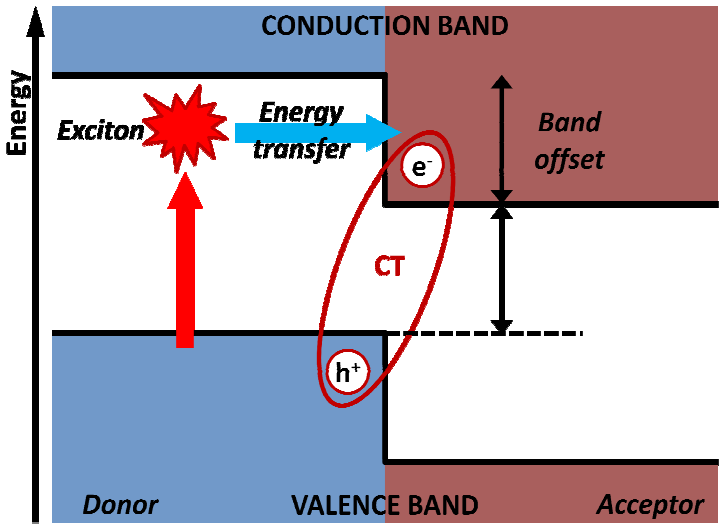

Figure 1.2 Valence and conductions bands of donor (blue) and acceptor (red) are shown. Photo-generated mobile exciton undergoes electron transfer at the interphase and CT state is formed

This role is accomplished by fullerene derivatives that act as electron acceptors (A) while the polymeric counterpart, which has a high light absorption coefficient, plays the role of electron-donor (D). BHJ solar cells allows the creation of an intimate interconnection between donor and acceptor (nm scale) and avoid recombination processes. Actually one of the most relevant problem about OPV devices deals with it (8, 9).

It's usual to refer to free charges generated after electron transfer as positive and negative polarons that can be treated as mobile quasiparticles as well (10). Once polarons are generated, the description of mechanism follows the general solar cell mechanism, in the next section, details of photophysical processes will be displayed.

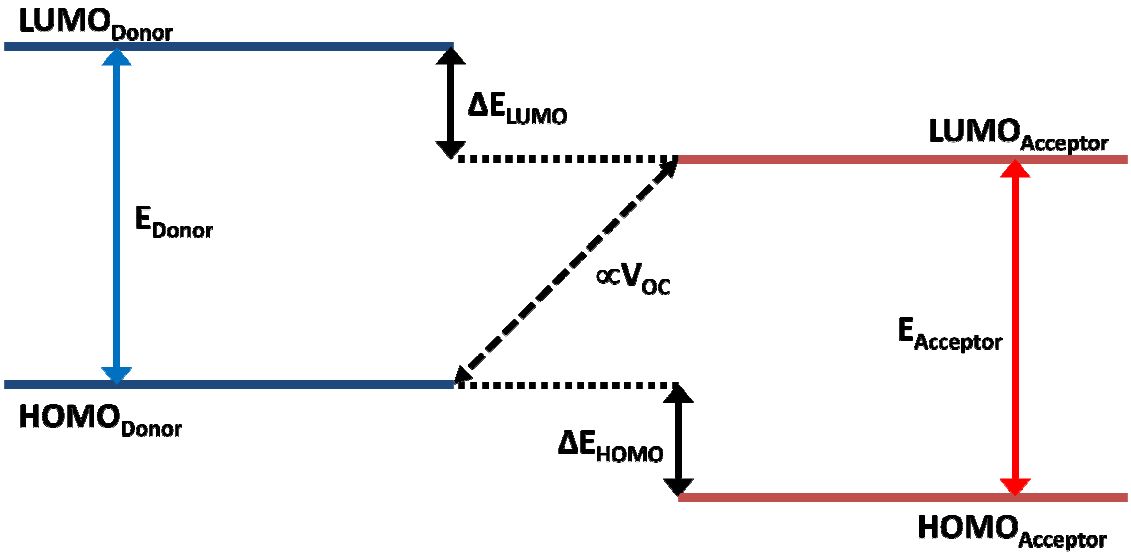

Figure 1.3 . Bands models is approximated by level diagrams of HOMO and LUMO orbitals of donor and acceptor. The V_{oc} is proportional to the energy gap between HOMO of acceptor and LUMO of donor. Increasing of acceptor LUMO energy brings to a higher efficiency of solar cell. LUMO energy of acceptor must be lower than LUMO of donor in order to electron transfer to take place.

The efficiency of organic solar cells can be given by $\eta = {I_{sc}V_{oc}ff}/{P_{light}}$ where I_{sc} is the short circuit current, V_{oc} the open circuit voltage, ff is the filling factor and P_{light} is the power of incident light. These parameters are obtained by $I-V$ curves (3, 11).
The V_{oc} is proportional to the energy gap between HOMO of donor and LUMO of acceptor (figure 1.3) and many acceptors have been studied to understand the role of LUMO energy in global efficiency (12). Morphological information about OPVs can be obtained by X-ray diffraction (XRD) experiments, by Atomic Force Microscopy (AFM), Transmission Electron Microscopy (TEM) and Scanning Probe Spectroscopy (13-15) . Moreover controlling of morphology has been proposed in order to enhance PCE (16). These techniques are generally used to estimate the degree of phase segregation, distances between chains in crystalline domain and the disposition of fullerene in the polymeric matrix.

1.2 Photophysical processes

Organic photovoltaic materials are electron-donor conjugated semiconductors and electron-acceptors high affinity materials. They can be treated using the solid state physic models or by molecular models which are more familiar to chemists' background. Generally physics deals with solid state by using bands theory where completely delocalized sates describe the valence and conduction bands, separated by an energy gap where localized sates, due to defects or doping, are present. When a photon with opportune energy is sent to semiconductor, an electron is promoted to conduction band and a positive hole is left on valence band. The system composed by electron and hole, interacting by Coulomb force, is called exciton and in case of a perfect crystal it can move all along the solid semiconductor. When molecular models are adopted, the valence band and conduction band of donor and acceptor are replaced by HOMO and LUMO orbitals and the mobile exciton as mobile singlet or triplet excited sate. In the this work of thesis, donor and acceptor molecules will be exclusively considered as conjugated organic polymer and fullerene derivatives, thus we will limited the photo-physical description to this case.

1.2.1 Solid state physic description

When triplet or singlet exciton is formed by irradiation, it must diffuse to interphase with electron acceptor in order to be dissociated by electron transfer. The length of exciton diffusion is about 100 nm, thus the two phases have to be closer than that. Once electron transfer takes place a Charge Transfer (CT) state, also called polaron pai state, is formed which at room temperature has lifetime of some nanoseconds (17). The CT state can undergo recombination to singlet ground state or triplet excited state by back electron transfer. Positive and negative polarons, generated by CT dissociation, can move, respectively, along the valence and conduction band or be trapped in some localized states inside the band-gap. Polarons transport to electrodes can be accomplished by direct motion along bands or by tunneling hopping between localized states. In figure 1.4 a qualitative representation of processes is displayed.

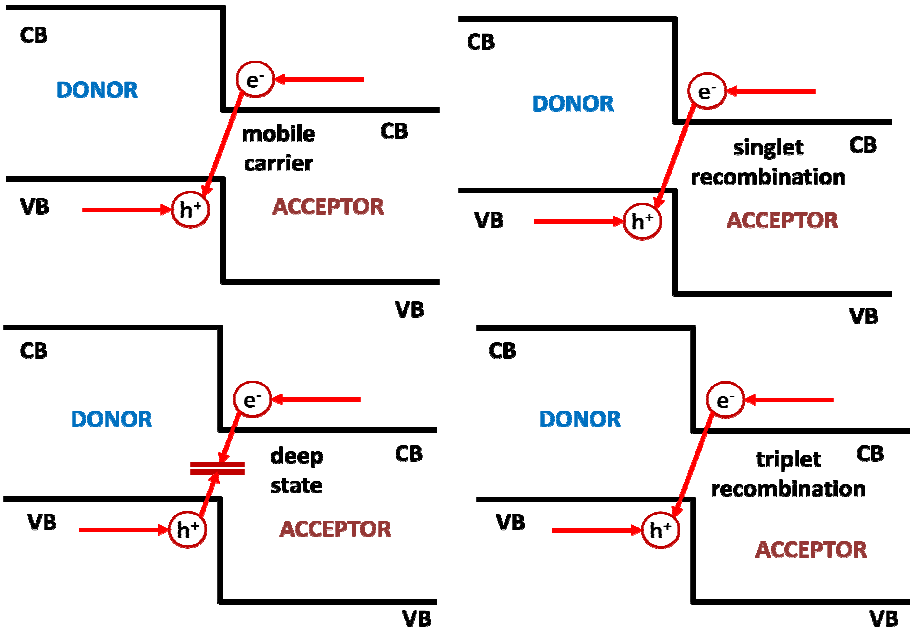

Figure 1.4 . Principal photophysical processes are shown in figure after CT state is formed. Polarons can diffuse along the solid bleds (up-left), they can recombine to singlet ground state (up-right) or to triplet excited state (down-right). During diffusion they can be trapped in some localized states (down-left).

1.2.2 Molecular description

The OPVs photophysics is usually described by Jablonsky diagrams (figure 1.5). When donor singlet excited state is formed by photon absorption, electron transfer can take place towards acceptor an give a CT/polaron pair state, described as one radical cation and one radical anion mutually interacting, efficient electron transfer is usually some femtoseconds long. From a spectroscopic point of view, CT state can be described as two interacting charged radicals ($S = 1/2$) also called Spin Correlated Radical Pair (SCRP) state (see section 2.3). Radicals can recombine to singlet donor ground state, giving back the initial conditions, or recombine to long-living triplet excited state of donor or acceptor. The latter causes the triplet sublevels to have out-of equilibrium population (see section 2.2.5) and it's called recombination triplet mechanism. When SCRP separates, cation radical is generally delocalized along polymer chain. The degree of wavefunction delocalization depends on the polymer nature (18) anyway generally it does not exceed a ten-monomers length. Radical cation can hop between molecules and can be trapped in some localized sate. Radical anion diffuses by hopping between fullerene molecules and can be trapped too. The degree of recombination of the two radicals is proportional to rapidity of their motions and density of localized states (DOS) (see section 4.1). If electron transfer is not efficient, ISC crossing of donor can take place after light absorption. ISC can give electron transfer to acceptor triplet excited state and give rise to SCRP with different spin-polarization. When electrode are present, mobile charges can easily be collected by them and the voltage generated can induced radical charges migration avoiding recombination. When singlet excited state has longer lifetime compared to electron transfer rate, Inter-System Crossing (ISC) can generate a triplet excited state with a peculiar populations (see sections 2.2.4 and 2.2.5), generally different from recombination triplets one. We can conclude stating that the photo-physical processes of a polymer-fullerene based solar cell is complex and not univocal.

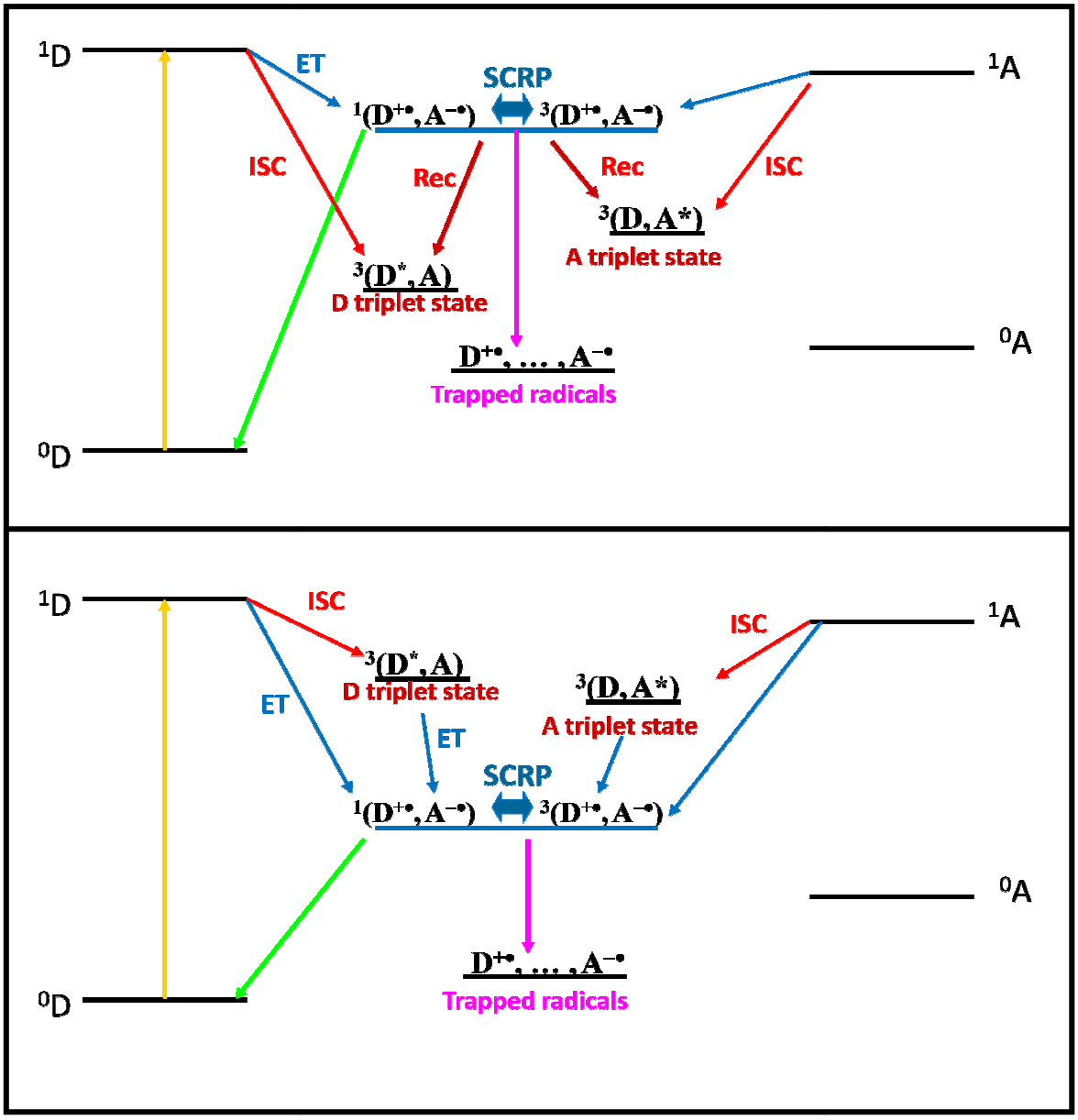

Figure 1.5 Jablonsky diagrams of donor-acceptor physic under irradiation. In figure are shown the two main photo-physical patterns that materials under inspection follow. D is donor molecule, A the acceptor and the number at up right of letter is the spin multiplicity of the state. Diagrams are plotted as a function of energy from bottom to top. ISC stands for Intersystem Crossing and Rec for recombination.

Upper figure shows the case where triplet donor and acceptor state lies lower in energy than SCRP. When a photon is absorbed by donor, it undergoes a transition (yellow line) to singlet excited state. Following the selection rules, spin multiplicity is kept. If electron transfer (ET - blue line) mechanism is efficient, ISC (red line) does not take place and a SCRP is formed. SCRP can separate and give recombination to singlet state (green line) or to triplet state (red line) or trapped radicals (pink line).

Lower figure shows an analogous situation in which triplets state lies higher in energy than SCRP state. In this case recombination to triplet state is avoided. When ET is not efficient ISC can take place generating triplet states. Donor and acceptor triplet state can be populated by ISC or by triplet-triplet energy transfer.

The study of photo-physics of materials for organic photovoltaic can be carried out by using many techniques as optical spectroscopies that can detect the photo-generated species, ratio of generation and recombination. Normally optical techniques have temporal resolution on the femtoseconds range (17, 19-21) and are able to see very fast dynamics up to steady-state processes.

In the last years Electron Paramagnetic Spectroscopy (EPR) has gained a lot of attention about the study of organic photovoltaic materials and of photo-generated species. It is able to detect species in different spin states, moreover it can distinguish three kind of species generated by visible radiation in photovoltaic materials:

- charged radical species, generated by photo-induced electron transfer, that have a spin quantum number S=1/2;
- triplet states by Inter System Crossing (ISC) or by recombination of charges, they are characterized by S=1;
- Spin Correlated Radical Pair (SCRP) species where two S=1/2 radicals interact by magnetic dipolar and exchange interaction and generated singlet-triplet mixed states

EPR techniques mostly used in the study of photovoltaic materials are:

- Light induced EPR (LEPR): it is a steady-state spectroscopy that allows to get the EPR spectra due only to photo-generated species
- Time-Resolved EPR (TREPR): it's a transient spectroscopy that detect EPR spectra as a function of time. This technique is typically used in the detection of short living species (from hundreds of nanoseconds to millisecond).
- Eco Detected Light ON EPR (EDlightON): it's a pulsed EPR spectroscopy where the signal is recorded while irradiating sample by microwave pulses. This technique can detect also spin relaxation time of species T1 and T2.

1.3 Materials

In this work of thesis we focused our attention on conjugated organic solid blends of polymers and fullerene derivatives. HOMO and LUMO energy levels of conjugated systems depends on the presence in polymeric chain of electro-rich and electron-poor units. In general, the energy gap of a material derived from a linear π-conjugated system can be expressed by the sum of 5 principal contributions:

$$Eg = E_{BLA} + E_{Res} + E_{\theta} + E_{Int} + E_{Sub}$$

where the five terms, in the right member, are respectively: the bond length alternation contribution, the aromatic stabilization energy, the energy related to the rotational disorder around single bonds, the intermolecular interaction contribution and the effect due to the substituents (22). These 5 contributions can be controlled by synthetic strategies improved for many years. The polymers discussed in this thesis have been chosen between well known P3HT, MDMO-PPV, PCDTBT, and new PTB7 which showed high PCE when coupled with fullerene. Acceptors studied are classical $PC_{61}BM$ and $PC_{71}BM$ and 1,2 and 1,4 C_{60} derivatives.

In the following section the description of material analyzed in this work is illustrated.

1.3.1 Conjugated polymers

P3HT

Poly(3-hexylthiophene-2,5-diyl P3HT is a semiconductive polymer commonly used in realization of OPV devices, OFET ("organic field-effect transistor'). Polymer is constituted by 3-exyle-substituted thiophene bound together by carbon atoms in 2 and 5 position. Polymer is a π conjugated system and this gives the good conductibility. The exyle groups add solubility to polymer in organic solvents mostly used for photovoltaic processing as toluene and chlorobenzene. P3HT has maximum absorption spectrum in the range between 450 and 600 nm. The indicative HOMO and LUMO energy are -5 eV and -3 eV (23).Polymer can be easily processed in solution for

deposition of thin films by spin coating or printing (24-27) .One of the most common method for P3HT synthesis is given by McCullough method (12). Structure of P3HT is shown in figure 1.6

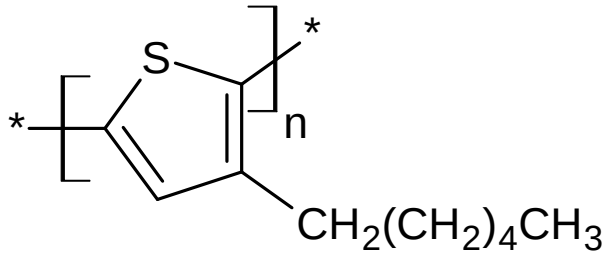

Figure 1.6

PCDTBT

Poly[*N*-9′-heptadecanyl-2,7-carbazole-*alt*-5,5-(4′,7′-di-2-thienyl2′,1′,3′benzothiadiazole)]) (PCDTBT). It is a low band-gap polymer constituted by electron-deficient benzothiadiaozole units and electron-rich thiophene units and aromatic carbazole units. This polymer has a 1eV lower energy band gap than P3HT and thus is able to absorb a greater portion of solar spectrum. It has generally a wide absorption band between 500 and 659 nm (28). Energy of HOMO is -5.5 eV while LUMO is -3.6 eV (29). Structure of PCDTBT is shown in figure 1.7

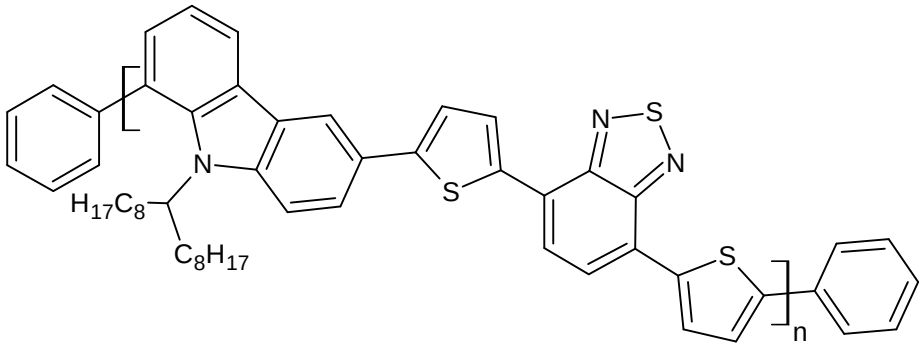

Figure 1.7

MDMO-PPV

Poly[2-methoxy- 5-[(3',7'-dimethyloctyloxy)-1,4-phenylenevinylene] (MDMO-PPV). Is a conjugated polymer composed by phenilene-vinylene units, used in the fabrication of polymeric LED and OPV solar cells. It has enhanced optical and electrical properties than other polymers and better morphology of MDMO-PPV/fullerene derivatives was found. Polymer is soluble in organic solvent as toluene, chloroform and dichlorobenzene. HOMO and LUMO energies are respectively -5.04 eV and -2.86 eV (30).Structure of MDMO-PPV is shown in figure 1.8

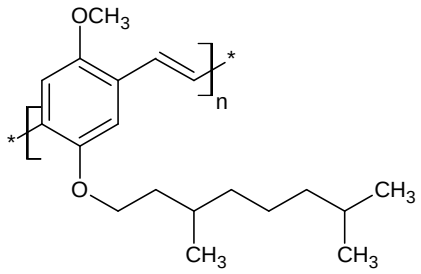

Figure 1.8

PTB7

Poly(4,8 - bis[(2 - ethylhexyl)oxy]benzo[1,2 - b:4,5 - b']dithiophene - 2,6 -diyl3 - fluoro - 2[(2 - ethylhexyl)carbonyl]thieno[3,4 - b]thiophenediyl] PTB7 is a recent polymer that increases greatly the photovoltaic efficiency. The monomer is constituted by one benzithiofenic and one thienothiofenic units. A fluorine atom is bound to the thienothiofenic unit and it is able to tune the energy levels of polymer and its photovoltaic properties. HOMO and LUMO energies have been measured by cyclic voltammetry (31) and are -5.15 eV and -3.31 eV. PTB7 is a low-band gap polymer and has an efficient absorption of photons of energy between 550 nm and 750 nm and between 300 nm and 550 nm. The synthesis is accomplished by Stille coupling (32). Structure of MDMO-PPV is shown in figure 1.9 (33).

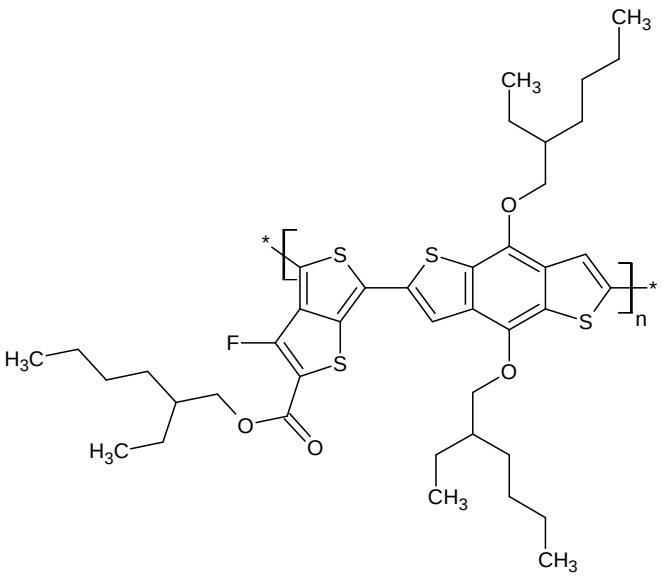

Figure 1.9

1.3.2 Fullerene derivatives

Fullerene derivatives have good electron acceptors properties and represent the most used molecules in OPV solar cells. The C_{60} molecule is one of the allotropic form of carbon, it has three degenerate LUMO orbitals that can host up to 6 electrons and guarantee an high electron affinity (33). This feature is due to higher dielectric constant than conjugated polymer which is able to stabilize the photo-induced CT state. Fullerene contributes to avoid back electron transfer (5) and recombination moreover, if not coupled with polymers, it has a very efficient ISC conversion form first triplet excited state (34). By getting advantage of the great reactivity of fullerene, there have been synthesized many fullerene derivatives in order to improve solubility and get better electronic and electric properties as higher conductivity (35), PCE (36) and slower photo-degradation (37). In this work of thesis, we studied the classical $PC_{61}BM$, $PC_{71}BM$ and 1,2 and 1,4 derivatives of C_{60}coupled with different polymers.

$PC_{61}BM$

(phenyl-C_{61}-butyric acid methyl ester) $PC_{61}BM$ is the most used fullerene derivatives for OPV solar cells. Structure of $PC_{61}BM$ is shown in figure 1.10

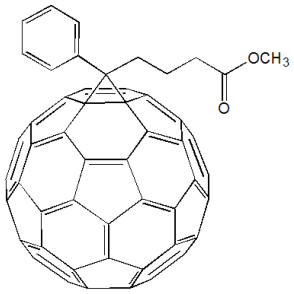

Figure 1.10

$PC_{61}BM$ has a better solubility in organic solvent as toluene or chlorobenzene thanks to the funzionalization of C_{60} with a methyl ester chain. $PC_{61}BM$ LUMO orbitals are almost degenerate due to weak lost of symmetry but it keeps all the electron properties found in C_{60}, moreover, the enhanced solubility makes $PC_{61}BM$ easily processable in solution.

C60 1,2 derivatives

the attention was focused on 1,2 C_{60} derivatives **C60H-1,2** and **C60MM-1,2**, which structures is shown in figure 1.11.

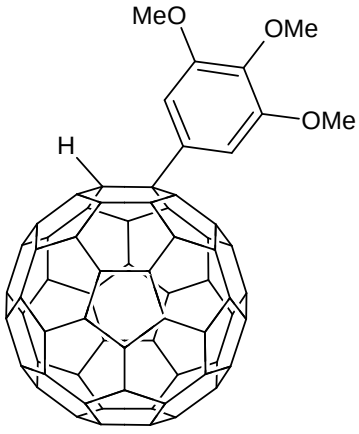

$C_{60}H$-1,2

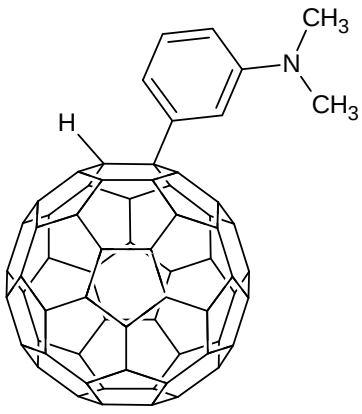

$C_{60}MM$-1,2

Figure 1.11

Some works on 1,2 derivatives for photovoltaic applications, can be found in (38, 39). They have electron-donor substituent group that increases LUMO level energy of about 100 meV and consequently the V_{OC} value.

C60 1,4 derivatives

1,4 derivatives studied were **C60-1,4-PhOMe** and **C60PH2-1,4,** shown in figure 1.12. The 1,4 derivatives display different properties than the 1,2 derivatives (40) .Role of substituent position was studied and comparisons with Hummelen et al (38) ,1,4 derivatives showed a greater LUMO energy than the 1,2 derivatives of about 35%.

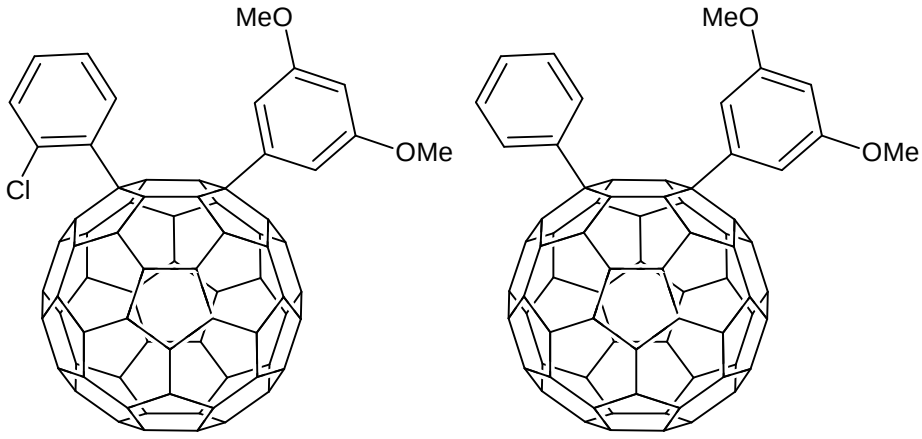

C_{60}PH2-1,4 **C_{60}-1,4PHO-Me**

Figure 1.12

$PC_{71}BM$

the ([6,6]-Phenyl C_{71} butyric acid methyl ester, mixture of isomers) $PC_{71}BM$ is a C_{70} derivative analogous to $PC_{61}BM$. Solar cells based on polymer/$PC_{71}BM$ blends, showed an improved photoabsoprtion and more efficient light harvesting with a consequent better PCE and higher current density than $PC_{61}BM$. HOMO and LUMO energy are -6eV and -3.9eV respectively. Structure is shown in figure 1.13

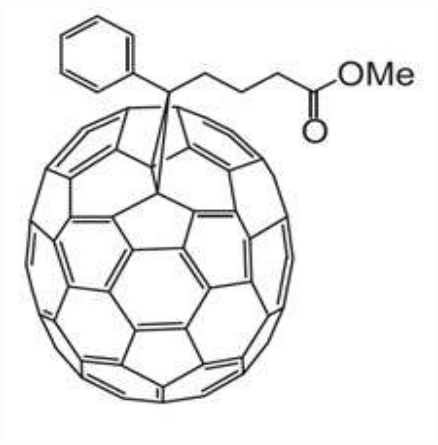

Figure 1.13

1.4 Thesis organization

This work of thesis deals with study of different properties of various polymer/fullerene solid blends by different EPR techniques. Samples were studied without presence of electrodes in order to study the natural photo-physics of systems. The preparation of samples will be described in detail in each section anyway, most of samples were prepared by spin-coating deposition or by slow evaporation of polymer/fullerene solution directly inside EPR tube. For section 4.1 and 4.2 peculiar applications of EPR spectroscopy was accomplished and in respective introductions details of models and assumption are explained. Below a brief resume of experimental part is displayed.

1.4.1 Light modulated EPR (LMEPR) for study of lifetimes of polymer/fullerene blends

Polymer and fullerene solid blends have a great intrinsic degree of disorder (41) that results in big number of localized states that interfere with radical charge transport and PCE. We propose a light modulated EPR (LMEPR) technique able to get some information to global distribution of localized states (DOS). (See section 4.1)

1.4.2 Wavelength dependence of EPR signal in photovoltaic blends

Wavelength dependent LEPR spectra were recorded in order to study energy dependence of photovoltaic processes (42). This EPR method, also called lambda-EPR, uses monochromatic light from 400 nm to 900 nm as source of illumination. A peculiar dependence of EPR signal on wavelength was found. (See section 4.2).

1.4.3 Partial Orientation Of Thin P3HT/$PC_{61}BM$ Blends

Thin films casted by spin-coating were studied with LEPR and TREPR changing orientation of thin field with respect to static magnetic field (43). Orientation dependent EPR signal was detected and simulated by assuming uniaxial orienting potential. At last a macroscopic orientation of polymer was obtained.(See section 4.3).

1.4.4 Effect Of Diiodooctane in photovoltaic PTB7/FULLERENE Blends

Effect of organic solvent of Diiodooctane (DIO) as additive on PTB7/$PC_{61}BM$ and PTB7/$PC_{71}BM$ blends (31, 44, 45). Samples were studied for bulk and thin film. Macroscopic orientation of polymer was found in all spin-coated samples, while, adding DIO, also a fullerenic oriented phase resulted. By simulation we were able to find the mutual orientation of molecules and give a model for the improved PCE for PTB7 based devices.

Chapter 2 - EPR Theory

2.2 Spin-Hamiltonians

2.2.1 Zeeman interaction

EPR spectroscopy is able to study paramagnetic systems. It's well know that it is possible to get information about: organic radicals, triplet states of molecules, transition metal ions, defect in crystals, conduction electrons and so on. The general concepts are similar to the Nuclear Magnetic Resonance (NMR) technique even though the EPR spin transition are observed for unpaired electrons. Let's consider a free electron that possesses an intrinsic spin angular momentum. Its modulus and projection with respect some arbitrary axis can be treated as a quantized physical quantities depending on spin quantum numbers s and m_s (46). If we indicate with $|s|$ and s_z respectively the modulus and the projection along z axis, then:

$$|\mathbf{s}|^2 = s(s+1)\hbar^2 \tag{2.1}$$

$$s_z = m_s\hbar \tag{2.2}$$

where quantum number $s = 1/2$ and m_s has values $s, s-1, \ldots -s$. For a single s=1/2 spin, we have $m_s = \frac{1}{2}$ and $m_s = -\frac{1}{2}$ which are respectively named after α and β sates. The two states, when no external magnetic field is applied, are degenerate.

To spin angular momentum is associated a spin magnetic momentum:

$$\boldsymbol{\mu} = -\frac{g_e\mu_B\mathbf{S}}{\hbar} \tag{2.3}$$

where $\mu_B = 9.27 \cdot 10^{-24}\ \mathrm{J/T}$ and $g_e = 2.0023$ is the g factor of free electron. When external magnetic field $\mathbf{B_0}$ is present, the two spin levels are no more degenerate, and

its expression it's given by the internal product of magnetic field with magnetic momentum:

$$E = -\boldsymbol{\mu} \cdot \mathbf{B_0} \tag{2.4}$$

From a quantum mechanical point of view, it's possible from (2.4) to define a spin Hamiltonian that describes the energy of the s=1/2 electron in presence of an external magnetic field. This is called Zeeman interaction and the Hamiltonian is:

$$\hat{H}_{Zeeman} = \frac{g_e \mu_B}{\hbar} \hat{\mathbf{S}} \cdot \mathbf{B_0} \tag{2.5}$$

where $\hat{\mathbf{S}}$ is the quantum mechanical operator relative to angular momentum. The energies of α and β states when $\mathbf{B_0}$ is parallel to z direction become:

$$E_\alpha = \frac{g_e \mu_B B_z}{2} \tag{2.6}$$

$$E_\beta = -\frac{g_e \mu_B B_z}{2} \tag{2.7}$$

it's possible now, with an opportune external electromagnetic perturbation, to generate transition between this two states and the recording of these two transitions is the basis of EPR spectroscopy. The resonance condition is fulfilled when the energy of the incident photon is the same of the energy gap $E_\beta - E_\alpha$:

$$\hbar\omega = g_e \mu_B B_z \tag{2.8}$$

Normally in EPR experiment, the frequency is kept fixed while the external magnetic field is swept around the resonance conditions. Generally transitions are allowed when $\Delta m_s = \pm 1$.

When we consider the case of an electron occupying some orbital in an atom, we have to take into account the effect of the other electrons, and nuclei interactions with the unpaired electron. It's possible to define a spin Hamiltonian similar to (2.5):

$$\widehat{H} = \mu_B g \cdot \hat{\mathbf{J}} \cdot \mathbf{B_0} \tag{2.9}$$

Where $\hat{\mathbf{J}}$ is the total angular momentum operator given by: $\mathrm{J} = \mathrm{S} + \mathrm{L}$ and the g factor is given by the expression (46):

$$g = \frac{3j(j+1) + s(s+1) - l(l+1)}{2j(j+1)} \tag{2.10}$$

where l are the orbital angular momentum quantum number and j is the total angular momentum and can assume value $j = s + l, s + l - 1, \ldots |s - l|$. If more than one electron is involved, expression (2.10) becomes:

$$g = \frac{3J(J+1) + S(S+1) - L(L+1)}{2J(J+1)} \tag{2.11}$$

where S, L, J are the quantum number given by the sum over spin, orbital and total angular momentum of each electron. When the orbital occupied by unpaired electron is non degenerate, orbital angular momentum is perfectly quenched and (2.5) holds.
Generally orbital angular momentum is not totally quenched thanks to spin-orbit coupling, in this case (2.11) must be taken into account. Moreover when the restore of angular momentum by spin-orbit coupling is present, an orientation dependence of g factor is found, thus it has to be treated like a second rank tensor (3X3 matrix) and the spin Hamiltonian is (46):

$$\widehat{H} = \mu_B \mathbf{B_0} \cdot \mathbf{g} \cdot \hat{\mathbf{S}} \tag{2.12}$$

where $\mathbf{g} = \begin{pmatrix} \mathbf{g_{xx}} & \mathbf{g_{xy}} & \mathbf{g_{xz}} \\ \mathbf{g_{yx}} & \mathbf{g_{yy}} & \mathbf{g_{yz}} \\ \mathbf{g_{zx}} & \mathbf{g_{yx}} & \mathbf{g_{zz}} \end{pmatrix}$. By diagonalizing the matrix, it's possible to find the principal values and principal reference frame of *g* tensor that assumes the from:

$$\mathbf{g} = \begin{pmatrix} \mathbf{g_X} & \mathbf{0} & \mathbf{0} \\ \mathbf{0} & \mathbf{g_Y} & \mathbf{0} \\ \mathbf{0} & \mathbf{0} & \mathbf{g_Z} \end{pmatrix} \tag{2.13}$$

when paramagnetic species is in solution, the rapid rotational and translational motions eliminates the anisotropic effect and the g factor is taken to be the averaged trace of (2.13). When paramagnetic defect in crystal phase are considered, anisotropy is present and it can deviate a lot the spectrum profile. In figure (2.1) an example it's shown.

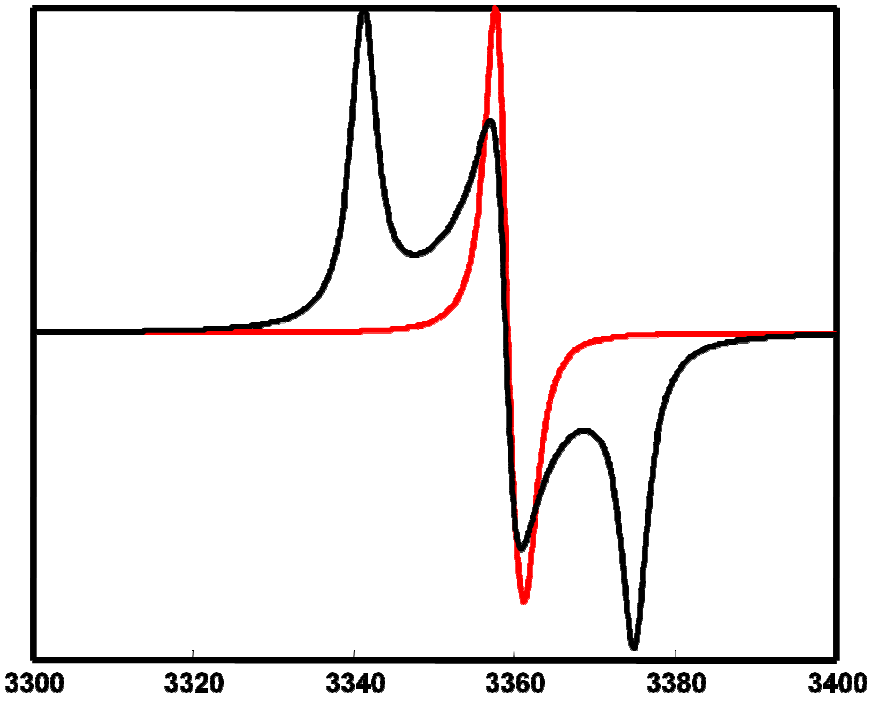

Figure 2.1 Powder spectrum(black line), the three transitions correspond to the principal values of g tensor. Solution spectrum where all anisotropy are mediated to the average of g tensor trace.

Experimental EPR magnetic field usually uses magnetic field of thousand of Gauss thus the spin transitions, following the field-dependence of energies (2.6, 2.7), are in the microwaves region of electromagnetic spectrum.

2.2.2 Hyperfine interaction

When nuclei with nuclear spin angular momentum are present, electrons can interact with them by hyperfine coupling that is described by (46, 47):

$$E_{hf} = \mathbf{S} \cdot \mathbf{a} \cdot \mathbf{I} \tag{2.14}$$

where $\mathbf{I}$ is the spin angular moment of nucleus and $\mathbf{a}$ is the hyperfine coupling tensor. This interaction is anisotropic and when molecular motion is fast enough it is mediated to hyperfine isotropic coupling constant a. For each coupled nucleus with hyperfine constant a,each EPR line is split in $2I + 1$ lines. We won't go any further with hyperfine interaction because generally, for photovoltaic materials, g anisotropy is greater and hyperfine coupling can be neglected.

2.2.3 Exchange interaction

Two or more unpaired electrons in different atomic or molecular orbitals can interact by their coulombic mutual action and this is called exchange interaction. The latter is a purely quantum effect and comes from the fact that electron are indistinguishable fermions thus the wavefunction of global system considered must be antisymmetric with respect to electrons exchange. The Hamiltonian of two interacting electrons by exchange interaction in presence of an external magnetic field is (46):

$$\widehat{H} = -\mathbf{2}J\hat{\mathbf{s}}_{\mathbf{1}}\hat{\mathbf{s}}_{\mathbf{2}} \tag{2.15}$$

where J is the scalar exchange constant, $\hat{\mathbf{s}}_1$ and $\hat{\mathbf{s}}_2$ are the spin angular momentum operators of electron 1 and electron 2. Hamiltonian (2.15) can be rewritten using ladder operators:

$$\widehat{H} = -2J\left(\hat{s}_{1x}\cdot\hat{s}_{2x} + \hat{s}_{1y}\cdot\hat{s}_{2y} + \hat{s}_{1z}\cdot\hat{s}_{2z}\right)$$
$$= -2J\left[\frac{1}{4}(\hat{s}_{1+} + \hat{s}_{1-})(\hat{s}_{2+} + \hat{s}_{2-}) - \frac{1}{4}(\hat{s}_{1+} - \hat{s}_{1-})(\hat{s}_{2+} - \hat{s}_{2-}) + \hat{s}_{1z}\cdot\hat{s}_{2z}\right] \quad (2.16)$$

By using the uncoupled basis set $\alpha\alpha$, $\alpha\beta$, $\beta\alpha$, $\beta\beta$ the (2.16) and calculating the matrix elements, (2.16) becomes:

$$H = J\begin{pmatrix} -\frac{1}{2} & 0 & 0 & 0 \\ 0 & \frac{1}{2} & -1 & 0 \\ 0 & -1 & \frac{1}{2} & 0 \\ 0 & 0 & 0 & -\frac{1}{2} \end{pmatrix} \quad (2.17)$$

The eigenvalues are:

$$E_{T-1} = E_{T0} = E_{T1} = -\frac{J}{2}$$
$$E_S = 3/2J \quad (2.18)$$

and eigenfunctions

$$T_{+1} = \alpha\alpha$$
$$T_0 = \frac{1}{\sqrt{2}}(\alpha\beta + \beta\alpha)$$
$$T_{-1} = \beta\beta \quad (2.19)$$
$$S = \frac{1}{\sqrt{2}}(\alpha\beta - \beta\alpha)$$

The (2.18) are called triplet and singlet states and are respectively symmetric and antisymmetric function with respect to the exchange of electrons.

When $J < 0$ triplet sublevels lie higher in energy and the echange coupling is antiferromagnetic while for $J > 0$ the coupling is ferromagnetic. Incidentally (2.18) are eigenfunction also of Zeeman interaction (2.12).

Finally in order to be consistent when exchange interaction will be invoked later on this section, we write the (2.15) in terms of total spin angular momentum operator S(48):

$$\widehat{H} = -J\left(\hat{S}^2 - \hat{s}_1^2 - \hat{s}_2^2\right) = -J\left(\hat{S}^2 - s(s+1) - s(s+1)\right) = -J\left(\hat{S}^2 - \frac{3}{2}\right) \tag{2.20}$$

Then we redefine the zero of energy adding an amount of $+\frac{J}{2}$ to (2.19)

$$\widehat{H} = J\left(\hat{S}^2 - 1\right) \tag{2.21}$$

and the shifted eigenvalues are

$$\begin{aligned} E_{T-1} &= E_{T0} = E_{T1} = -J \\ E_S &= J \end{aligned} \tag{2.22}$$

2.2.4 Dipolar interaction

When an atom or a molecule have two unpaired electrons, triplet state is found characterized by total quantum number $S = 1$. If we consider this magnetic interaction as two magnetic interacting dipoles, it's possible to use the classical dipolar-dipolar interaction to formulate the appropriate spin-Hamiltonian.

The Hamiltonian of dipolar interaction depends on mutual distance of electrons and from their spin angular momenta (47):

$$H_{dip} = \frac{\mu_0}{4\pi}(g\mu_B)^2\left[\frac{\hat{\boldsymbol{s}}_1 \cdot \hat{\boldsymbol{s}}_2}{r^3} - \frac{3(\hat{\boldsymbol{s}}_1 \cdot \boldsymbol{r})}{r^5}\right] \tag{2.23}$$

By integration on spatial coordinates, it's possible to rewrite (2.23) into:

$$H_{ZFS} = \widehat{\boldsymbol{S}} \cdot \boldsymbol{D} \cdot \widehat{\boldsymbol{S}} = 2\hat{\boldsymbol{s}}_{\mathbf{1}} \cdot \boldsymbol{D} \cdot \hat{\boldsymbol{s}}_{\mathbf{2}} \tag{2.24}$$

when $\boldsymbol{D}$ is the dipolar tensor also called Zero-Field Splitting tensor (47). This name is due to energies splitting observed when two electrons are interacting in absence of an external magnetic field.

$\boldsymbol{D}$ has principal values:

$$\boldsymbol{D} = \begin{pmatrix} -D_x & 0 & 0 \\ 0 & -D_y & 0 \\ 0 & 0 & -D_z \end{pmatrix} \tag{2.25}$$

for convention their magnitude is considered as $D_z > D_y > D_x$. The dipolar $\boldsymbol{D}$ is a traceless and state the anisotropy of the dipolar interaction. When fast molecular motion is present, $\boldsymbol{D}$ reduces to its trace which is zero. Before diagonalization, it's useful to define the Zero-Field splitting parameters (46):

$$D = \frac{3}{2} D_z \tag{2.26}$$

$$E = \frac{D_y - D_x}{2} \tag{2.27}$$

and (2.21) becomes:

$$\widehat{H}_{ZFS} = D\left(\hat{S}_z^2 - \frac{1}{3}S(S+1)\right) + \frac{1}{2}E(\hat{S}_+^2 + \hat{S}_-^2) \tag{2.28}$$

where $\hat{S}_-$ and $\hat{S}_+$ are the ladder operators.

If we consider as basis of function the eigenfunctions of exchange coupling for triplet state: T_{-1}, T_0, T_{+1} we can calculate the matrix elements of (2.28) by integration

$$H_{ZFS} = \begin{pmatrix} \frac{1}{3}D & 0 & E \\ 0 & -\frac{2}{3}D & 0 \\ E & 0 & \frac{1}{3}D \end{pmatrix} \tag{2.29}$$

we can now perform diagonalization of (2.29) and get eigenvalues and eigenfunctions

$$\begin{aligned} E_x &= \frac{1}{3}D - E = -D_x \\ E_y &= \frac{1}{3}D + E = -D_y \\ E_z &= -\frac{2}{3}D = -D_z \end{aligned} \tag{2.30}$$

the dipolar interaction, as anticipated before, lift the degeneracy of triplet states even when there's no external magnetic field and thus it's called Zero-field splitting.
The eigenfunctions of (2.29) are (46) :

$$\begin{aligned} T_x &= \frac{1}{\sqrt{2}}(T_{-1} - T_{+1}) \\ T_y &= \frac{1}{\sqrt{2}}(T_{-1} + T_{+1}) \\ T_z &= T_0 \end{aligned} \tag{2.31}$$

when external magnetic field we must define a new Hamiltonian given by the sum of dipolar and Zeeman interaction:

$$\widehat{H} = \mu_B \mathbf{B_0} \cdot \mathbf{g} \cdot \hat{\mathbf{S}} + D\left(\hat{S}_z^2 - \frac{1}{3}\hat{S}(\hat{S}+1)\right) + \frac{1}{2}E(\hat{S}_+^2 + \hat{S}_-^2) \tag{2.32}$$

the set of function (2.25) are not eigenfunctions of the total Hamiltonian (2.32) but we can use them to determinate the new set. The (2.32) in the (2.31) set is (46):

$$H_{ZFS} = \begin{pmatrix} \frac{1}{3}D - E & g\mu_B B_0 l_z & -ig\mu_B B_0 l_y \\ g\mu_B B_0 l_z & \frac{1}{3}D + E & g\mu_B B_0 l_x \\ ig\mu_B B_0 l_y & g\mu_B B_0 l_x & -\frac{2}{3}D \end{pmatrix} \tag{2.33}$$

where $l_i (i = x, y, z)$ are the cosine directors of magnetic field with respect to dipolar tensor principal frame. Matrix (2.33) can only be diagonalized for one arbitrary direction of external magnetic field and usually the principal directions of dipolar tensor $\boldsymbol{D}$ are chosen:

when $B_0 \parallel x$

$$\begin{aligned} E_+ &= -\frac{1}{2}\left(\frac{1}{3}D - E\right) + \left\{\frac{1}{4}(D+E)^2 + (g\mu_B B_0)^2\right\}^{1/2} \\ E_0 &= \frac{1}{3}D - E \\ E_- &= -\frac{1}{2}\left(\frac{1}{3}D - E\right) - \left\{\frac{1}{4}(D+E)^2 + (g\mu_B B_0)^2\right\}^{1/2} \end{aligned} \tag{2.34a}$$

when $B_0 \parallel y$

$$\begin{aligned} E_+ &= -\frac{1}{2}\left(\frac{1}{3}D + E\right) + \left\{\frac{1}{4}(D-E)^2 + (g\mu_B B_0)^2\right\}^{1/2} \\ E_0 &= \frac{1}{3}D + E \\ E_- &= -\frac{1}{2}\left(\frac{1}{3}D + E\right) - \left\{\frac{1}{4}(D-E)^2 + (g\mu_B B_0)^2\right\}^{1/2} \end{aligned} \tag{2.34b}$$

when $B_0 \parallel z$

$$E_+ = \frac{1}{3}D + \{E^2 + (g\mu_B B_0)^2\}^{1/2} \tag{2.34c}$$

$$E_0 = -\frac{2}{3}D$$

$$E_{-} = \frac{1}{3}D - \{E^2 + (g\mu_B B_0)^2\}^{1/2}$$

The Zero-field splitting eigenfunctions (2.22) are still eigenfunction when magnetic field is taken to be parallel to the direction associated to them. For strong applied field the eigenfunctions are considered the T_{-1}, T_0, T_{+1} set which are eigenfunctions of Zeeman and exchange interaction. The effect of magnetic field in changing the energies from zero-field splitting ones is shown is figure (2.2) (47) .Some typical pattern of a powder thermalized triplet spectra is shown in figure 2.3

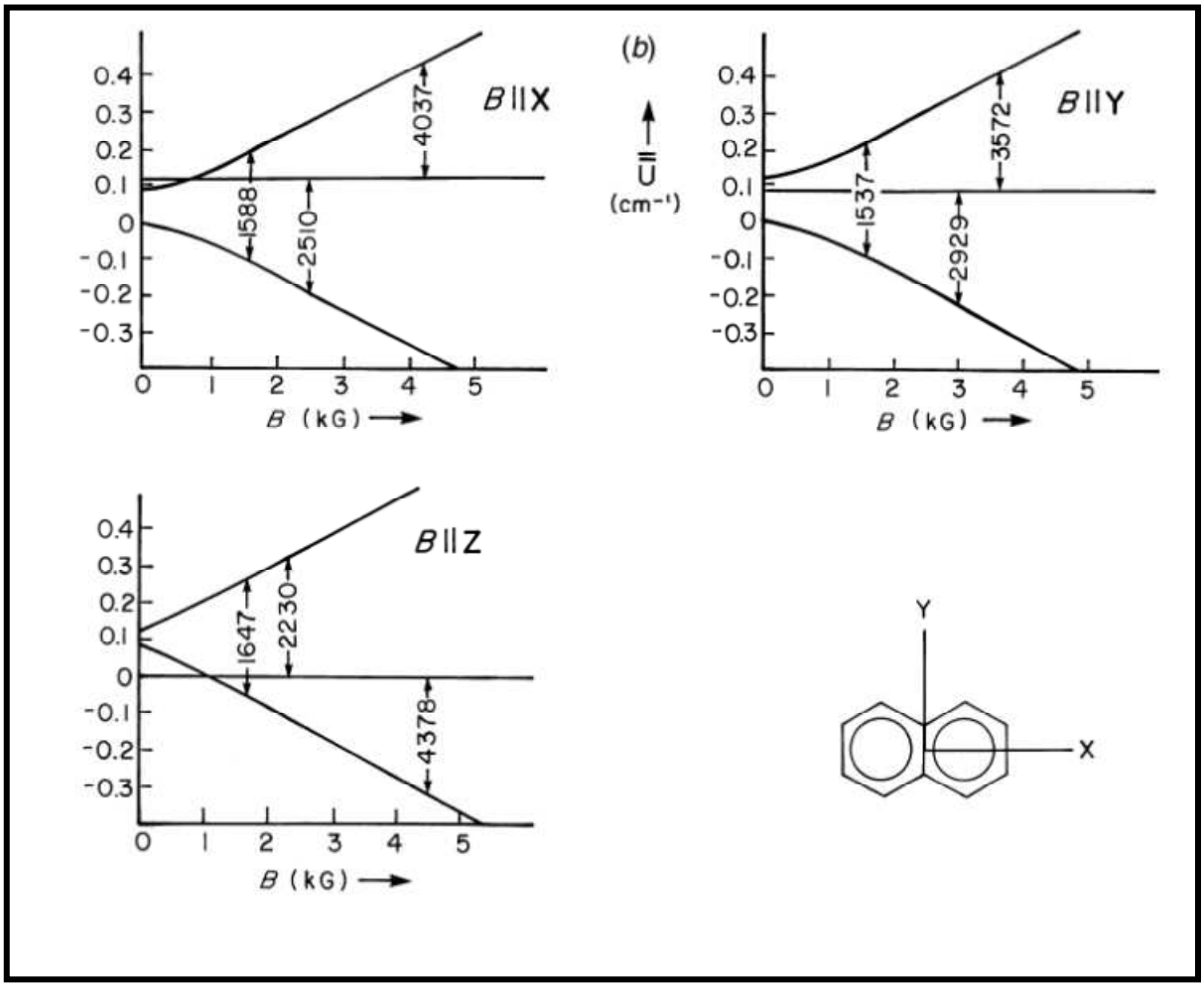

Figure 2.2

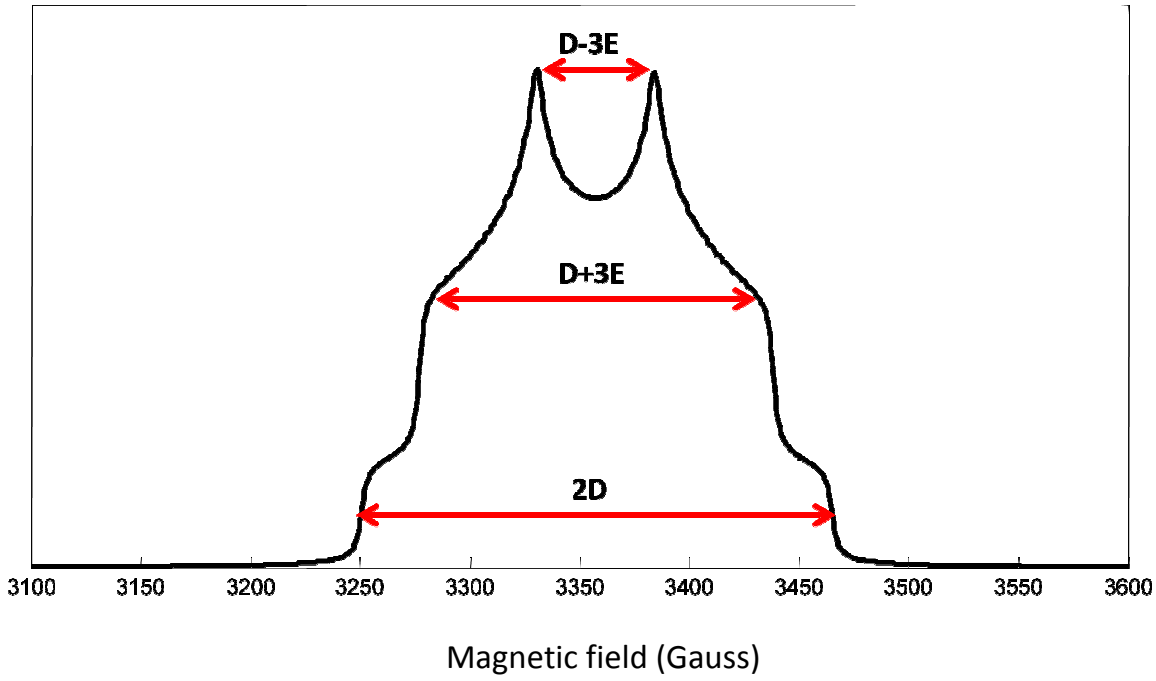

Figure 2.3 powder spectra of thermalized triplet species. The three principal transitions are shown in red.

2.2.5 Spin Polarization of triplet state

Dipolar interaction between two unpaired electrons in the same atom or molecule is responsible for the Zero-Field-Splitting effect that removes the degeneracy from the three triplets states. Triplet ground states are generally very rare and most of the times excited triplet sates are considered. Following the basic selection rules for photon absorption, it's not possible to excite an electron directly from a singlet ground state to a triplet excited state thus ISC from singlet excited state to triplet excited state must be taken into account. Normally ISC mechanism is proportional by the spin-orbit Hamiltonian:

$$H_{SO} = -\lambda \hat{\mathbf{S}}\hat{\mathbf{L}} \tag{2.35}$$

where $\hat{\mathbf{S}}$ and $\hat{\mathbf{L}}$ are the total spin and orbital angular momentum of system. The triplets and singlet functions (2.18) are not eigenfunctions of (2.31) that globally mixed all the four states.

The mixing of S state with T_{+1}, T_0, T_{-1} states is dependent on symmetry functions and is generally not of the same magnitude. Consequently T_{+1}, T_0, T_{-1} will have different degree of population transfer from S that is triplet states is spin-polarized and cannot be described by Boltzmann distribution. The ISC mechanism is said to be spin-selective and EPR spectrum of triplet states will have emission and absorption features. This is generally called ISC triplet and it is represented in figure 2.4.

Triplet states can be polarized also by recombination from a charge transfer state that, as displayed in chapter 1, is called Spin Correlated Radical Pair (SCRP) state. The spin Hamiltonian of SCRP state is widely explained in next section, anyway two of the four levels can give spin-selective population transfer to T_0 level and thus polarizes the triplet states. ISC crossing and recombination triplet states have same ZFS parameters D and E but peculiar polarization patterns thus they can be recognized by spectra simulations. The recombination mechanism is shown is figure 2.5.

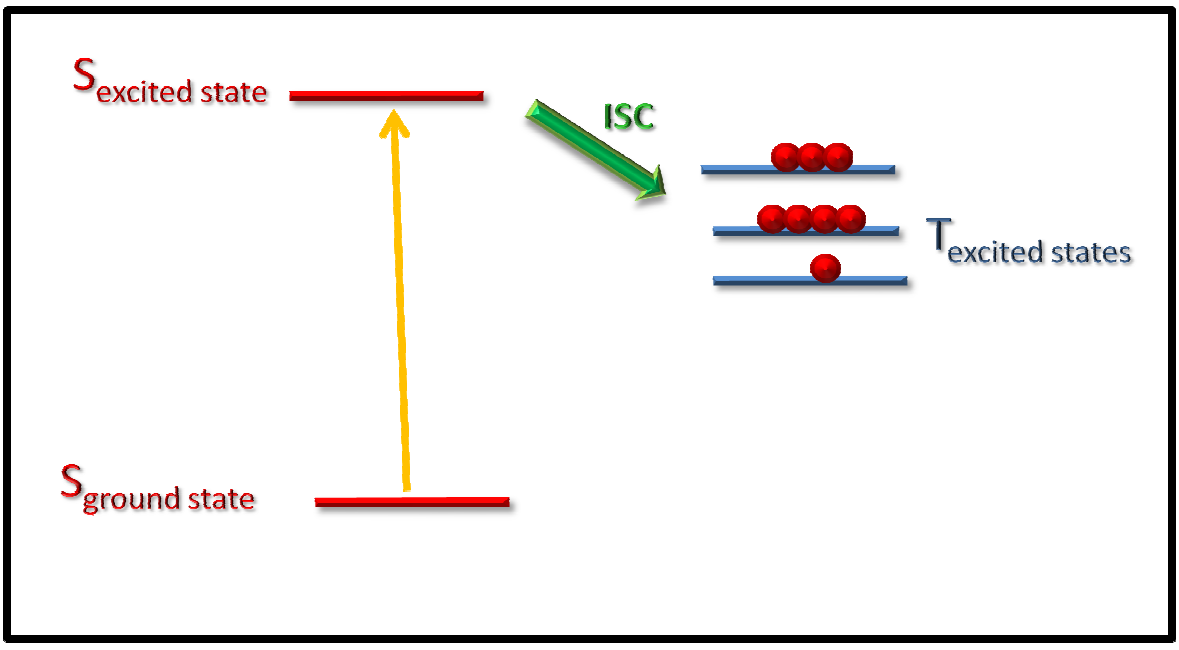

Figure 2.4 ISC mechanism is shown as spin-selective process that causes populations of triplet sublevels to be spin-polarized.

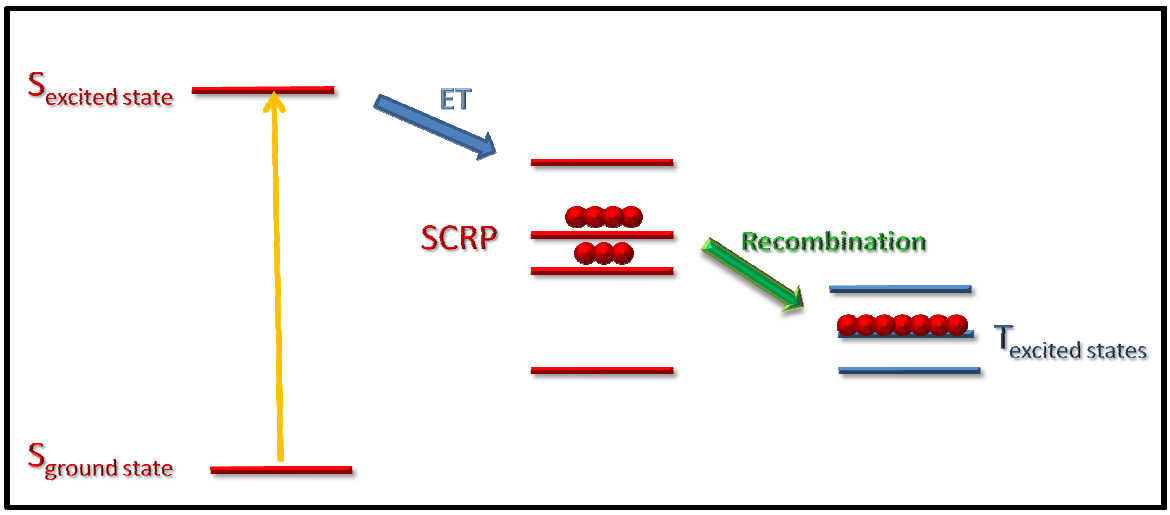

Figure 2.5 Recombination mechanism is shown by green arrow. Populations of two sublevels of SCRP states are transferred to T_0. Triplets states result to be spin-polarized.

2.3 Spin Correlated Radical Pair (SCRP)

2.3.1 Spin Hamiltonian of SCRP

The intensity of exchange and dipolar couplings are dependent from the average distance between two unpaired electrons. When electrons are characterized by a great exchange interaction, their spin states are (2.19) that is electrons are considered to form a total coupled spin system. As outlined in section 2.2.4 , two electrons can interact also by dipolar coupling that has no effect on T_0 and S_0 states of (2.19) and mix T_{-1} and T_{+1} states. The global Hamiltonian can be expressed as the sum of (2.20) and (2.24)

$$H = -J(S^2 - 1) + D\left(\hat{S}_z^2 - \frac{1}{3}S(S+1)\right) + \frac{1}{2}E(\hat{S}_+^2 + \hat{S}_-^2) \qquad (2.36)$$

When electrons are far apart but still interacting, point dipole approximation holds and dipolar tensor $\mathbf{D}$ is considered to have axial symmetry. And (2.36 becomes)

$$H = -J(S^2 - 1) + +D\left(\hat{S}_z^2 - \frac{1}{3}\hat{S}(\hat{S}+1)\right) \tag{2.37}$$

where $E = 0$ was set in (2.36). Hamiltonian (2.37) is diagonal in the basis set (2.19) T_{+1}, S, T_0, T_{-1}

$$H = \begin{pmatrix} -J + \frac{D}{3} & 0 & 0 & 0 \\ 0 & J & 0 & 0 \\ 0 & 0 & -J - \frac{2}{3}D & 0 \\ 0 & 0 & 0 & -J + \frac{D}{3} \end{pmatrix} \tag{2.38}$$

If and external magnetic field is applied, the Zeeman interaction must be taken into account. It should keep in mind that we are treating the case of two separated weakly interacting electrons that two species with different *g* factors slightly coupled.

Considering the anisotropic case, when we add the Zeeman contribution to (2.37) it becomes (48):

$$H = \mu_B \mathbf{B_0} \cdot \mathbf{g_1} \cdot \hat{\mathbf{S}}_\mathbf{1} + \mu_B \mathbf{B_0} \cdot \mathbf{g_2} \cdot \hat{\mathbf{S}}_\mathbf{2} - J(S^2 - 1) + D\left(\hat{S}_z^2 - \frac{1}{3}\hat{S}(\hat{S}+1)\right) \tag{2.39}$$

The anisotropy of $\mathbf{g}$ and $\mathbf{D}$ tensors can be expressed in terms of $g(\vartheta, \varphi)$ and $D(\vartheta)$, where ϑ, φ are the polar angles and D depends only on ϑ for the $\mathbf{D}$ tensors is axial (48-50)

$$\begin{aligned} H = \mu_B g_1(\vartheta, \varphi) S_{z1} + \mu_B g_2(\vartheta, \varphi) S_{z2} - J(S^2 - 1) \\ + D(\vartheta)\left(\frac{3}{2}\hat{S}_z^2 - \frac{1}{2}\hat{S}(\hat{S}+1)\right) \end{aligned} \tag{2.40}$$

where:

$$\left(g_i(\vartheta,\varphi)\right)^2 = g_{ix}^2 \sin^2\vartheta\cos^2\varphi + g_{iy}^2 \sin^2\vartheta\sin^2\varphi + g_{iz}^2\cos^2\vartheta \qquad i = 1{,}2 \tag{2.41}$$

$$D(\vartheta) = D\left(\cos^2\vartheta - \frac{1}{3}\right) \tag{2.42}$$

We now consider the isotropic Zeeman interaction case and separate the relative Hamiltonian into a symmetric and antisymmetric contributes (49):

$$\begin{aligned} H_A &= \frac{1}{2}(g_{1z} - g_{2z})\mu_B B_0\left(\hat{S}_{z1} - \hat{S}_{z2}\right) \\ H_S &= \frac{1}{2}(g_{1z} + g_{2z})\mu_B B_0\left(\hat{S}_{z1} + \hat{S}_{z2}\right) \end{aligned} \tag{2.43}$$

the antisymmetric contribute mixes the T_0, S and this mixing is maximum when exchange and dipolar couplings are similar to H_A interaction. We now express (2.40) in the (2.19) basis (48)

$$H = \begin{pmatrix} \omega - J + D(\vartheta) & 0 & 0 & 0 \\ 0 & J & Q & 0 \\ 0 & Q & -J - \frac{D}{2}(\vartheta) & 0 \\ 0 & 0 & 0 & -\omega - J + D(\vartheta) \end{pmatrix} \tag{2.44}$$

where $Q = \frac{1}{2}(g_{1z} - g_{2z})\mu_B B_0$ and $\omega = \frac{1}{2}(g_{1z} + g_{2z})\mu_B B_0$. The eigenvalues of (2.44) are:

$$\begin{aligned} E_1 &= \omega - J + D(\vartheta) \\ E_2 &= -D(\vartheta) + \Omega \\ E_3 &= -D(\vartheta) - \Omega \\ E_4 &= -\omega - J + D(\vartheta) \end{aligned} \tag{2.45}$$

where $\Omega^2 = \left(\mathrm{J} + \mathrm{D}(\vartheta)\right)^2 + \mathrm{Q}^2$. The eigenfunctions are given by:

$$\begin{aligned}\varphi_1 &= T_1\\ \varphi_2 &= \cos\psi\, S + \sin\psi\, T_0\\ \varphi_3 &= -sin\,\psi\, S + \cos\psi\, T_0\\ \varphi_4 &= T_{-1}\end{aligned} \tag{2.46}$$

where $\tan 2\psi = \frac{Q}{J+D/2}$. This spin system is called Spin Correlated Radical Pair (SCRP) and can be detected by EPR spectroscopy.

The allowed transitions are:

$$\begin{aligned}\omega_{12} &= \omega - \Omega - J + \frac{D(\vartheta)}{2}\\ \omega_{34} &= \omega - \Omega + J - \frac{D(\vartheta)}{2}\\ \omega_{13} &= \omega + \Omega - J + \frac{D(\vartheta)}{2}\\ \omega_{24} &= \omega + \Omega + J - \frac{D(\vartheta)}{2}\end{aligned} \tag{2.47}$$

It's possible to get the dipolar D parameter from simulation of SCRP spectra. By using (47)

$$\langle r^3\rangle = \frac{-\frac{3}{8}\mu_0 \cdot (g\beta)^2}{D} \tag{2.48}$$

the mean distance between radicals can be calculated

2.3.2 Spin polarization of SCRP (50)

SCRP is a four fold spin system which is described by (2.39). In many cases, SCRP state is generated by electron transfer between a donor and an acceptor. The two radical ions that result after electron-transfer have generally different isotropic g values and weak exchange and dipolar interactions. Before electron transfer, the spin state of the system is given by the eigenfunction (2.19) and there is still no mixing between S and

T_0 states. If we assume the two unpaired electrons to be in a singlet state, the population at the moment of the electron transfer is given by:

$$\boldsymbol{\rho(0)} = \begin{pmatrix} 0 & 0 & 0 & 0 \\ 0 & 1 & 0 & 0 \\ 0 & 0 & 0 & 0 \\ 0 & 0 & 0 & 0 \end{pmatrix} \tag{2.49}$$

where $\rho(0)$ is the density matrix of initial state in T_{+1}, S, T_0, T_{-1} basis set. When system undergoes electron transfer, Zeeman interaction mixes S, T_0 states, and population start to oscillate between these two states, that is the diagonal elements of (2.49) become dependent in time for ρ_{SS} and $\rho_{T_0T_0}$. If we transform the (2.49) in the eigenstates of (2.40), we get:

$$\boldsymbol{\rho_E(0)} = \mathbf{V}' * \boldsymbol{\rho(0)} * \mathbf{V} \tag{2.50}$$

where $\mathbf{V}$ is the matrix of eigenvectors that transforms from T_{+1}, S, T_0, T_{-1} to $\varphi_1, \varphi_2, \varphi_3, \varphi_4$ basis

We get:

$$\boldsymbol{\rho_E(0)} = \begin{pmatrix} 0 & 0 & 0 & 0 \\ 0 & \cos^2\psi & \sin\psi\cos\psi & 0 \\ 0 & \sin\psi\cos\psi & \sin^2\psi & 0 \\ 0 & 0 & 0 & 0 \end{pmatrix} \tag{2.51}$$

The diagonal elements of (2.51) states that populations of SCRP levels at time of electron transfer from a singlet state. We will refer to it as singlet precursor and this represents a common situation in photovoltaic processes. Anyway population of SCRP level are not at Bolztmann equilibrium because level φ_2, φ_3 are the only populated levels. System is said to be spin-polarized and the expected EPR spectra for $J > 0$ and $D = 0$. The polarization of levels is shown in figure 2.6

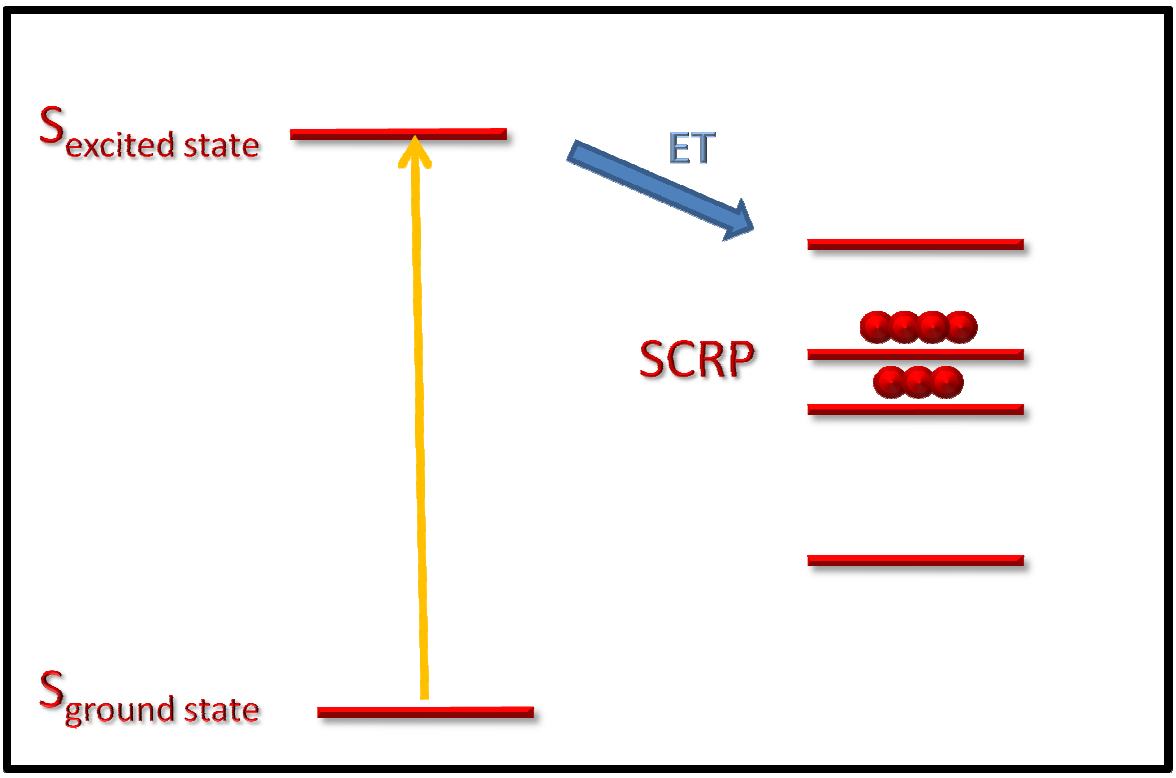

Figure 2.6 SCRP spin-polarization of levels. The spin-selective electron transfer mechanism populates the central levels that correspond to φ_2 and φ_3 eigenstates.

Chapter 3 - EPR technique

3.1 Steady stated EPR experiments

3.1.1 Continuous wave EPR (cw-EPR)

EPR experiments deals with microwave induced spin transitions when an external magnetic field is applied. The EPR spectrometers are classified by frequency of electromagnetic radiation used and on resonance conditions. The most common EPR spectrometers uses microwaves in X Band of about 9-10 GHz and magnetic field intensity of some thousand of Gauss.

EPR spectra are recorded using a resonant cavity at a precise microwave frequency and then magnetic field is swept in order to get the resonance condition. The spectra is a measurement of absorbance of microwaves as a function of magnetic field. Anyway the direct measure of microwaves intensity is inefficient and sensibility is very low. A 100 KHz modulation of some gauss is superimposed to static magnetic field and this produces an oscillating output that can be easily detected by a Lock-in amplifier that amplifies signal and as cut-off filter for noise. The modulation applied causes the spectra to be detected in first derivative.

3.1.2 Light-Induced EPR (LEPR)

LEPR is a continuous wave EPR technique that focuses its detection on photo-generated species. It is widely used in studying system which undergoes photo-induced processes generating paramagnetic species. Thus LEPR is mostly used in analysis of photovoltaic processes. LEPR spectra is obtained by subtraction of cw-EPR spectrum recorded under light on condition with the cw-EPR spectrum under light off condition. When continuous white light illumination is used, the intensity of LEPR spectra can be considered proportional to the ratio of formation and of annihilation of photoinduced species that guarantees a sufficient steady state concentration. When lifetime of species is too low, LEPR signal is basically undetectable. For this reason, as outline in chapter 1, LEPR technique applied to photovoltaic organic blends, allows to

detect only trapped photo-generated paramagnetic species for their long lifetimes. These radicals are $S = 1/2$ species and have negligible hyperfine and dipolar interactions thus we expect an EPR one-line spectrum for each species.

3.1.3 Time Resolved EPR (TREPR)

TREPR is a transient spectroscopic technique that is able to detect an EPR spectrum of photo-induced species as a function of time and of magnetic field intensity.

Samples are irradiated by 5 ns laser pulses at a certain magnetic field strength and then a transient decay is recorded in the range of microseconds. By sweeping the magnetic field intensity, it possible to detect a collection of decay curves around the spin-transition resonance condition. Laser pulses length is considered to be a Dirac delta function in the time-range considered thus TREPR is able to detect paramagnetic species with short lifetime (from hundreds of nanosecond to ten of milliseconds). This technique is able to detect SCRP and triplet state species that cannot be seen by LEPR. As outlined in sections 2.3.2 and 2.2.5 the populations of levels of these species is spin-polarized and thus relative TREPR spectra have emission and absorption features. TREPR spectra of triplet states populated by ISC and Recombination have different polarization patterns and the possibility to distinguish between them is very useful in understating the photo-physic of system.

SCRP species are short living species that can be detected by TREPR. These species are spin-polarized by electron transfer mechanism that transfers population from singlet excited state of donor to φ_2 and φ_3 SCRP state by ST_0 mixing. The pattern of polarization generally depend on the spin sate of donor, the sing of exchange constant J and the sign of $D(\vartheta)$.

When SCRP species is formed by interacting radicals that can migrate, it's possible to detect by TREPR some spectra of polarized isolated radicals. They have the same spectral line shapes of two independent $S = 1/2$ species and their spin-polarization arises from radical pair mechanism that causes single radicals to inherit the polarization of SCRP when they are no more interacting. Generally line of two radicals

are polarized in an antiphase pattern. In figure 2.7 theoretical LEPR and TREPR spectra of studies species are shown.

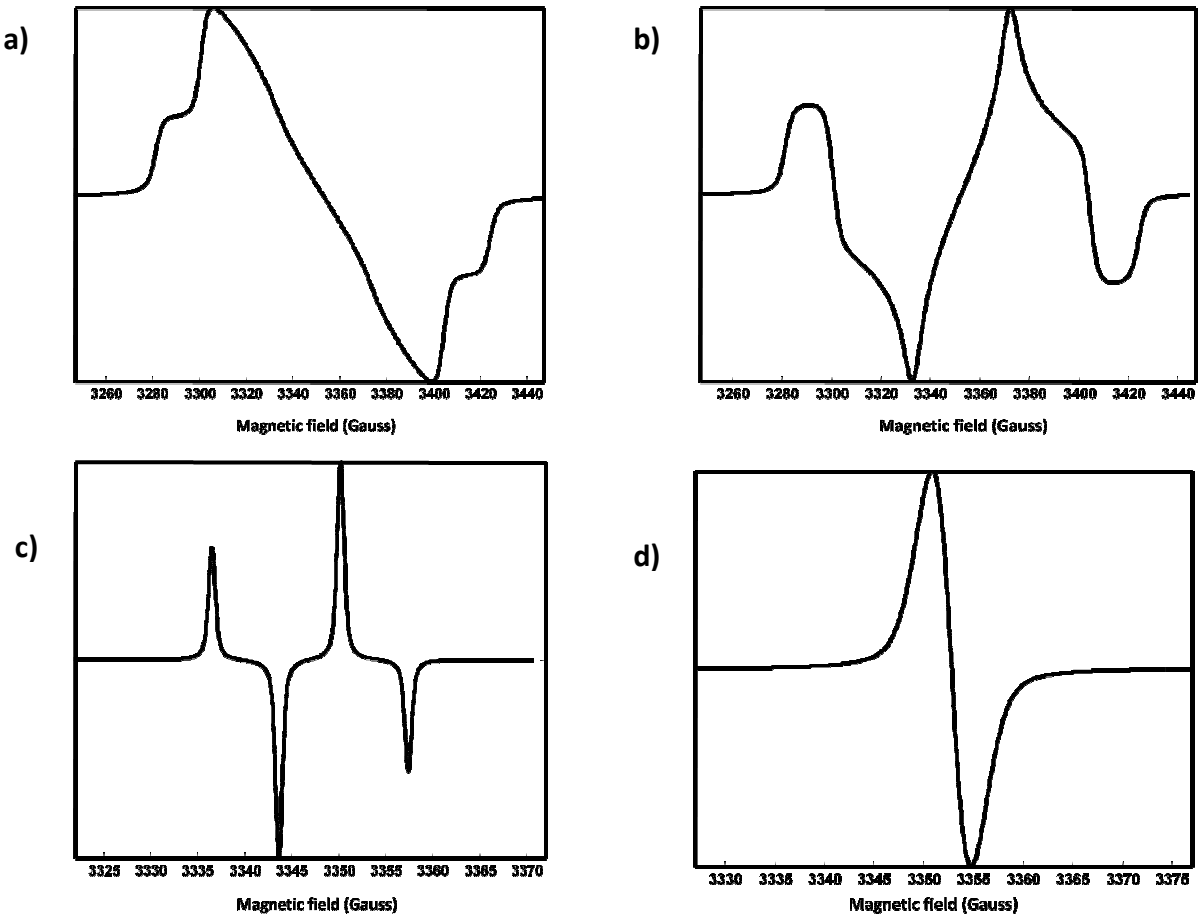

Figure 2.7 Theoretical spectra of a) ISC triplet state, b)Recombination triplet, c) SCRP for J>0 and D=0, d) $S = 1/2$ radical. g factors are considered isotropic for all cases.

3.1.4 Linewidth and Lineshape

The characteristics of spectral line in EPR experiment are usually treated by solving Bloch equations. When steady state solution is considered, it's possible to find the expression for complex magnetic susceptibility χ

$$\chi' = \chi_0 \frac{\omega_B(\omega_B - \omega)T_2^2}{1 + (\omega_B - \omega)^2 T_2^2 + \gamma_e^2 B_1^2 T_1 T_2}$$
$$\chi'' = \chi_0 \frac{\omega_B T_2}{1 + (\omega_B - \omega)^2 T_2^2 + \gamma_e^2 B_1^2 T_1 T_2} \quad (3.1)$$

where χ' and χ'' are respectively the real and imaginary part of χ, ω_B is the classical Larmor frequency, ω is the microwave frequency, T_1 and T_2 are the longitudinal and transversal relaxation time constants, γ_e is the gyromagnetic ratio of free electron.. The EPR spectrum represents the microwave power absorption from the spin system and its profile is given by the imaginary part of (3.1). The $\gamma_e^2 B T_1 T_2$ term is negligible in low microwave power regime and the resulting curve is a Lorenztian function. Under this approximation, the linewidth can be expressed as:

$$\Gamma = \frac{1}{|\gamma_e| T_2} \tag{3.2}$$

when stationary state condition hold, the linewidth is proportional only to T_2 , and is said to be homogeneous. Generally the unpaired electrons in a system are not equivalent thanks to different local lattice geometry, weak unresolved hyperfine or dipolar coupling with different nuclei that can be strongly anisotropic. These interaction usually changes lineshape from Lorenztian type to Gaussian type that can be considered as an envelope of various Lorenztian function each one centered at different frequency. The latter is called inhomogeneous broadening. This considerations are valid for all the EPR experiments described above. When microwaves pulses are used, things can get more complicated.

3.2 Pulsed EPR experiments

3.2.1 Spin-Echo

When pulsed microwaves are used spin system interacts with a strong oscillating magnetic field which are usually tens of nanoseconds long. In this case, solutions of Bloch equations can be performed only under particular boundary conditions and they cannot give information about phase coherences evolutions of system. For a complete description of dynamic is often used the Liouville equations or the formalism of product operators. Anyway the spin-Echo experiment can still be described by Bloch

formalism thus by using the vectorial picture, that considers the vector magnetization as preceding around the axis of quantization given by an external magnetic field. When an external magnetic field $\mathbf{B_0}$ is applied on a sample, magnetization vector $\mathbf{M}$ is generated. $\mathbf{M}$, which is given by the sum of all the magnetic momenta of electrons, will start to precedes around $\mathbf{B_0}$ direction (considered as z axis) with damped oscillating dynamic for the relaxation processes T_1 and T_2 that forces $\mathbf{M}$ to align along the z axis in the equilibrium configuration. When an oscillating magnetic field $\mathbf{B_1}$ such as microwave pulse with polarization perpendicular to $\mathbf{B_0}$ field, the magnetization start its precession motion around $\mathbf{B_1}$ axis at the Raby frequency dependent on intensity of $\mathbf{B_1}$**.** If we imagine to apply a $\mathbf{B_1}$ field for a time long t_p, then the angle rotation of $\mathbf{M}$ is:

$$\alpha = -\gamma|\mathbf{B_1}|t_p \tag{3.3}$$

Usually, the microwave pulse is directed to the sample with an intensity and duration adapted to produce $\pi/2$ or π flip angles. After a single $\pi/2$ pulse, a transverse magnetization in the xy plane is produced. After the pulse, all spin packets start a precession motion around B0 with their Larmor frequency. However, not all of them precedes around B0 with the same frequency and therefore, after a short time (often shorter than the response time of the pulsed EPR instruments) they spread out in the xy plane producing a vanishing total magnetization. π pulse is generally sent after an evolution time τ and it causes an inversion of magnetization. Afterwards, the single spin packets continue to precedes but are refocused exactly after a second delay time τ . The refocusing of the magnetization is named spin echo and a graphical representation of the sequence of events (“Hahn echo pulse sequence”) is shown in figure 2.8

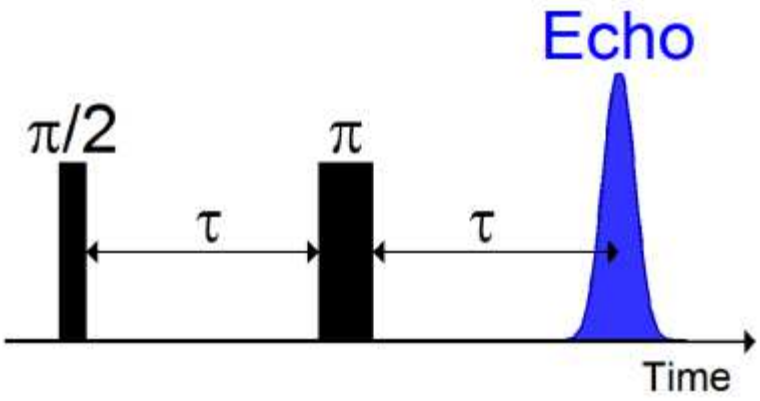

Figure 2.8 The effect of $\mathbf{B_1}$ field with two $\pi/2$ and π pulses is shown. Magnetization is rotated in the xy plane by the first pulse then after τ is inverted and refocus along $-x$ axis after τ.

3.2.2 Echo-detected EPR

Field-swept pulsed experiments are used to acquire broad EPR spectra in which it is impossible to excite the whole spectrum with a single short microwave pulse. In a usual Echo-Detected EPR (EDEPR) experiment, an echo pulse sequence is used and the echo intensity is measured at every magnetic field position. Spectrum recorded is analogous of cw-EPR one even if intensity of single species can have different intensity according to different T_2 relaxation times. If species has great difference in T_2 magnitude, it's possible to eliminate the contribute of all species with $T_2 < \tau$.

3.2.3 Relaxation Times

Because the electron spins interact with their surroundings, after a $\pi/2$ pulse, the magnetization in the xy plane decays away and eventually returns to alignment with the z axis. This process is called relaxation and is characterized by two constants, T_1 and T_2. The spin lattice relaxation time, T_1, describes how quickly the magnetization returns to its equilibrium value (only z-component) while the transverse relaxation time, T_2, describes how quickly the magnetization in the xy plane (i.e. transverse magnetization) disappears.

Spin-Lattice Relaxation Time. T_1 relaxation time is generally measured by Echo Detected Inversion Recovery sequence. A π pulse rotates magnetization is reversed along $-z$ axis. population is now inverted. The restore of equilibrium polarization is performed by T_1 relaxation also called Spin-Lattice Relaxation Time. After the time T, a two pulse echo sequence is performed and magnetization is refocused after $T + 2\tau$ time. The pulse sequence is shown in figure 2.9.

The echo intensity as function of the time T is recorded and the curve obtained is fitted by the following formula, from which T_1 can be obtained:

$$y = A - Be^{-t/T_1} \tag{3.4}$$

Spin-Lattice Relaxation Time. Transverse (or spin-spin) relaxation time refers to the magnetization decay in the xy plane. In the case of inhomogeneous broadening, each spin packet feels a slightly different local magnetic field and the distribution of local fields gives a large number of spin-packets with a distribution of Larmor frequencies.

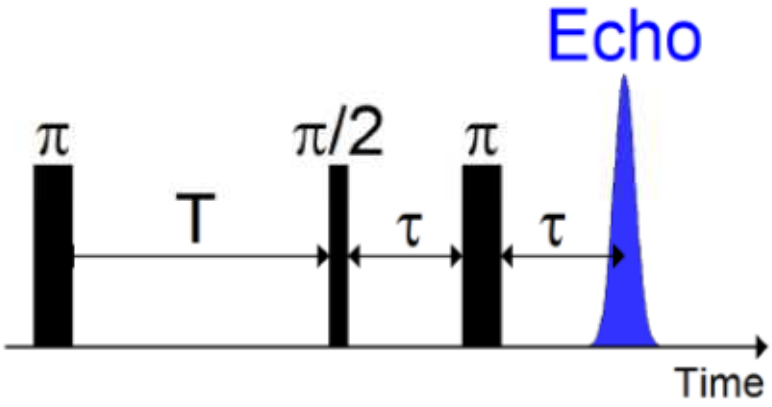

Figure 2.9 Inversion recovery experiment is displayed. The pulse sequences allows determination of T_1 relaxation time.

In the vectorial sum of each component, many
components cancel each other out and decrease the transverse magnetization. In case of homogeneous broadening even though all spins experience the same magnetic field, there are spins that interact with each other resulting in mutual and random spin flip-flops. In general, the decay of the transverse magnetization is exponential with T_2 characteristic time:

$$y = Be^{-t/T_2} \tag{3.5}$$

To measure the relaxation time T_2 of a sample it is often used the Hahn echo decay pulse sequence, where the Echo intensity is measured at different τ values. The decay curve thus produced is fitted by the above exponential decay function, from which the characteristic time T2 is obtained.

Chapter 4 – Experimental Results

4.1 LIGHT MODULATED EPR (LMEPR) FOR STUDY OF LIFETIMES DEFECTS OF POLYMER/FULLERENE BLENDS

4.1.1 Disordered Organic Semiconductors

This section focuses its attention on localized states of polymer/fullerene solid films (51, 52). OPV solar cells are generally based on solid state blends able to generate radical charges under illumination (53). The principal photo-physical processes can be described using a molecular picture, see section 1.2.2, but it should be kept in mind that the evaporated blends are very disordered solid materials with a generally casual amount of amorphous and crystalline phase. The amorphous phase is generally characterized by a more intimate interconnection between polymer and fullerene thus it is the main responsible for the efficient electron transfer. On the other side, the charge transport fenomena that the photovoltaic process needs, avoiding recombination, is clearly enhanced in a more ordinate phase such as a crystal (54). There's no clear evidence on the best ratio between crystalline and amorphous phase to get the best efficiency, anyway the number of defects of the solid matrix can influence heavily the final efficiency (55). The standard theory in an ideal crystalline semiconductor is based on the band theory which formally uses Bloch wavefunctions to describe a wholly delocalized state along all the volume of solid. Low degree of disorder generally modifies the electron wavefunctions and relative energies only slightly and transport description can still be based on Bloch functions with some random potential taking into account the deviations from ideal crystal (41, 56).

In noncrystalline materials it's still possible to find a short-range order and the density of state is generally influenced by the degree of disorder. Generally it's possible to distinguish an high electron density state region, that keeps the feature of a band, and a lower density state region where delocalization can be reduced to single molecule state. The energy level that separates these two regions is called the *mobility edge* with an energy ε_c typical of semiconductor. The energy interval between the mobility edges of valence and conducting band is called *mobility gap* and the states inside it the

are localized. By term localized we consider states with low degree of extension along the solid blends. The density of state inside the mobility gap is an important factor in charge transport mechanism anyway the spectrum of energy is not known for almost all disordered materials. Experimental techniques can give only an esteem but the problem is still far from a complete solution (51, 57). In Figure 4.1 a general representation of the density of state is displayed. Even if density dies out very fast for states with lower energy than mobility edge, a great amount of states is still present and this makes the biggest difference with ordered materials. State below ε_v and above ε_c denotes the mobility edge for the valence and conduction bands respectively. In the presence work we deal with photo-generated holes and electrons trapped in some localized state inside the mobility gap.

For polymer/fullerene solids blends, we considered localized states occupied by positive polaron (P^+) and negative polaron (P^-) which represent the polymer radical cation and fullerene radical anion generated by photo-induced electron transfer. These localized states have different lifetimes depending on the energy and are considered as traps for polarons. The purpose of this section is to get some information about lifetimes of solid blends localizes state distribution by using light modulated EPR technique.

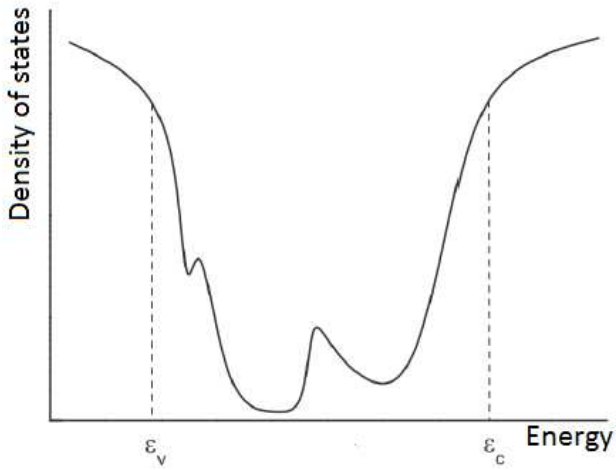

Figure 4.1 Hypotetical density state distribution is displayed. States are considered more denser above and under the two mobility edges for conduction and valence band while they are seen as localized inside the mobility gap.

4.1.2 Principles of modulated techniques in BHJ substrates

Let's consider a species in an excited state with relaxes with a general time function $I(t)$. The temporal range can always be represented by a time constant τ i.e. the lifetime. When sample is stimulated by some modulated excitation of the form $L(t) = b \cdot \sin(\omega t)$, system responds with a modulated signal with different amplitude and phase but same frequency $S(t) = B \cdot \sin(\omega t + \varphi)$. When the period of excitation $T = 2\pi/\omega$ is greater than τ, $S(t)$ follows exactly the profile of excitation with no phase shift $(\varphi = 0)$ and same normalized amplitude. This happens when lifetime is shorter enough to restore completely the system in one oscillation time. When $T \approx \tau$ or $T < \tau$ the response of system is cumulative along one period of oscillation and the global output has lower amplitude and its phase is shifted (Fig 4.2a).

Eventually when $T \ll \tau$ amplitude is zero $(B = 0)$ and phase-shift is maximum $(\varphi = \pi/2)$. This technique was first carried out for frequency-domain fluorescence experiments in order to detect singlet lifetime of fluorophores. In Fig 4.2b it shown a typical trend for two fluorophores having 10ns and 2.5 ns lifetimes (58).

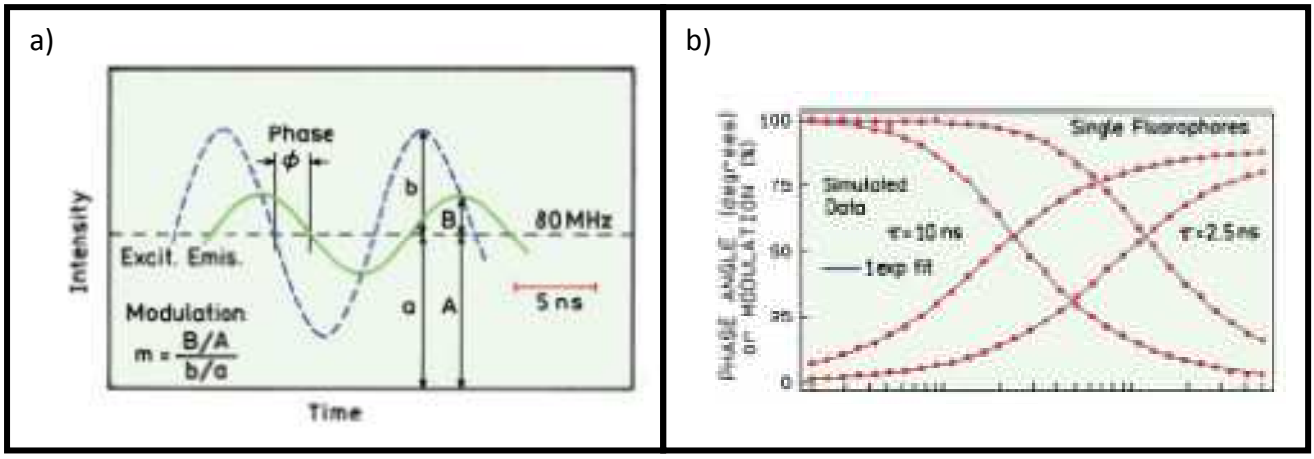

Figure 4.2 figures are taken from Lakowicz's *Principle of fluorescence spectroscopy* (58) . Figure 4.1a shows the effect of an alternating stimulation (blue dotted line) to a system with lifetime τ. When inverse of stimulation frequency is near to lifetime range, the response of system (green line) is phase shifted and has lower amplitude. Fig 4.1b show amplitude decrease and phase shift increase for two fluorophores with different lifetimes as a function of frequency of stimulation. Spectra are shown in logarithmic scale.

A general output signal, in time domain, can always be described as a convolution between input signal $L(t)$ and the time response function (RF) of the system $I(t)$

$$S(t) = \int_0^\infty dt' L(t')I(t-t')dt' = \int_0^\infty dt' L(t-t')I(t')dt' \tag{4.1}$$

In the present case the RF is the decay in time of an excited specie which is generally assumed to be exponential $I(t) = \mathrm{e}^{-t/\tau}$. Oscillating excitation can be written as a complex function of time: $L(t) = b \cdot \mathrm{e}^{i\omega t}$. We get:

$$\begin{aligned} S(t) = \int_0^\infty b\,\mathrm{e}^{i\omega(t-t')}\,\mathrm{e}^{-\frac{t}{\tau}}\,dt' = b\mathrm{e}^{\mathrm{i}\omega\mathrm{t}} \int_0^\infty e^{-\left(\frac{1}{\tau}+i\omega\right)t'}dt' = \\ = b \cdot e^{i\omega t}\frac{\tau}{1+i\omega\tau} = R(\omega,\tau)\cdot be^{i\omega t} \end{aligned} \tag{4.2}$$

the frequency domain response function

$$R(\omega,\tau) = \frac{\tau}{1+i\omega\tau} \tag{4.3}$$

modifies amplitude and phase of $L(t)$. From (4.2) we can obtain:

$$S(t) = B \cdot e^{i(\omega\tau+\varphi)} \tag{4.4}$$

with $B = |S(t)| = \frac{b\tau}{\sqrt{1+(\omega\tau)^2}}$ and $\varphi = \arctan\frac{Im(S(t))}{Re(S(t))} = \arctan(\omega\tau)$

Light Modulated LEPR (LMEPR) is a magnetic continuous wave spectroscopy able to study radical charges generated by modulated light at different frequencies using the same principles previously outlined. Lifetime of photogenerated trapped radicals is

considered as the time when P^+ and P^- get off the site of traps toward the mobility edges where they can recombine and generated again the neutral species (polymer and fullerene). Modulation of light at a certain frequency allows to cut off all contributes of radicals trapped in site with lifetime longer than the inverse of modulation frequency. As modulation frequency increases, a gradual phase shift and a decrease in EPR intensity should be found.

Expression of $R(\omega,\tau)$ in (4.3) is valid only for system with a single lifetime and it's analogous to Debye model for dielectric constant (59) in electric polarization processes. Debye model assumes a first order kinetic relaxation, that can be well describe with a single lifetime. Photovoltaic film produced by thin or bulk evaporation methods are characterized by a great disorder of samples due the intrinsic difficulties of polymers to generated ordered crystalline phases. This results in a wide possible distribution of lifetimes of species located mostly in the amorphous phase. Cole-Cole (60) propose an empirical model by adding an exponential parameter α to Debye formula:

$$R(\omega,\tau) = \frac{\tau}{1 + (i\omega\tau)^{\alpha}} \tag{4.5}$$

α can be considered as a parameter that can globally account for the overall kinetic of processes (61, 62). When $\alpha = 1$ we obtain again the Debye formula. In this case, τ assumes the phenomenological meaning of apparent lifetime and it represents the global distribution of lifetimes studied. It can be used as comparison parameter between different samples, thus samples with a smaller τ will have a greatest amount of short living species.

As alternative to Cole-Cole (2.4), it's possible to assign a monoexponential decay to each trap that are so considered as an ensemble of Debye contributions ie. single lifetime species. In other words, a continuous lifetimes distribution $a(\tau)$ is considered that acts as weight function for each Debye contribution:

$$I(t) = \int_0^\infty a(\tau) e^{-t/\tau}\, d\tau \tag{4.5}$$

which leads to

$$R(\omega) = \int_0^\infty \frac{\tau \cdot a(\tau)}{1 + i\omega\tau} d\tau \tag{4.6}$$

by calculating the inverse formula of (2.6), it's theoretically possible to get the lifetime distribution $a(\tau)$. Anyway the model assumes for each trap a first order kinetic of decay, which is generally not the case. Radicals trapped in the matrix defects can have a more complex dynamics before recombination, moreover the correlation between lifetime distribution and energy distribution is not trivial and not follow necessarily an activated (Arrhenius-like) process.

In this work we will consider both Debye (4.3) and Cole-Cole (4.5) model in data discussion. In Figure 4.3 the real and imaginary part of (4.3) and (4.5).

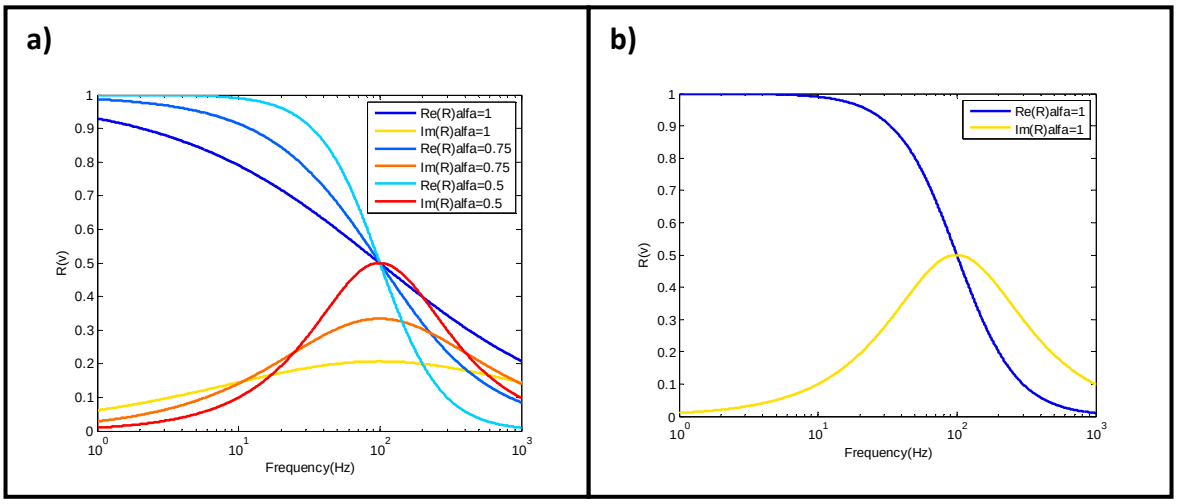

Figure 4.3 Fig.4.3a shows real and imaginary part of Cole-Cole formula (4.4) for $\tau = 10\, ms$ and $\alpha = 1{,}0.75{,}0.5$. For each value of α, when linear frequency is $(2\pi\tau)^{-1}$ real part is 0.5 and the imaginary part has a maximum. In Fig.4.3b real and Imaginary part of Debye formula is shown for the same lifetime as Cole-Cole. Debye model is just a single case of Cole-Cole model when $\alpha = 1$

4.1.3 Light Modulated EPR - LMEPR

Light-Modulated EPR (LMEPR) is a non-conventional EPR technique based on the principles of modulated spectroscopy outlined in the previous section. After photo-generation, negative polarons and positive polarons can occupy some localized states inside the mobility gap. These species are S=1/2 radicals and thus can be detected by EPR technique. We combined a modulated photo-excitation with the classical cw-EPR spectroscopy in order to discriminate the contribution of negative and positive polarons by the time of stay inside the traps, The great amount of defects and the efficient electron transfer of materials give rise to steady state concentration of radicals high enough to detect spectra with good signal to noise ratio. In Figure 4.4 a schematic representation of experimental set-up is displayed.

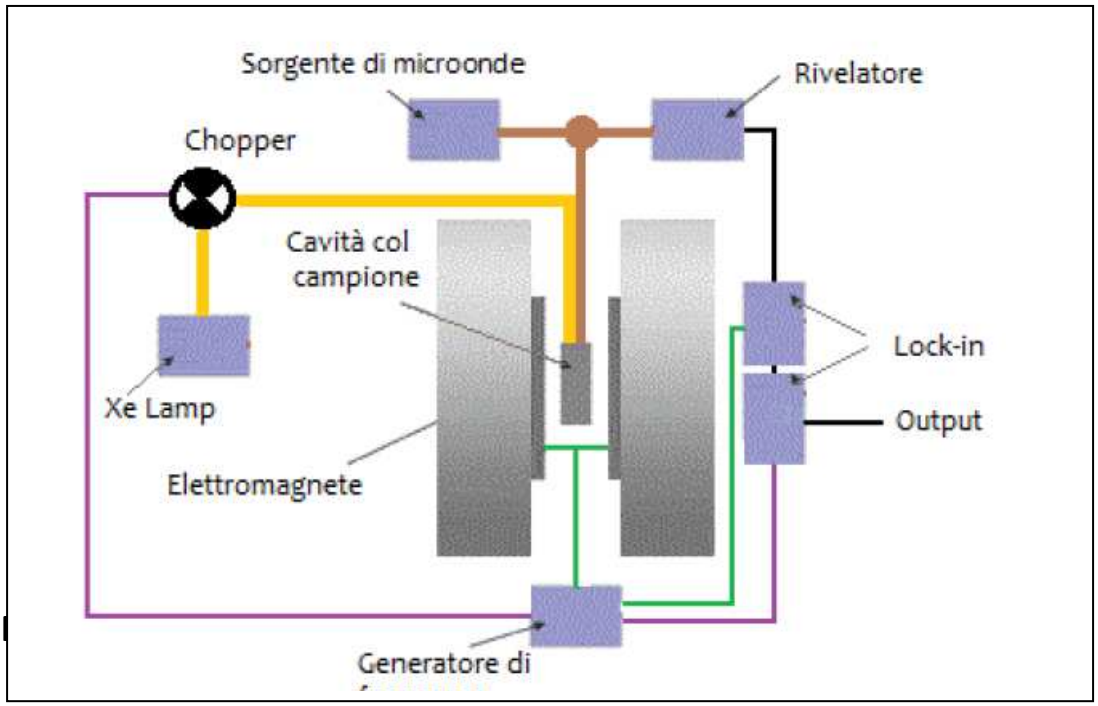

Figure 4.4 A continuous white light source from Xe-Lamp is modulated by a chopper at difference frequencies. Modulated light is then headed inside the EPR cavity and illumines the sample. Since output signal is modulated by high oscillating field modulation and slowly oscillating white light excitation, two lock-in put in series are needed in order to recover the LEPR signal

4.1.4 Experimental

The different role of polymer and fullerene was studied for two different set of samples. the first set considers P3HT blended with different fullerene: PC60PhOMe, C60MM12, $PC_{61}BM$, C60H12, C60Ph2,1-4 the second set $PC_{61}BM$ blended with different polymers: P3HT,MDMOPPV,PCDTBT,PTB7. Solution of polymer:fullerene=1:1 weight ratio blends were prepared in 1,2 chlorobenzene (ODCB) at open air. Films were prepared by slowly pumping the solutions directly in 3x4 mm EPR quartz tubes till complete evaporation of solvent. XBand-LEPR (Lightinduced EPR) experiments were performed at 130 K using a microwave cavity (Bruker ER200D), white light modulated excitation of 100mW power. Modulation were performed by an optical Thor Labs chopper that can generated oscillating curves between 1Hz and 1000Hz with logarithmic step. Signal is recovered by an external SR830 DSP Lock-in Amplifier just after the internal Lock-In of spectrometer. Signal has been recorded in in-phase and out-of-phase traces in order to get information on both phase and intensity variation of signal. Anyway the phase shift seemed to randomly change as frequency of modulation increases and follow neither the Debye (4.3) nor the Cole-Cole (4.5) models . Probably this chaotic phase change is due to the EPR instrumentation. Moreover all signals were phased by a numerical rotation, in the complex plane, that takes the intensity of one of the trace to vanish. The information of the phase is lost but the modulus of the complex vector can be used.

4.1.5 Results and discussion

P3HT with different fullerene derivatives

LEPR spectra of all samples showed two signals due to negative and positive polarons. Following previous studies (63, 64), we assigned the low field signal to the polymer polaron and the high field signal to the fullerene polaron. Before illumination all samples show a weak signal due to polymeric species already in a charged state. In Figure 4.5 experimental LEPR spectra and simulations are shown. Simulation were carried out by using a Matlab home-made program for fitting/simulation of isotropic

solid state radicals EPR spectra. Fullerenes derivatives have different line positions stating differences g factors. Anyway the various substituents modify only slightly the C_{60} wavefunction and this results in a little differences in g factors principal values that can be appreciated. The EPR lines of the two species are not well resolved thus the attribution of g principal values in simulation have a certain degree of arbitrariness. Table 4.1 shows the results of simulations for P3HT:fullerene_derivatives samples.

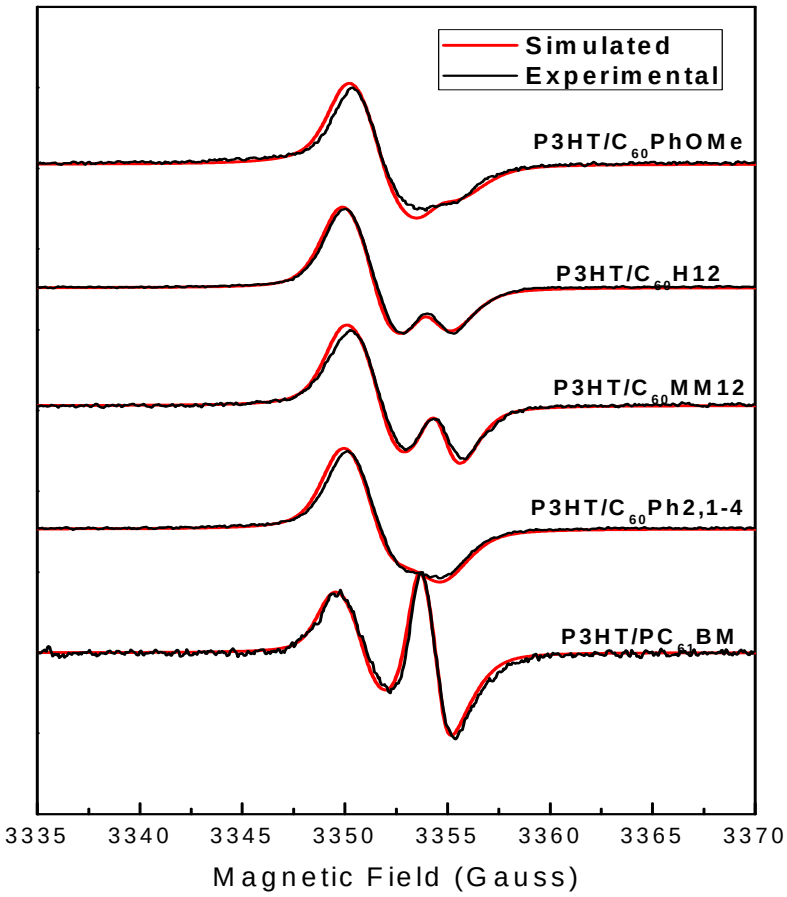

Figure 4.5 LEPR experimental spectra (black line) and simulations (red line) of P3HT/fullerene derivatives. Simulations were carried out considering a weighted sum of two non-interacting S=1/2 species.

Table 4.1

g tensor principal values of P3HT/fullerene derivatives samples. Simulations were carried out considering a weighted sum of two non-interacting S=1/2 species. Error on g factors is evaluated as ± 0.0002.

Blends	g1	g2	g3
P3HT/PC60PhOMe	2.0031/2.0030	2.0021/2.0001	2.0009/2.000
P3HT/C60H12	2.0031/2.0004	2.0021/2.0003	2.0009/2.0003
P3HT/C60MM12	2.0031/2.0003	2.0021/2.0002	2.0009/2.0001
P3HT/C60Ph2,1-4	2.0031/2.0008	2.0021/2.0004	2.0009/2.0004
P3HT/$PC_{61}BM$	2.0031/2.0003	2.0021/1.9996	2.0009/1.9992

LMEPR measurements were thus performed on P3HT/fullerene derivatives set of samples. Generally a decrease of signal is seen as modulation frequency increases. An example of LMEPR is shown in figure 4.6 for some frequencies of excitation. As modulation frequency ω increases, EPR signal of all localized states with a lifetime equal or greater than $1/\omega$ does not contribute to signal, thus the higher the frequency, the lower the intensity. The difference in rate of intensity decrease between samples can give information on the global distribution of localized states.

Simulation of spectra at single modulation frequencies were carried out keeping the same parameters of Table 4.1 and changing the relative weight of the two S=1/2 contributions. Intensity obtained as double integration of simulated spectra was compared with subtraction between maximum and minimum (example shown in figure 4.7). Anyway they appeared to differ only slightly then we chose, for seek of simplicity, maximum less minimum gap for data elaboration.

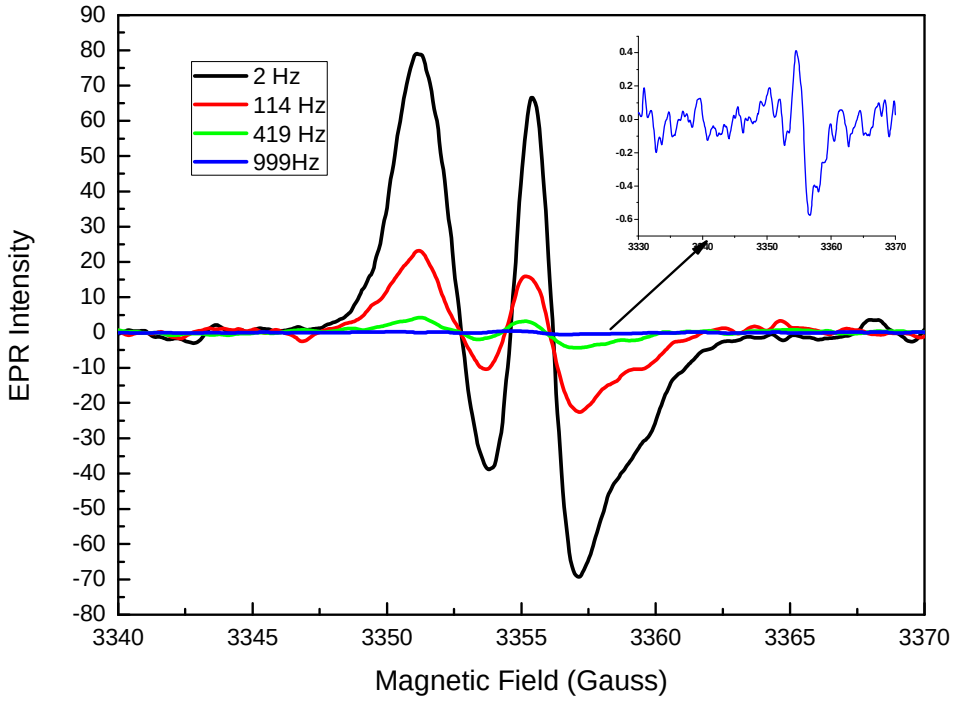

Figure 4.6 LMEPR at 2 Hz ,114 Hz 419 Hz, 999 Hz modulation frequency. Intensity of spectra decreases as modulation frequency increases denoting a change of about 2 orders of magnitude

We performed fitting using the Debye model and the Cole-Cole models. In Figure 4.8. it's shown a comparison between fitting performed with the two models on P3HT/$PC_{61}BM$ blend: data were all normalized to maximum of intensity in order to perform the fitting . Debye fitting results to be worse than Cole-Cole one, and this is what is expected since Debye model holds only for specie with single lifetime. In the case of polymer/fullerene blends there's a lifetime distribution and this complicate things. Cole-Cole formula takes into account deviation from Debye behavior that is when the exit mechanism from localized state it's not a simple exponential (65, 66). Even if at first approximation, recombination process can be considered dependent only by detrapping time which leads to a simple first order kinetic process (67), there could be some deviations due to other mechanism, such as diffusion or collision of polarons

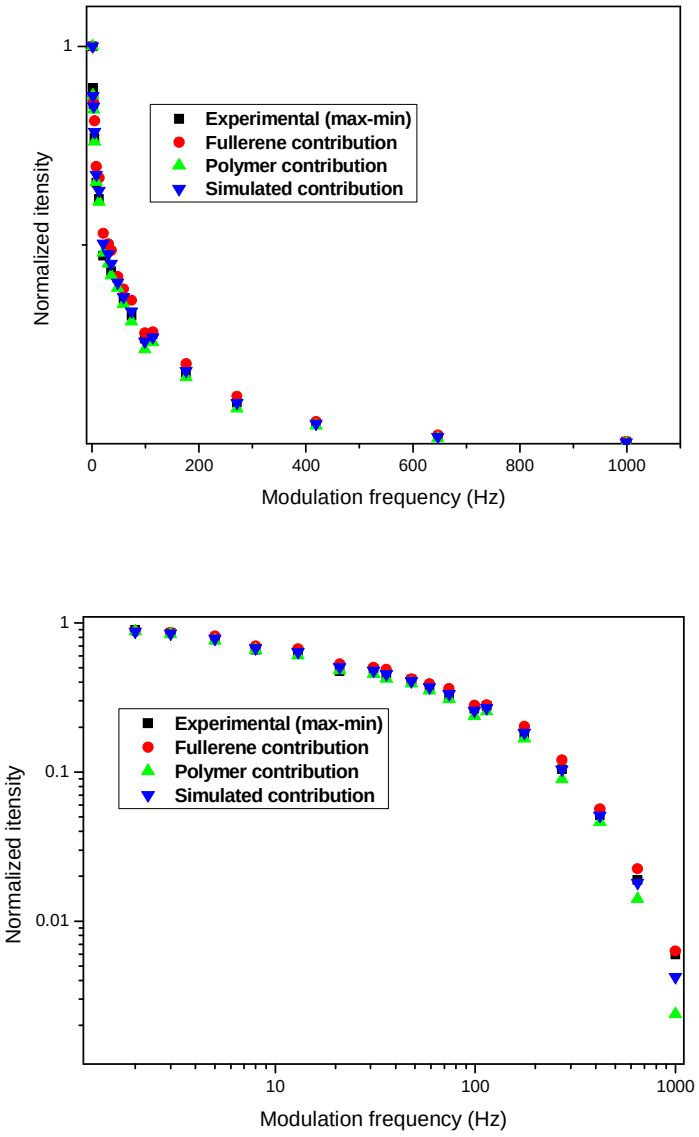

Figure 4.7 LMEPR spectra intensity of P3HT/Pc_{61}BM samples are shown as max - min subtraction and double integrated spectra. Simulations allows to determinate the contributions of single polarons that globally follow the same trend. Decays are shown in double logarithmic scale.

with same charge that result in a more complex kinetic. The exponent α of the Cole-Cole model adds a degree of freedom to Debye one and this generally can take into account this deviation. Anyway both cases cannot work well when distribution of lifetime is presence. Cole-Cole data fitting were considered to determine the apparent lifetimes of blends that can be generally used as comparison parameter.

Figure 4.9 shows the fitting and Table 4.2 summarizes the results of Cole-Cole fitting. As pointed out in the previous sections, the apparent lifetime has no particular physical meaning but can be used as comparison parameter between blends. It's not even possible to consider it as some kind of algebraic average between the various lifetimes of traps but can be considered as a phenomenological parameter that points out if a blend has, globally, a greatest number of low energy traps with respect to another

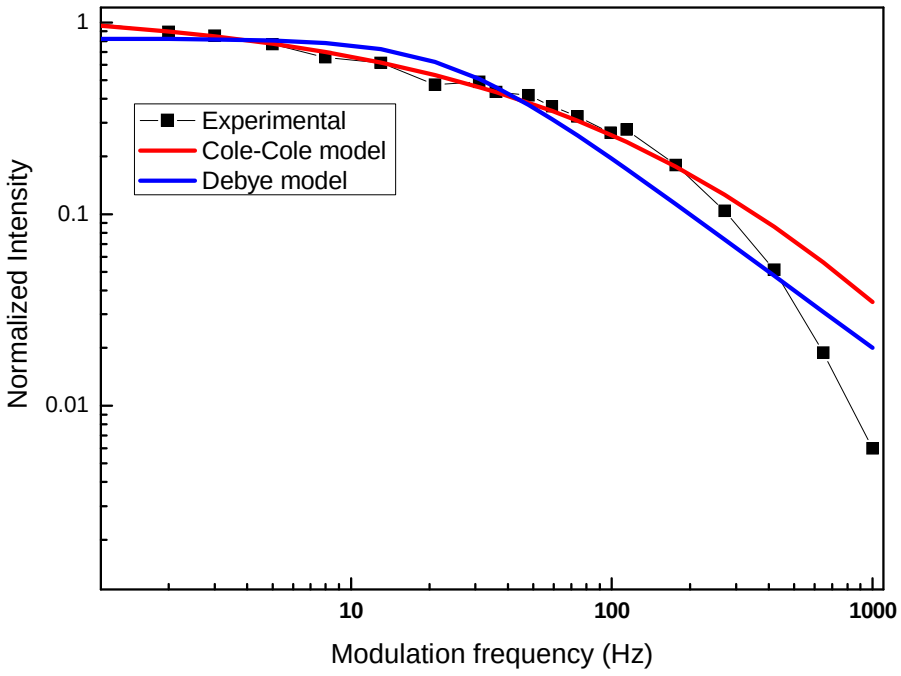

Figure 4.8 Fitting performed using modulus of Debye model (blue line) and Cole-Cole model (red line) . Debye model appears not to fit well experimental data while Cole-Cole follows the profile excluding the last three points. Decays are shown in double logarithmic scale.

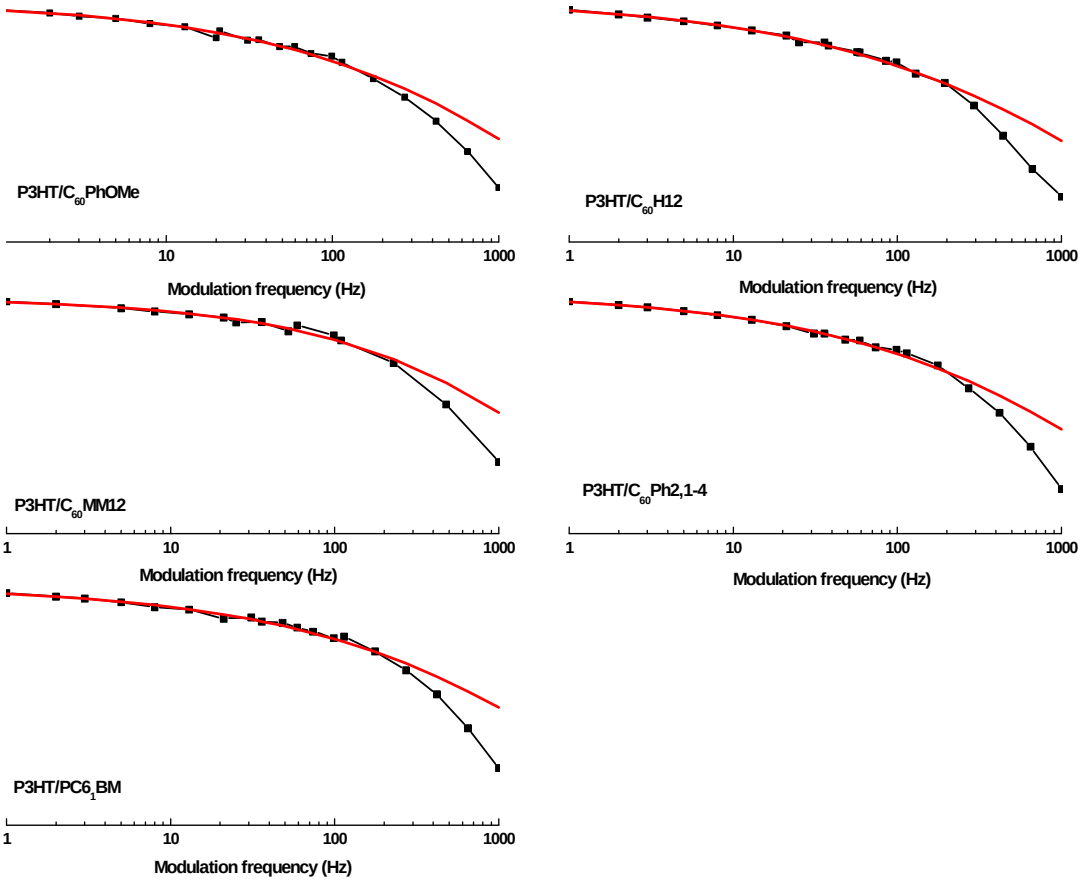

Figure 4.9 fitting (red line) of P3HT/fullerene derivatives blends using modulus of Cole-Cole models. Normalized intensity and frequency of modulation are plotted in double logarithmic scale. At high frequencies, experimental decay is not well fitted, this is attributed to experimental reasons.

Table 4.2

Apparent lifetime, and α exponent for P3HT/fullerene blends are displayed. Errors were calculated considering 90% as confidence interval and fitting is performed excluding intensity the three last frequency for each blends. Since we used an angular frequency to carry out the fit, τ is expressed in ms/rad.

Blends	α	τ(ms/rad)
P3HT/PC60PhOMe	0.62 ± 0.07	9.11 ± 3.3
P3HT/C60H12	0.61 ± 0.06	12.50 ± 3.00
P3HT/C60MM12	0.62 ± 0.11	7.41 ± 1.92
P3HT/C60Ph2,1-4	0.63 ± 0.06	10.30 ± 3.32
P3HT/$PC_{61}BM$	0.61 ± 0.09	7.86 ± 3.84

Apparent lifetimes found for P3HT/fullerene blends are in the range of ten of milliseconds (from about 7.5 ms to 12.5 ms). Considering the experimental and the fitting error, calculated as 90% of confidence interval, we can conclude that generally blends with different fullerene derivatives and the same polymer (P3HT) keep, globally, almost the same energy profile for the traps. The apparent lifetimes should be take into account to have a general look to the rate of recombination process. The steady state concentration of radicals that gives LEPR and LMEPR signals, is proportional to the number of polarons generated less number of polarons recombining per unit time. Efficiency of recombination is inversely proportional to the apparent lifetime that is if charges are trapped in low energy localized states LEPR

signals should be greater. This is generally true if efficiency of polarons formation and migration rate are similar and does not interfere much with global kinetic.

The reasons why at high frequencies the intensity decreases faster than the fitted curve arise from a too high instrumental cut off constant. Anyway it should be kept in mind that Cole-Cole model does not take into account a distribution of lifetimes but only the deviation from a single-exponential decay from some localized state. Intensity at high frequency is slowly varying with respect to low frequency region so their contribution to the goodness of fittings is negligible.

$PC_{61}BM$ with different polymers

In this section we focus on polymers/$PC_{61}BM$ solid blends. We used the same methodology of P3HT/fullerene derivatives for data analysis, for further information see previous section. LEPR spectra were performed for all samples and simulations were performed considering two not interacting S=1/2 spin systems. The high field signal is attributed to negative polaron while at low field is attributed to positive polaron. All samples showed a weak signal before illumination due to polymer species already in charged state. In figure 4.10 experimental LEPR spectra and simulations are shown while Table 4.3 shows the results of simulations. LMEPR spectra were performed, and decrease of intensity is observed as modulation frequency increases. Intensity was taken as maximum less minimum value of EPR spectrum and follows the same trend as double integrated simulated spectra intensity. Simulation of LMEPR spectra were performed changing the relative weight of the two polarons contribution. Debye and Cole-Cole fitting was performed for intensity decrease of all samples. As the previous case Cole-Cole models appears to suit well to the data.

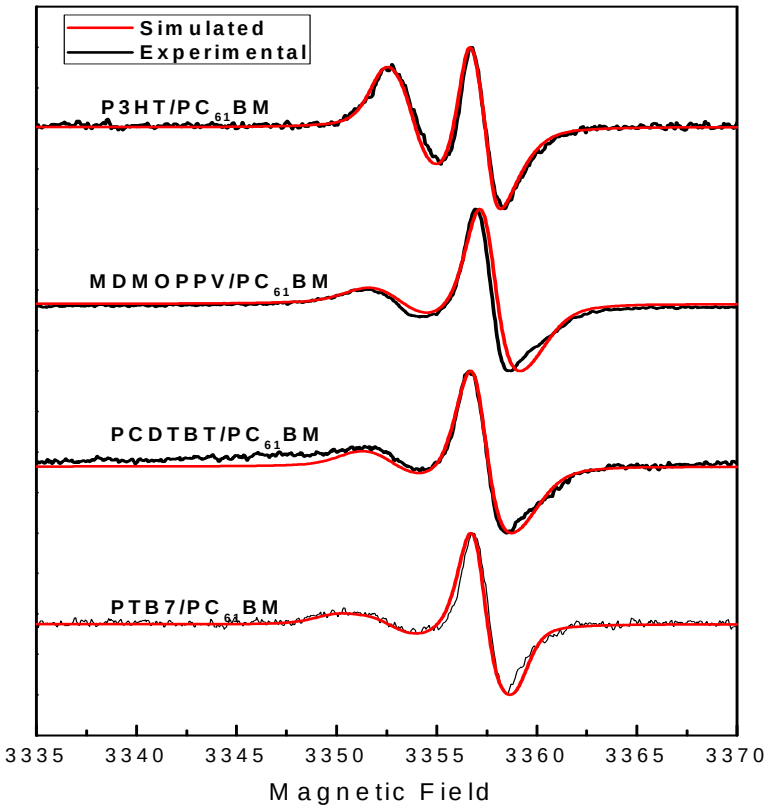

Figure 4.10 LEPR experimental spectra (black line) and simulations (red line) of polymer/$PC_{61}BM$. Simulations were carried out considering a weighted sum of two non-interacting S=1/2 species.

Table 4.3

g tensor principal values of polymer/$PC_{61}BM$ samples. Simulations were carried out considering a weighted sum of two non-interacting S=1/2 species. Error on g factors is evaluated as ± 0.0002.

Blends	g1	g2	g3
P3HT/$PC_{61}BM$	2.0031/2.0003	2.0021/1.9996	2.0009/1.9992
MDMOPPV/ $PC_{61}BM$	2.0035/2.0003	2.0025/1.9996	2.0015/1.9992
PCDTBT/ $PC_{61}BM$	2.0035/2.0003	2.0025/1.9996	2.0013/1.9992
PTB7/ $PC_{61}BM$	2.0045/2.0003	2.0021/1.9996	2.0018/1.9992

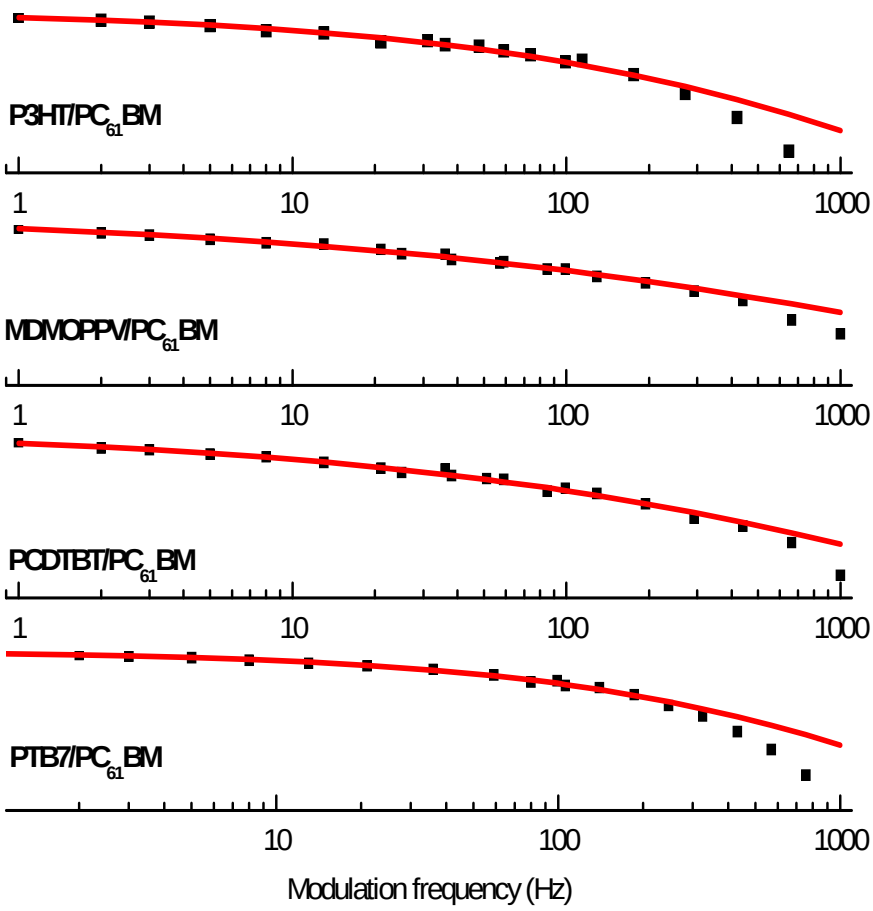

Figure 4.11 Fitting (red line) of polymer/$PC_{61}BM$ blends using modulus of Cole-Cole model . Normalized intensity and frequency of modulation are plotted in double logarithmic scale. At high frequencies, experimental decay is not well fitted, this is attributed to experimental reasons.

The kinetic process are analogous to those describe for P3HT/fullerene derivatives samples and represent the dynamics of signal decrease due to complex decay that cannot be described by a single exponential. Cole-Cole takes into account of this deviation by exponent α. figure 4.11 shows the fitting and Table 4.4 summarizes the results of Cole-Cole fitting.

Table 4.4

Apparent lifetime, and α exponent for P3HT/fullerene blends are displayed. Errors were calculated considering 90% as confidence interval and fitting is performed excluding intensity the three last frequency for each blends. Since we used an angular frequency to carry out the fit, τ is expressed in ms/rad.

Blends	α	τ(ms/rad)
P3HT/ $PC_{61}BM$	0.61 ± 0.09	7.86 ± 3.84
MDMOPPV/ $PC_{61}BM$	0.60 ± 0.06	31.51 ± 2.11
PCDTBT/ $PC_{61}BM$	0.53 ± 0.07	15.00 ± 3.12
PTB7/$PC_{61}BM$	0.75 ± 0.09	8.13 ± 2.01

while for the polymers/$PC_{61}BM$ blends we found a wider range of lifetimes going from about 8 ms to 30 ms while the change of polymer, brings a deeper modification of the traps energy distribution. Even if a clear correlation between morphology studies (AFM, STM, SEM etc.) and energy of traps is not straightforward, we can conclude that probably the polymer counterpart influences deeply the morphology of film and is responsible for the great difference of apparent lifetimes for the second set of blends. This is in good agreement with the fact that polymer, thanks to the long chains, is able to generate good solid films under evaporation bulk or by spin-coating while fullerene molecules can't give a good film alone.

4.3 WAVELENGTH DEPENDENCE OF EPR SIGNAL IN PHOTOVOLTAIC BLENDS.

4.3.1 Introduction

Polymer and fullerene based solar cells, as widely outlined in the previous sections, are able to generate electric current under continuous white light illumination. The photo-physics of this kind of materials, which is written in detail in the main introduction, deals with direct excitation of an electron to the conductive band by light absorption, generation of a mobile singlet exciton and eventually electron transfer at the interface with the fullerene phase. Low-band gap polymers are able to collect a great number of photon since all wavelengths composing white light, have enough energy to excite an electron to the conduction band. Work of Stoichko et al (42) shows that the wavelength dependence is particularly evident when polymer is irradiated below and above the mobility edge. In their model, as shown in figure 4.12, they consider hot excitons formation when photon energy is above the mobility edge. The term "hot" refers to excited electronic or vibrational state. Excess energy is transferred to CT states when electron transfer takes place and hot CT states are generated. The same amount of energy retained is responsible for a more efficient CT dissociation thanks to greater probability for Coulombic interaction in CT to be overcome.

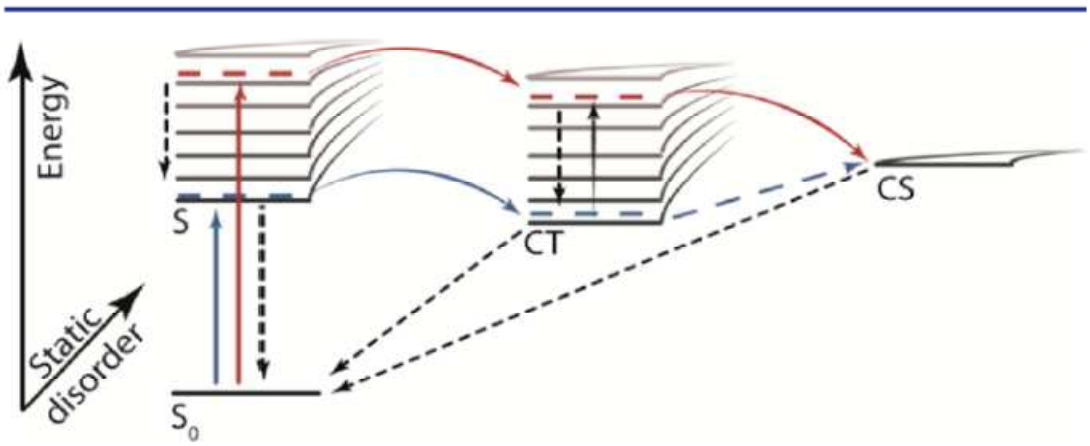

Figure 4.12 Figure, taken from (42), shows the hot exciton states populated by above band edge photon absorption. Hot and relaxed CT state are generated and rate of dissociation in separated charges (CS) is dependent on the energy of CT initial state.

When above mobility edge photons are absorbed, relaxed CT states with insufficient excess of energy are formed, decreasing the charge dissociation efficiency and increasing recombination. This mechanism is also supported by Bakulin et al (68) where hot CT states were considered to have a high level of delocalization. On the other hand Lee et al (69) outlines that hot CT states are not responsible for efficient charge separation but the directly population of CT state by appropriate wavelength usually in infrared region. Here we proposed EPR spectra detection by changing the wavelength of excitation on various photovoltaic polymer/fullerene blends. We assume valid the model in Stoichko's work (42) and due to low absorption coefficient in infrared spectrum we consider negligible the effect of direct population of CT state.
Spectra were weighted by number of incident photons and intensity was thus calculated as difference of maximum and minimum values and by double integration of simulated spectra. Finally we found that EPR intensity doesn't follow the absorption spectra of samples proving that the photo-physical picture of these blends is more complex. It should be keep in mind that, as underlined in previous chapter by LMEPR measurements, polymer and fullerene solid blends are very disordered materials which implies a great variety of defects along the film surface. Consequently it's not surprising that photo-physics behavior can deviate from the more classical models of conductivity of inorganic semiconductors.

4.3.2 Experimental

In order to study the different role of polymer and fullerene, we studied two sets of samples. the first set considers P3HT blended with different fullerene: PC60PhOMe, C_{60}MM12, $PC_{61}BM$, C_{60}H12, C_{60}Ph2,1-4 the second set $PC_{61}BM$ blended with different polymers: P3HT,MDMOPPV,PCDTBT,PTB7. Solution of polymer:fullerene=1:1 weight ratio blends were prepared in chlorobenzene (CB) at open air. Films were prepared by slowly pumping the solutions directly in 3x4 mm EPR quartz tubes till complete evaporation of solvent. XBand-LEPR (Lightinduced EPR) experiments were performed at 130 K using a microwave cavity (Bruker ER200D). Monochromatic light was

generated by OMNI 150 Lot-Oriel from 100 mW white light illumination. For power detection we use a power meter Thor Labs PM 100D. In Figure 4.13 the recorded emission spectra of the lamp and the responsivity function of power meter are plotted as a function of wavelength. Generally monochromatic light power on the range of units of mW was measured.

For taking into account that the monochromator selects a 5 nm range of the incoming

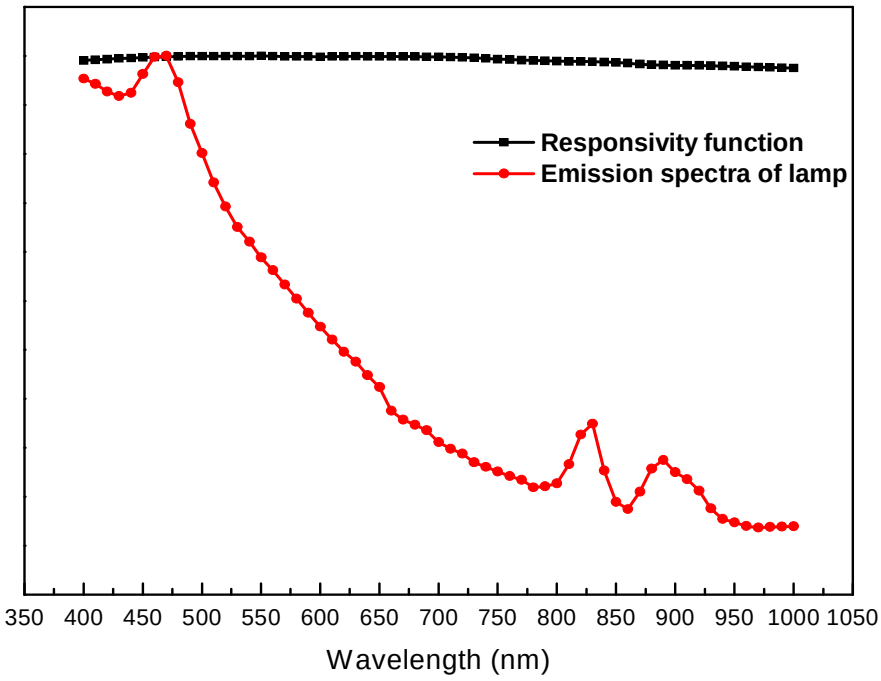

Figure 4.13 Responsivity function of power meter (black scattered line) and emission spectrum (red scattered line) . Both functions were normalized at the maximum of intensity.

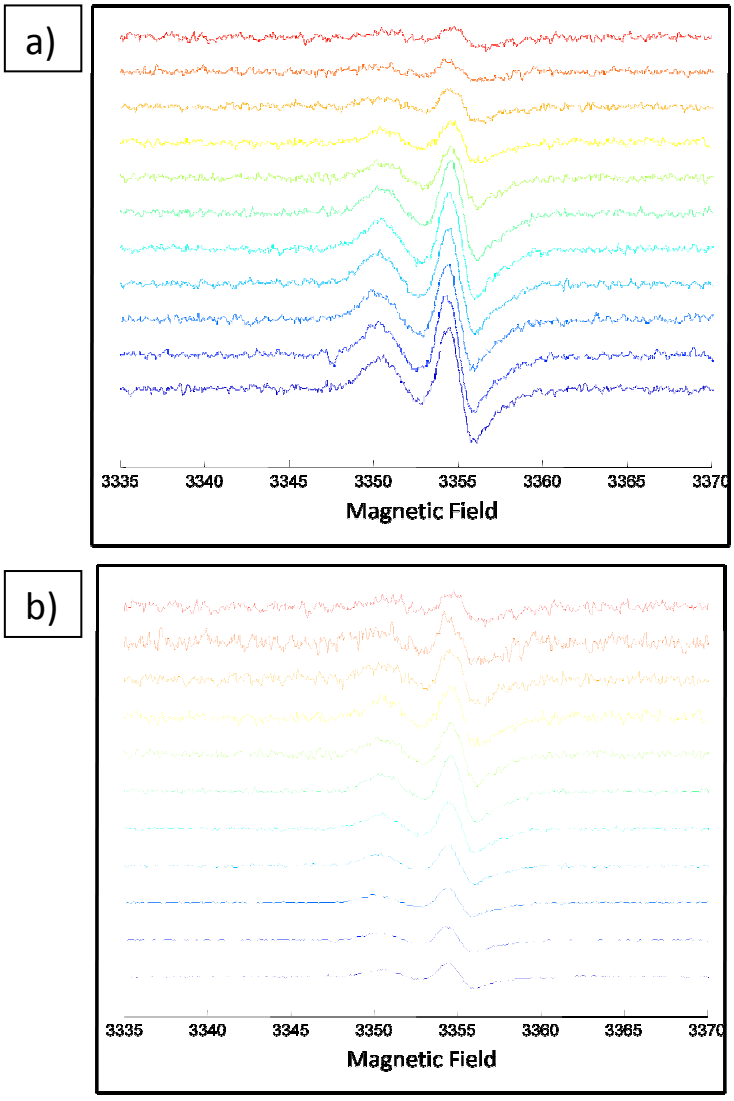

Figure 4.14 Experimental spectra (a) and weighted spectra (b) by number of incident photons of P3HT/Pc_{61}BM film. Spectra are recorded from 400nm (blue line) to 900nm (red line). EPR intensity changes at each wavelength.

beam instead of a perfectly monochromatic light, the number of incident photons for unit time and for each wavelength was calculated by the numerical integration of the emission curve on the wavelength:

$$n = \int_{\lambda_1}^{\lambda_2} \frac{P(\lambda) \cdot \lambda}{hc} d\lambda \qquad (4.7)$$

EPR spectra intensity were thus weighted for n. In figure 4.14 set of experimental and weighted by *n* spectra for P3HT/PC_{61}BM are shown as examples. We will refer to experimental spectra as raw data and to weighted as spectra divided by number of photons.

4.3.3 Results and Discussion

P3HT with different fullerene derivatives blends

LEPR spectra of all samples show two signals due to negative and positive polarons. Since samples are the same studied with Light Modulated EPR, we will follow the same analysis of spectra performed in previous chapter. In figure 4.15 experimental LEPR spectra and simulations are shown. Simulation were carried out by using a Matlab home-made program for fitting/simulation of isotropic solid state radicals EPR spectra. Fullerenes derivatives have different line positions stating differences g factors.

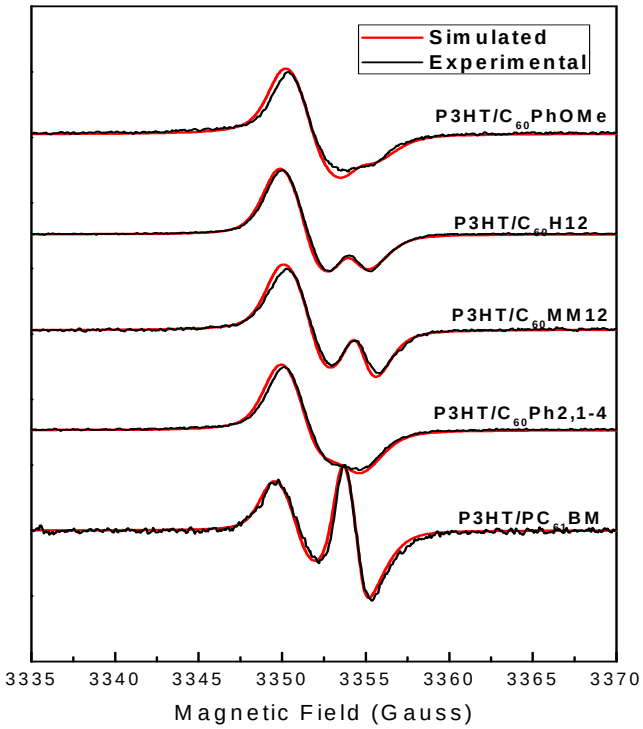

Figure 4.15 LEPR experimental spectra (black line) and simulations (red line) of P3HT/fullerene derivatives. Simulations were carried out considering a weighted sum of two non-interacting S=1/2 species.

Table 4.5

g tensor principal values of P3HT/fullerene derivatives samples. Simulations were carried out considering a weighted sum of two non-interacting S=1/2 species. Error on g factors is evaluated as ± 0.0002.

Blends	g1	g2	g3
P3HT/PC60PhOMe	2.0031/2.0030	2.0021/2.0001	2.0009/2.000
P3HT/C60H12	2.0031/2.0004	2.0021/2.0003	2.0009/2.0003
P3HT/C60MM12	2.0031/2.0003	2.0021/2.0002	2.0009/2.0001
P3HT/C60Ph2,1-4	2.0031/2.0008	2.0021/2.0004	2.0009/2.0004
P3HT/$PC_{61}BM$	2.0031/2.0003	2.0021/1.9996	2.0009/1.9992

Anyway the various substituents modify only slightly the C_{60} wavefunction and this results in a little differences in g factors principal values that can be appreciated. The EPR lines of the two species are not well resolved thus the attribution of g principal values in simulation have a certain degree of arbitrariness. Table 4.1 shows the results of simulations for P3HT:fullerene derivatives samples. Weighted spectra were calculated taking into account the number of incident photons at each wavelength by using (4.7). Intensity of spectra is observed to change as wavelength varies (figure 4.14). Intensity of weighted spectra were calculated by double integration of simulated ones and show the same trend of maximum less minimum gap. In Figure 4.16 P3HT/$PC_{61}BM$ weighted EPR spectra intensity it's shown as a function of wavelength. figure 5.6 displays normalized intensity of EPR spectra taken as subtraction between maximum and minimum. Intensity is shown before and after taking into account of number of incident photons. The emission of the lamp, as shown in figure 4.16 has not

the same intensity for all the wavelengths, thus intensity of EPR spectra changes its trend when number of incident photons is taken into account.

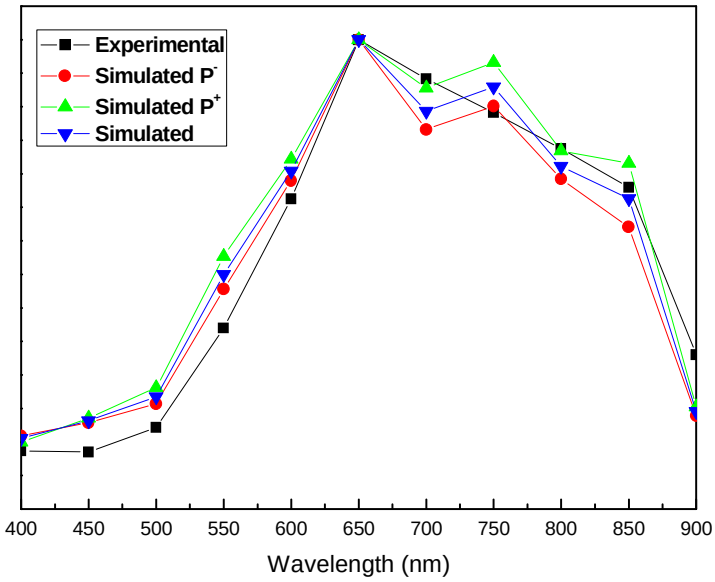

Figure 4.16 Weighted EPR spectra intensity of P3HT/$Pc_{61}BM$ samples are shown as max - min subtraction and double integrated spectra. Simulations allows to determinate the contributions of single polarons that globally follow the same trend. Decays are shown in double logarithmic scale.

Polymeric counterpart is the main responsible for light harvesting when blend is put under a light source. Following Stoichko's work (42) we should expect that at high wavelength photons absorption, hot CT state are populate by hot excitons dissociation and a greater number of separated charges (non-interacting radicals) is formed. This anyway must be weighted for the absorption curve of polymer in order to taking into account the number of photons absorbed. Generally we expect the number of non-interacting radical to be maximum at maximum of absorption and EPR intensity to follow exactly absorption curve profile. When weighted intensity are compared with the absorption curve of blends (figure 4.18), it's possible to see that intensity profile does not follow this is not generally and an almost regular 100 nm shift of maximum is observed. When we excite at wavelengths inside the absorption band, we are

populating hot CT states with higher degree of delocalization, mobility and dissociations efficiency .

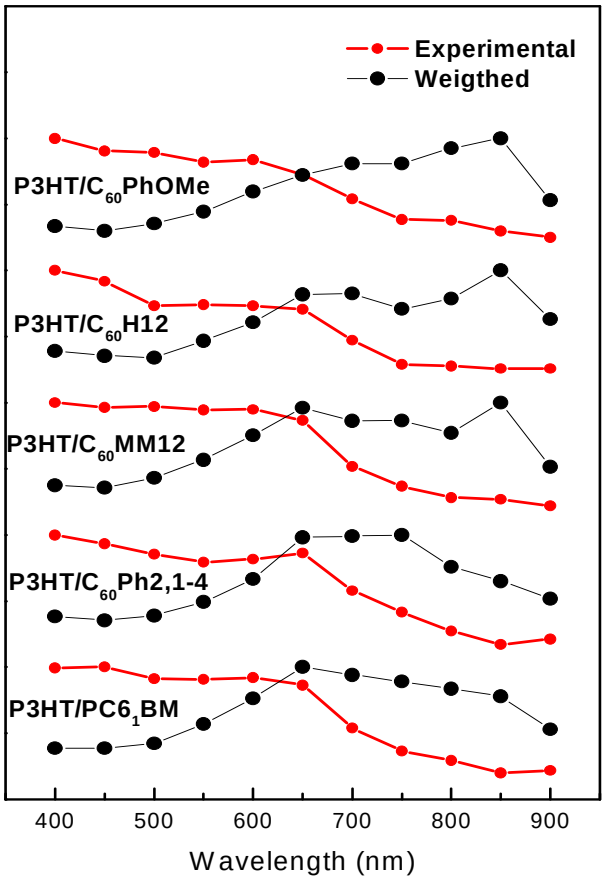

Figure 4.17 Weighted and normalized (black scattered line) and experimental (red scattered line) EPR intensity of P3HT/fullerene derivatives samples. Intensity changes its profile as number of incident photons is taken into account.

Polarons, generated by hot CT states dissociation, will occupy high energy states with high degree of delocalization and mobility, thus they can recombine easily, making their steady state concentration low and EPR is not sensible enough to detect them. For wavelengths much greater than 500 nm, we are populating relaxed CT state with

low level of dissociation, anyway polarons arising from their dissociation will occupy low energy state and their lifetimes range is much more detectable by EPR.

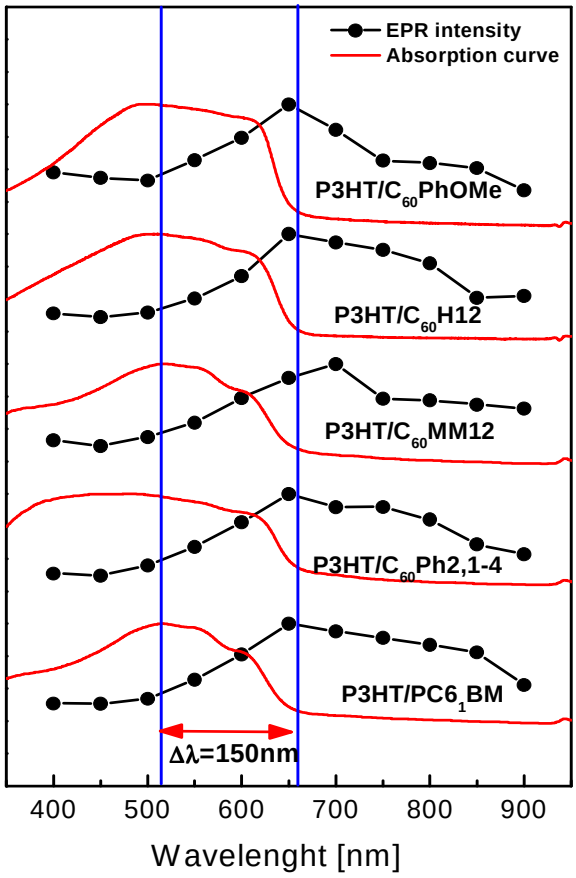

Figure 4.18 Weighted, normalized (black scattered line) EPR intensity and absorption curve. The profile of absorption does not follow the EPR intensity.

In (63) it's considered the possibility of bipolarons formation when the maximum of polymer absorption is excited. Bipolarons are spinless species that generate from collision of mobile positive polarons toward a singlet state. Anyway this mechanism assumes generation of a large number of charge carriers in the mobility edge and this

cannot be generally true considering the low intensity of monochromatic beam used (units of mWatt). Trend of intensity has a maximum at about 650 nm for P3HT/PC60PhOMe, P3HT/$PC_{61}BM$, P3HT/C60H12, P3HT/C60Ph2,1-4 blends while for P3HT/C60MM12 maximum is observed at 700 nm. We can conclude that fullerene does not affect greatly the photo-physic of charge generation for all kind of mechanisms outlined above. This is not surprising since polymer acts the role of absorbitive part. Anyway it seems that, at greater wavelengths, the populated localized state are mostly given by polymer states and the presence of fullerene states does not influence photo-mechanisms. It's possible to find a correlation with LMEPR measurements displayed in the previous chapter. LMEPR is a technique able to detect an apparent lifetime for solid blend denoting a general trend of the distribution of localized states lifetimes. Table 4.2 displays that apparent lifetime constants go from about 8 ms to 12 ms but taking into account the experimental error they can be considered to differ only slightly. If we associate a distribution function to apparent lifetime, we expect blends to have a similar number of localized states inside mobility gap. The latter are responsible for maximum EPR intensity in figure 4.17 because, by irradiating at about 650 nm, we are directly generating them by relaxed CT states dissociation. Moreover we can conclude that polymer is the main responsible for localized state generation inside the band gap of the solid blends, and this explains why for a similar apparent lifetime we have similar trend in the EPR intensity.

4.3.2 $PC_{61}BM$ with different polymers

Wavelength-dependent EPR measurements were carried out for of polymer/ $PC_{61}BM$ derivatives: we adopted the same methodology and consideration in data analysis as previous section. LEPR spectra and simulations were performed considering two not interacting S=1/2 spin systems. The assignment of spectral features to polaronic species is characterized by a low field polymeric signal and the high field fullerenic signal. In Figure 4.19 experimental LEPR spectra and simulations are shown while Table 4.6 shows the results of simulations.

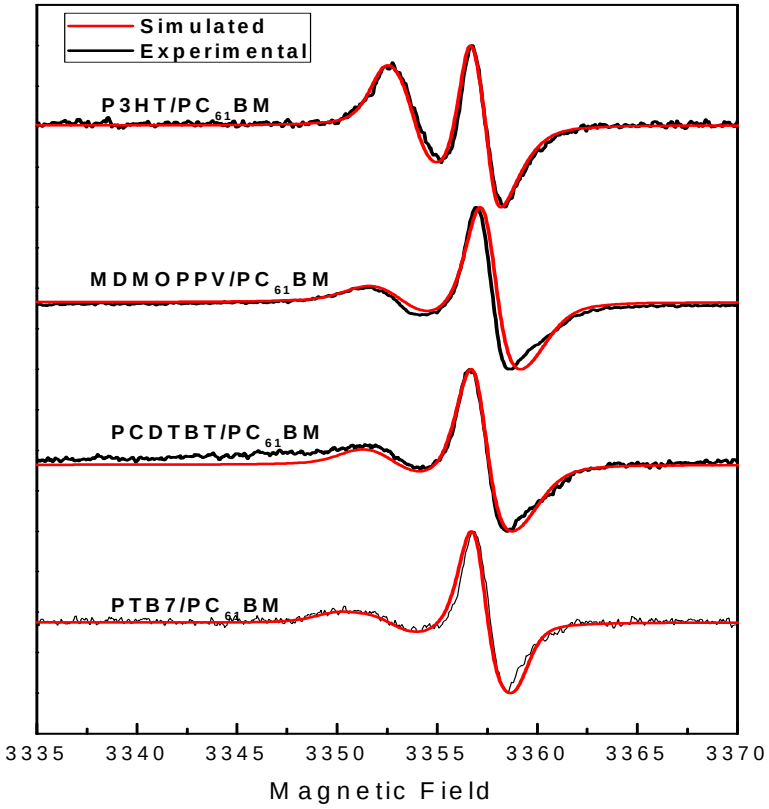

Figure 4.19 LEPR experimental spectra (black line) and simulations (red line) of polymer/$PC_{61}BM$. Simulations were carried out considering a weighted sum of two non-interacting S=1/2 species.

Table 4.6

g tensor principal values of polymer/$PC_{61}BM$ samples. Simulations were carried out considering a weighted sum of two non-interacting S=1/2 species. Error on g factors is evaluated as ± 0.0002.

Blends	g1	g2	g3
P3HT/$PC_{61}BM$	2.0031/2.0003	2.0021/1.9996	2.0009/1.9992
MDMOPPV/ $PC_{61}BM$	2.0035/2.0003	2.0025/1.9996	2.0015/1.9992
PCDTBT/ $PC_{61}BM$	2.0035/2.0003	2.0025/1.9996	2.0013/1.9992
PTB7/ $PC_{61}BM$	2.0045/2.0003	2.0026/1.9996	2.0018/1.9992

LEPR spectra were recorded for polymer/$PC_{61}BM$ samples changing wavelength of excitation. Intensities show a change in their profiles when weighted for number of incident photons. Comparison of experimental and weighted intensity is displayed in figure 4.20. We invoke the same considerations of previous section relative to P3HT/fullerene derivatives samples. When absorption curves is compared to the weighted EPR intensities and it's possible to see that the differences between maximum absorption signal and EPR one vary a lot changing the polymer. Intensities profile of samples were compared to the absorption curves (figure 4.21) We found that EPR intensity does not follow the profile of absorption curve and shifts in maximum position vary more markedly. For MDMOPPV/$PC_{61}BM$ we found $\Delta\lambda \cong 250$ nm shift, for PCDTBT/$PC_{61}BM$ $\Delta\lambda \cong 200$ nm and for P3HT/$PC_{61}BM$ $\Delta\lambda \cong 150$ nm for PTB7/$PC_{61}BM$ $\Delta\lambda \cong 100$. The EPR intensity profiles have a wider change for the three blends from the absorption curves. The reasons underneath the shift are considered analogous as for P3HT with different fullerene derivatives blends and can be resumed:

- Enhanced recombination of polarons from hot CT states dissociation

- Long living localized polarons by relaxed CT state dissociation
- Formation of spinless bipolarons species.

Localized state, can have a very long lifetime thus charges contribute way much more to LEPR steady state concentration. It's possible to find an analogous link to LMEPR measurements of apparent lifetime of such blends.

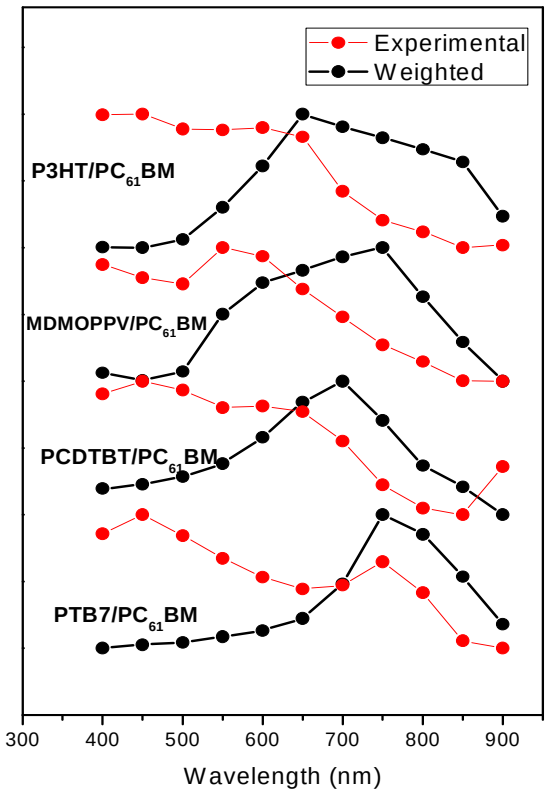

Figure 4.20 Weighted and normalized (black scattered line) and experimental (red scattered line) EPR intensity of polymer/$PC_{61}BM$ samples. Intensity changes its profile as number of incident photons is taken into account.

Looking to Table 4.6 we found that the apparent lifetimes for MDMOPPV/$PC_{61}BM$, P3HT/$PC_{61}BM$ PCDTBT/$PC_{61}BM$ and PTB7/ $PC_{61}BM$ are respectively about 8 ms, 15 ms 31 ms and 8 ms. Blends with longer apparent lifetime have distribution of lifetimes with biggest number of low energy states. Considering dissociation from relaxed CT state, we expect a greater red-shift of maximum EPR intensity as apparent lifetime increases. Finally we can conclude that the mechanism that most of all contributes to shift of maximum is the population of long living localized states by low energy CT states mechanism. Even if it's not possible to get the exact profile distribution function of the localized state in the mobility gap (see section 4.1) we can confirm the LMEPR data and get some new information on the global shape of the distributions. From a photovoltaic point of view it's not necessarily an advantage to have polymers with high energy state. Charge mobility is influenced a lot by the presence of traps on the solid matrix and low living state can be occupied by charges generates at first time and allow the others to diffuse more easily toward the electrodes. All the experiments seen up to now are carried out without electrodes, and this may change things since polarized electrodes generate a static electrical field that induce migration of polarons and can make all the mechanisms of charge motion more difficult and complex.

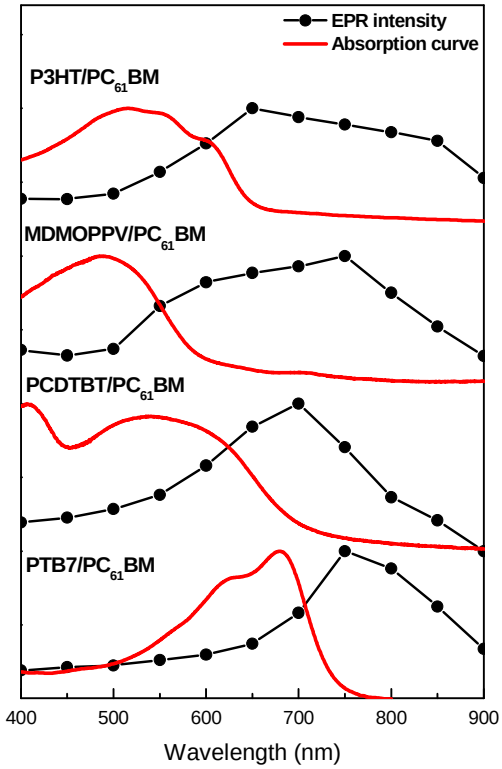

Figure 4.21 Weighted, normalized (black scattered line) EPR intensity and absorption curve. The profile of absorption does not follow the EPR intensity.

4.4 PARTIAL ORIENTATION OF THIN P3HT/PC_{61}BM BLENDS

4.4.1 Introduction

The photo-active layer of Polymer/Fullerene based solar cells is usually prepared by spin-coating from a 20 mg/ml solution of 1:1 weight ratio between the two components. Spin coating deposition method allows the casting of a small amount of solution (50-60 μL) that forms a film of hundreds of nm of thickness. This method has been chosen among the others for its easy application and fast processing of cells. Anyway one can wonder if this kind of deposition, that forces sample to be radially spread over the substrate, influences somehow the degree of order of the polymeric or fullerene phase. Usually, polymer/fullerene active film, are considered extremely disordered materials, anyway there should be a good degree of crystalline phase in order to allow charge diffusion and yet a degree of amorphous phase where electron transfer can take place. In this section we perform LEPR measurements of spin coated P3HT/PC_{61}BM samples and try to find out if any kind of order is imposed to samples. We recorded LEPR data, changing the orientation of surface substrate with respect to the direction of the static magnetic field. Taking advantage of the anisotropy of *g* tensor, we were able to prove that polymer molecules get a partial order along the surface of deposition while the fullerene molecules keep an isotropic phase. We assumed an uniaxial orienting potential and were able to perform simulations at various orientations. We performed TREPR measurements in order to test if the SCRP state was influenced by the polymer orientation that is if the electron transfer was more efficient along some particular directions. In this case we took advantages of anisotropy of dipolar tensor and found that there's no evident preferential direction for electron transfer.

4.4.2 Oriented phase

In order to describe the partial orientation of chain polymer it's possible to use the same model of nematic phase where molecules have a high degree of order. First a certain direction axis, called director, is defined, in the presence case, it is taken to be perpendicular to plane of deposition. We assumed that deposition by spin-coating

causes polymer chain to radially spread over the surface and that very few molecules lies perpendicular to it. Thus the resulting distribution of orientation would depend only by the angle ϑ formed between the direction and the axis of preferential orientation. The latter is considered as the axis lying on the polymer chains. The distribution function is then defined as $p(\vartheta)$ so that the probability to find a chain with ϑ within $\vartheta_1$and ϑ_2 is:

$$P = \int_{\vartheta_1}^{\vartheta_2} \int_0^{2\pi} p(\vartheta) sin\vartheta d\vartheta d\varphi \tag{4.8}$$

where the normalization condition holds

$$\int_0^{\pi} \int_0^{2\pi} p(\vartheta) sin\vartheta d\vartheta d\varphi = 1 \tag{4.9}$$

it's possible to define an order parameter S as the average of the second Legendre polynomial $P_2(cos\vartheta)$:

$$S = \langle P_2(cos\vartheta) \rangle = \frac{\int_0^{\pi} \int_0^{2\pi} p(\vartheta) \left(\frac{3}{2} cos^2\vartheta - \frac{1}{2}\right) sin\vartheta d\vartheta d\varphi}{\int_0^{\pi} \int_0^{2\pi} p(\vartheta) sin\vartheta d\vartheta d\varphi} \tag{4.10}$$

When no order is present, the function $p(\vartheta)$ is constant for all values of ϑ, it can be taken off the integral and the order parameter S would be zero. In case of total alignment with director S is equal to unit. The distribution function can be expressed as a function of an orienting potential $U(\vartheta) = k_B T \cdot u(\vartheta)$, in the form:

$$p(\vartheta) = \frac{1}{Z} e^{-u(\vartheta)} \tag{4.11}$$

Where Z is the partition function. $u(\vartheta)$ can be expressed using Legendre Polynomial:

$$u(\vartheta) = \sum_{L=1}^{n} P_L\,(cos\vartheta) \tag{4.12}$$

where the sum is restricted only to even polynomials. The simplest model for potential considers only the second contribution of (4.12). We can finally write the orienting potential and the distribution function as:

$$U(\vartheta) = k_B T \cdot u(\vartheta) = -\frac{\varepsilon_{2,0}}{2}(1 - 3cos^2\vartheta) \tag{4.13}$$

$$p(\vartheta) = \frac{1}{Z} e^{-\frac{\varepsilon_{2,0}}{2}(1-3cos^2\vartheta)} \tag{4.14}$$

where $\varepsilon_{2,0}$ is called coefficient potential and has the dimension of an energy. It is related to the degree of order S and generally for $\varepsilon_{2,0} > 0$, and $0 \geq S \geq 1$ and for $\varepsilon_{2,0} < 0$ then $-0.5 \geq S \geq 0$ and for $\varepsilon_{2,0} = 0,\ S = 0$.

4.4.3 Experimental

Samples were prepared starting from a solution of 20 mg/ml of P3HT and $PC_{61}BM$ in (1,2dichlorobenzene) ODCB. (Polyethilentereftaalte) PET was chosen as substrates of deposition. PET is a common material used in processing OPV solar cells and does not interfere with EPR measurements. Films were cast by spin-coating, where drops of solution are put under fast rotation in order to get the film. Solvent evaporates rapidly during deposition and generally this causes the film to have a greater degree of disorder phase with respect to film studied in previous sections. For discussion we will refer to "thin" film for spin coated film.

XBand-LEPR (Lightinduced EPR) experiments were performed at 130 K using a microwave cavity (Bruker ER200D), white light continuous excitation of 100mW power. The TR-EPR signal evoked by the light pulse in the EPR cavity was amplified by a wideband pre-amplifier (bandwidth 20 Hz–6.5 MHz) and recorded by a digital oscilloscope (LeCroy 344LT). No field modulation was used and the TREPR spectra represent true absorption or emission at 130 K with pulsed laser excitation of about 5 mJ for single pulse at 532 nm.

For both experiments spectra were recorded changing the orientation of static magnetic field with respect to the surface of deposition. Orientations chosen are: 0°,45°,90° using a goniometer mounted on the EPR tube

4.4.4 Results and discussion

LEPR measurements

In order to get information on *g* tensor principal values, we first performed LEPR spectra and simulations of P3HT/PC_{61}BM in isotropic film. This is obtained by slowing evaporating a small amount of the same solution used for spin-coating deposition directly inside the EPR tube.

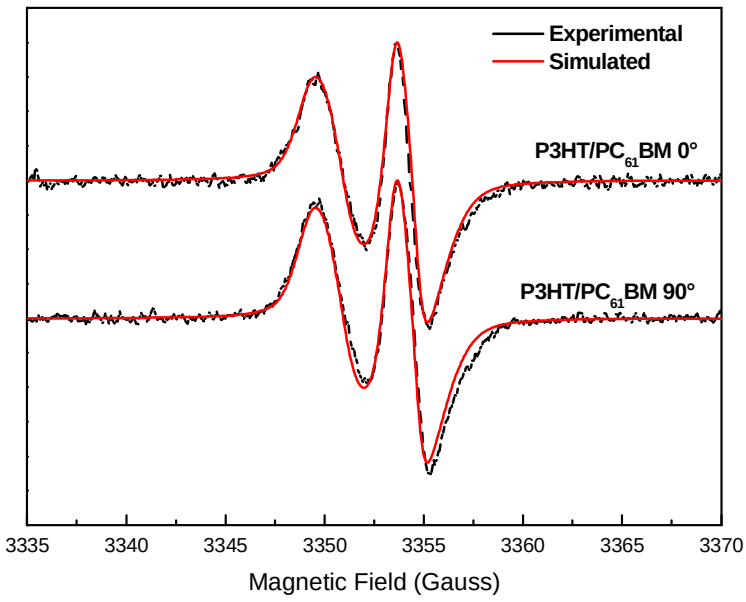

Figure 4.22 Experimental (black line) and simulated (red line) LEPR spectra of bulk P3HT/PC_{61}BM sample. Measurements taken at 0° and 90° with respect to static magnetic field, show that phases are isotropic.

Table 4.7

g-tensors[a] of radical cation P3HT$^{\cdot+}$ and radical anion $PC_{61}BM^{\cdot-}$

	g_1	g_2	g_3
P3HT	2.0029	2.0020	2.0009
$PC_{61}BM$	2.0003	1.9997	1.9994

[a]Error on g factors is evaluated as ± 0.0002.

This method generates film of some micron thickness and this is generally considered a bulk isotropic sample. Figure 4.22 displays the spectrum and simulations. Spectra show the typical positive polaron and negative polaron signals and we can assign the low-field signal to positive polar (polymer radical cation) and the high field one to fullerene radical anion.

Simulations were performed by home-developed program in MatLab language for simulation of solid state S=1/2 radicals in oriented and isotropic phase, considering a sum of two S=1/2 non interacting spin systems. In Table 4.7 parameters of simulation are shown. Isotropic spectra were recorded rotating sample of 0° and 90° with respect to static magnetic field and no substantial difference was found.

LEPR spectra of thin samples at 0°. 45° and 90° orientation with respect to static magnetic field were thus performed and the result is displayed in figure 4.23.

In this case we found a different shape of spectra for the various orientations. Spectra were adjusted for the frequency of microwave: fullerene signals coincided for all orientations while polymer contribution appeared to vary. The overall change of profile spectra is due to different contribution of polymer. Simulations were performed using the same parameters of isotropic spectra and taking into account the preferential orientation of chains polymer by using (4.14). From previous work (43, 70-72)

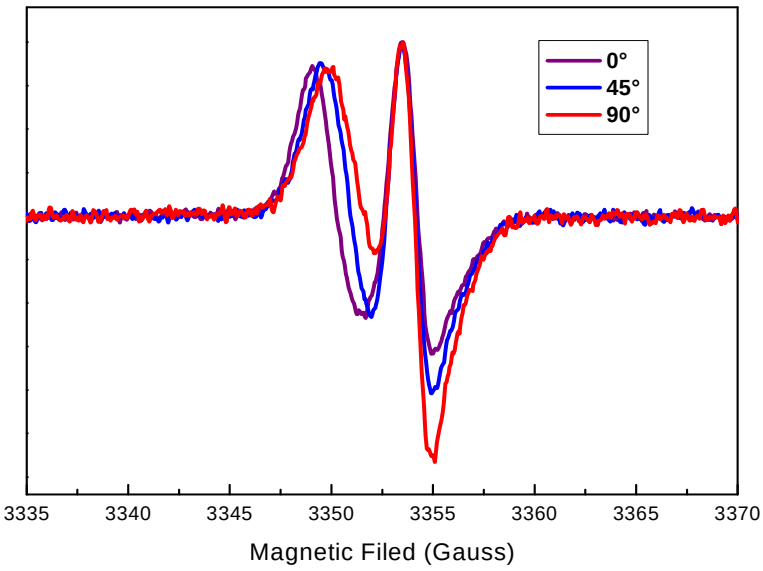

Figure 4.23 Experimental LEPR spectra of spin-coated P3HT/$PC_{61}BM$ sample at 0°,45°,90° of orientations with respect to static magnetic field. Profile of spectra changes as different orientations becomes more relelvant.

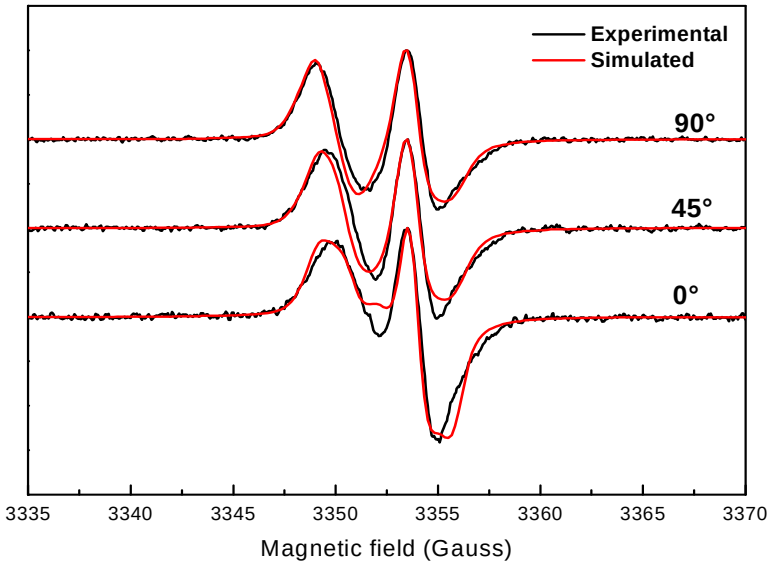

Figure 4.24 Experimental (black line) and Simulated (LEPR) spectra of spin-coated P3HT/$PC_{61}BM$ sample at 0°,45°,90°. Simulations were performed assuming uniaxial orienting potential and a negative coefficient potential $\varepsilon_{2,0}$

the direction associated to the lowest principal value of polymer *g* tensor (g_3=2.0009) was assigned to the inter-chain direction, thus we assumed it as axis of preferential orientation while the director was taken to be perpendicular to surface deposition. The sign of parameter $\varepsilon_{2,0}$ of (4.14) determines two kind of possible distribution functions. If positive, distribution has a maximum at $\vartheta = 0° \text{ and } 180°$ thus molecules are supposed to orient parallel to director, for negative $\varepsilon_{2,0}$ distribution has a maximum at $\vartheta = 90°$ and molecules are mostly perpendicular to director. Thin samples are assumed to have polymer chains radially spread over the substrate so we must consider a negative value of $\varepsilon_{2,0}$. Once chosen the orientational distribution we performed the simulations, shown in figure 4.24. Parameters of simulation are displayed in Table 4.8. It was not possible to determine $\varepsilon_{2,0}$ univocally and -4,-5,-6 values was found to have an slightly effect on spectra simulations. This is mostly due to the partial overlap of the two species when seen at X-Band spectrometer. Even if simulations don't suit perfectly the spectral profile it's possible to find a global trend that confirm the hypothesis of a partial orientation of polymer.

Table 4.8

g-tensors[a] of radical cation P3HT$^{\cdot+}$ and radical anion $PC_{61}BM^{\cdot-}$

Species	g_1	g_2	g_3	$\varepsilon_{2,0}$
P3HT	2.0029	2.0020	2.0009	-4;-5;-6
$PC_{61}BM$	2.0003	1.9997	1.9994	0

[a]Error on g factors is evaluated as ± 0.0002.

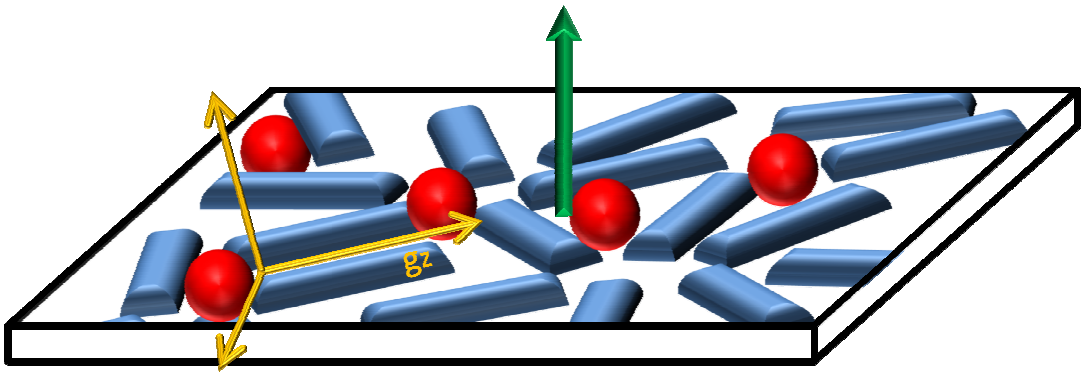

Figure 4.25 representation of thin film order where sticks represent polymer chains and red spheres the fullerene molecules. The green arrow is the director while the g_z axis of *g*-tensor is taken as axis of preferential orientation. Molecules of polymer are mostly spread over the surface of deposition.

By using (4.10) ,order parameter S was calculated in a range from -0.38 to -0.42 . The assumption of an unixial orienting potential is surely one of to be the simplest model that can be use for oriented phase. Anyway there can be more complex distribution function depending on φ angle. Moreover the preferential orientation could be slightly tilted from the surface of deposition figure 4.25 shows a qualitative picture of the order found

TREPR measurements

Time Resolved EPR (TREPR) spectra were thus recorder in order to understand if the degree of order influences the process of electron transfer. If the charge transfer (CT) state is long living (some μs) TREPR technique is able to detect it. The latter is commonly called polaron pairs state or spin correlated radical pair (SCRP) state. As outline in chapter 2, this state is given by two S=1/2 radicals that interact by dipolar and exchange interaction. Generally for dipolar interaction, point dipole approximation is considered and dipolar tensor is taken to be axial. Even if anisotropy of dipolar interaction is smaller than the *g* anisotropy, one must take into account the energy of interaction in order to performed simulation. SCRP is generated from the singlet exciton state of polymer and this causes the four fold sublevels of SCRP to be spin-polarized. The sign of dipolar constant D is usually taken negative and exchange

constant J is optimized by fitting simulation for a singlet precursor population. Figure 4.26 shows the TREPR spectra recorded after 500 ns after laser pulse. The spectra pattern was simulating ad SCRP species with D=5 Gauss and J=1.1 Gauss. The sign of J outlines an antiferromagnetic coupling. From the values of D it's possible to get the distance between the two radicals by using the formula:

$$r^3 = \frac{-\frac{3}{8}\mu_0 \cdot (g\mu_B)^2}{D} \tag{4.15}$$

where g_{iso} is the average of the traces of the two g tensors, μ_B is the Bohr magneton. We found an average distance of about 2nm between polymer and fullerene molecules. In point dipole approximation, the interspin distance is taken as the z direction of dipolar tensor, no orientation dependence was found between this direction and the static magnetic field one.

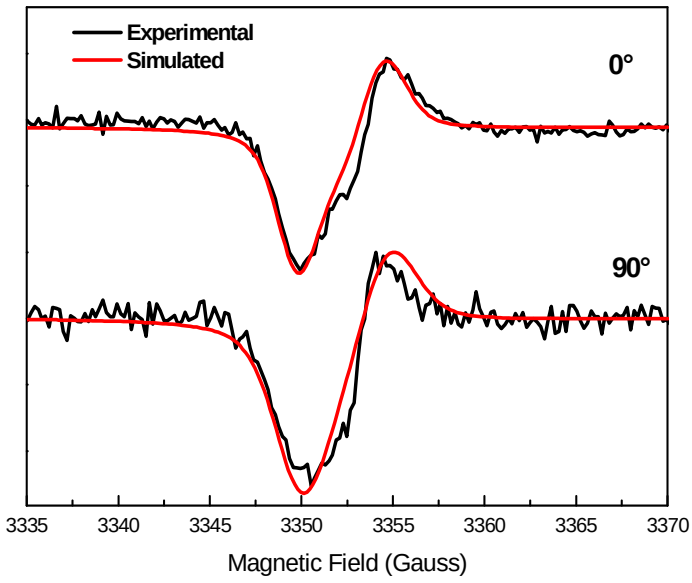

Figure 4.26 Simulated (red line) and Experimental (black line) of SCRP of spin-coated P3HT/$PC_{61}BM$ sample. Simulations were performed considering a dipolar constant D=-5 Gauss and exchange constant J=1.1 Gauss. Singlet precursor is assumed. Spectra were recorded after 500 ns

Table 4.9

SCRP simulation parameters

Blend	D(Gauss)	J(Gauss)	$\varepsilon_{2,0}$
P3HT/$PC_{61}BM$ $_{SCRP}$	-5	1.1	0

Populations of SCRP sublevels from the lowest in energy to highest is taken: 0.006:0.401: 0.470: 0.124

4.5 EFFECT OF DIIODOOCTANE IN PHOTOVOLTAIC PTB7/FULLERENE BLENDS

4.5.1 Introduction

This section focuses its attention on the study of organic photovoltaic blends, based on organic polymer and fullerene derivatives processed with organic additive Diiodooctane (DIO). In the last ten years, significant progresses have been made on increasing efficiency of organic solar cells. Power conversion efficiency (PCE) has been improved from 1% up to about 8% (31), however, the efficiency is sill significantly lower than the inorganic cells. Lately a new kind of low-band gap polymer poly[[4,8-bis[2-ethylhexyl)oxy]benzo[1,2-b:4,5-b']dithiophene-2,6-diyl][3-fluoro-2[(2ethylhexyl) carbonyl][thieno[3,4b]thiophenediyl]] abbreviated as PTB7 (structure is shown in figure 4.21), gained lots of interest thanks to the enhanced efficiency of PTB7-based solar cells, coupled with classical Phenyl-C61/C71-butyric acid methyl ester abbreviated as $PC_{61}BM$ and $PC_{71}BM$ (31, 44, 73-75). Processing PTB7-based blends with organic additive as Diiodiooctane (DIO) manage to improve the PCE up to 7.4%. The role of DIO has been widely discussed in term of enhanced morphology and crystallinity of photoactive films (31, 44, 73-75) stating that DIO helps to create a finer structure of solid blend where polymer and fullerene are more closely interlinked. Anyway a complete work concerning photophysical mechanisms, and a good reason for the increase of efficiency are still missing.

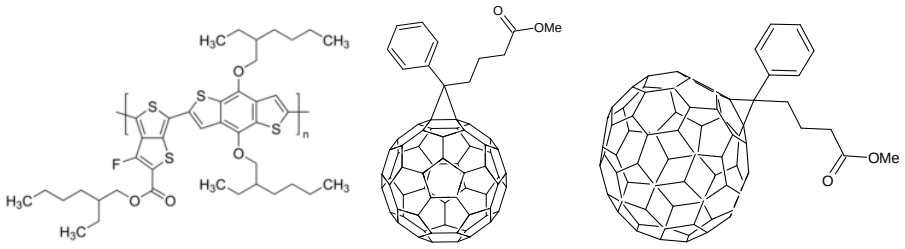

Figure 4.27. Chemical Structure of PTB7, $PC_{61}BM$ and $PC_{71}BM$ used in this section.

Here we proposed an EPR studied based on LEPR and TREPR and Eco Detected light ON EPR (EDlightON). LEPR and TREPR allows to have direct information on photo-physical dynamic, degree of order of samples induced by DIO while with pulsed techniques we focuses on the spin-dynamics and its change when DIO is present as additive

4.5.2 Experimental

Bulk Films

A PTB7:$PC_{61}BM$=1:1.5 and PTB7:$PC_{71}BM$=1:1.5 weight ratio blends were dissolved in chlorobenzene (CB) with 3% of diiodooctane (DIO). All solutions were prepared at open air. Films were prepared by slowly pumping the solutions directly in 3x4 mm EPR quartz tubes for 5 h. Analogous films were prepared without DIO for comparison.

XBand-LEPR (Lightinduced EPR) experiments were performed at 130 K and 80 K using a microwave cavity (Bruker ER200D), white light continuous excitation of 100mW power. The TR-EPR signal evoked by the light pulse in the EPR cavity was amplified by a wideband pre-amplifier (bandwidth 20 Hz–6.5 MHz) and recorded by a digital oscilloscope (LeCroy 344LT). No field modulation was used and the TR-EPR spectra represent true absorption or emission at 130 K with pulsed laser excitation of about 5 mJ for single pulse at 532 nm.

Thin Films

Solution of 15 mg/ml of PTB7 in chlorobenzene (CB) with amount of $PC_{61}BM$ and $PC_{71}BM$ in order to obtain PTB7:$PC_{61}BM$=1:1.5 and PTB7:$PC_{71}BM$=1:1.5 weight ratio, were spin-coated in glow-box[2] on polyethylene terephtalate substrates. Coated films were cut in strings and put in 3x4 quartz EPR tube and then sealed under nitrogen atmosphere.

XBand-LEPR (Lightinduced EPR) experiments were performed at 130 K and 80 K using a microwave cavity (Bruker ER200D), white light continuous excitation of 100mW power.

[2] Special thanks to Dr. Michele De Bastiani for realization of spin-coated samples

The TR-EPR signal evoked by the light pulse in the EPR cavity was amplified by a wideband pre-amplifier (bandwidth 20 Hz–6.5 MHz) and recorded by a digital oscilloscope (LeCroy 344LT). No field modulation was used and the TR-EPR spectra represent true absorption or emission at 130 K with pulsed laser excitation of about 5 mJ for single pulse at 532 nm.

Eco-Detected (ED) Spectra were recorded using 16ns pi/2 pulse and 32 ns pi pulse with 200ns delay between two pulses and ECO detection. For integration of the ECO we set a gate of 300 ns. Measurements were taken at 80K, under continuous white light irradiation in order to get both signal of P^+ and P^-.

T_1 and T_2 measurements were performed under white light continuous white light irradiation. T_1 and T_2 constants were found to differ even for some order of magnitude for various samples, so we set different time-increment dx, generally going from tens nanosecond to ten thousand nanoseconds.

4.5.3 Results and Discussion

Light Induced EPR (LEPR)

LEPR spectra were recorded for bulk PTB7/Fullerene, PTB7/Fullerene/DIO films and thin films PTB7/Fullerene and PTB7/Fullerene/DIO, where Fullerene=$PC_{61}BM$ and $PC_{71}BM$. Thin films measurements were carried out for parallel and perpendicular orientation of plane deposition to magnetic field. Since we didn't notice any differences in LEPR we will show spectra at one orientation.

PTB7/$PC_{61}BM$ and PTB7/$PC_{61}BM$/DIO films show weak EPR signal before irradiation, that can be assigned to stable paramagnetic defects generated during film formation or to species already in a charged state. These species are generally assigned to the polymer and thus are positive charged. Light Induced (LI) spectra of PTB7/$PC_{61}BM$ blend showed a signal at 3353 G and a new signal at 3355 G. Following previous studies (18) the signal at low field can be assigned to positive polaron $PTB7^{\cdot+}$ (P^+) and at high field to negative polaron $PC_{61}BM^{\cdot-}$ (P^-). After switching off the light, signals of both polarons suddenly shut down to dark value at 130 K while at 80 K signals persist

for several minutes due to inhibition of charge recombination process. This is observed for both spin coated and bulk evaporated films. PTB7/$PC_{61}BM$/DIO shows P^- EPR signal quite undetectable for all time of measurement. Only a small amount of negative polarons of bulk sample could be detected (figure 4.28). The great difference for negative polaron signals in the two kind of blends is attributed to DIO. P^- can possibly have a very short lifetime, less than EPR detection time (about 300 ns), so its steady state concentration is too low to be detected. DIO is a non-volatile good solvent for $PC_{61}BM$ and it is still present , trapped in film surface, after evaporation.

Simulations were performed by home-developed program in MatLab language for simulation of solid state S=1/2 radicals in oriented and isotropic phase. The two signals overlap, so it's not possible to assign unequivocally the *g*-factor principal values using and X-Band spectrometer. Using *g*-factors of work (18) it was possible to obtain a good simulation of spectra as linear weighted combination of two independent species confirming that the observed signals are related to species no longer interacting. The ratios between coefficients P^-/P^+, following the same order as figure 4.28 are: 2.1, 0, 2.1, 0.1. Spectrum for thin film PTB7/$PC_{71}BM$/DIO was not simulated for bad signal to noise ratio and the anion contribute is taken to be zero. We didn't observe any relevant change in line-width for both species. PTB7/$PC_{71}BM$ and PTB7/$PC_{71}BM$/DIO blend films show a similar behavior as that of $PC_{61}BM$. Light induces spectra show that Larmor frequency of $PC_{71}BM$, which now is considered P^-, lies lower than $PC_{61}BM$ thus the P^+ and P^- EPR signal are almost overlapped around 3353 Gauss region (Figure 4.29). Although it's harder to get good simulations, the *g* tensor components, listed in Table 4.10, agree with literature values (18). As expected, *g* values are higher than those of $PC_{61}BM$ yet we couldn't find any reasonable change in linewidths. The ratio between coefficients P^-/P^+, follows a similar trend of those shown for $PC_{61}BM$: 2, 0, 1,0. We can conclude that LEPR outlines, on a still qualitative level, the effect of adding DIO during processing of photovoltaic blends.

Table 4.10

g-tensors[a] of radical cation PTB7·$^{+}$ and radical anions $PC_{61}BM\cdot^{-}$ and $PC_{71}BM\cdot^{-}$

Species	g_X	g_Y	g_Z
PTB7	2.00450	2.0029	2.0018
$PC_{61}BM$	2.00026	2.0002	1.9991
$PC_{71}BM$	2.00310	2.0018	2.0018

[a]Error on g factors is evaluated as ± 0.0002.

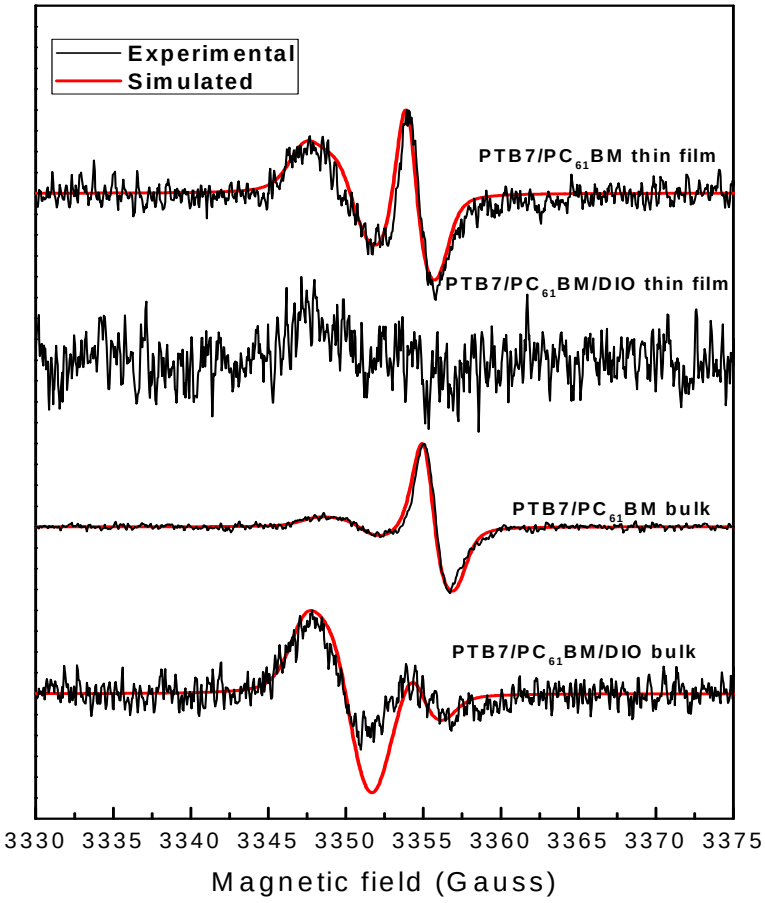

Figure 4.28 LEPR spectra (black line) and Simulations (red line) of bulk and thin film PTB7/$PCB_{61}BM$ samples. Simulations are considered as independent weigthed sum of two S=1/2 species. DIO causes fullerene signal to shut down.

Anyway it's hard to find a straightforward connection of recorded signals with literature works. As already said, most of them are related to morphologic and crystallographic studies of thin films, photophysical processes have not been deeply studied and only some general models had been proposed.(9, 31, 73, 74, 76).

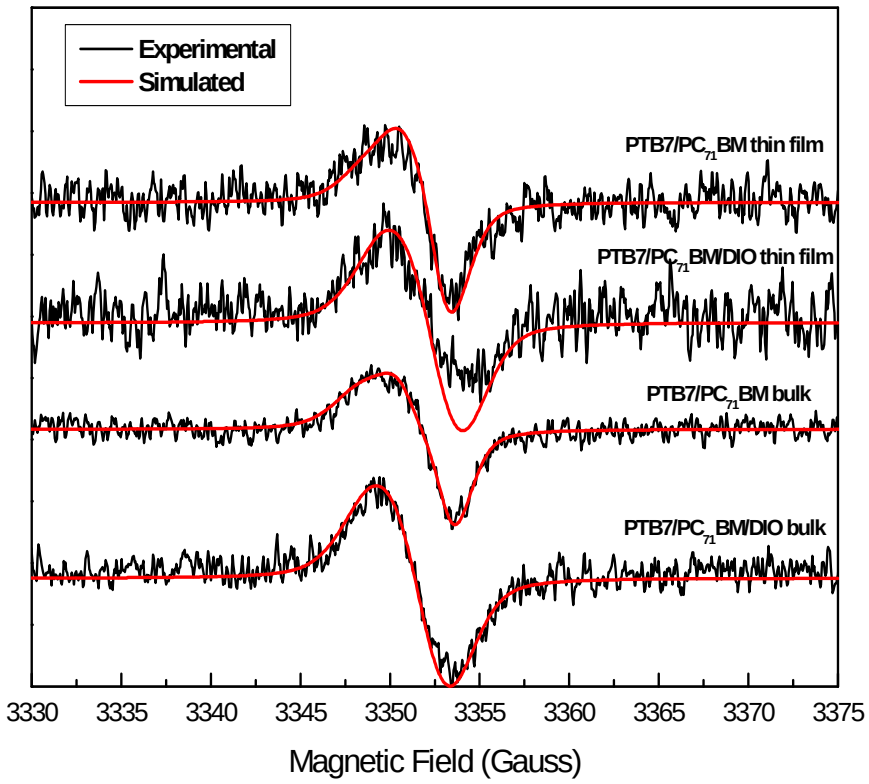

Figure 4.29 LEPR spectra (black line) and Simulations (red line) of bulk and thin film PTB7/$PCB_{71}BM$ samples. Simulations are considered as independent weigthed sum of two S=1/2 species. DIO causes fullerene signal to shut down.

Time Resolved EPR (TREPR)

TREPR spectra were recorded on the samples described above in order to detect transient radical species and triplet states generation. TREPR 50 Gauss sweep spectra, figure 4.30, for PTB7/$PC_{61}BM$ films show an emission signal at 3353 Gauss and an absorption signal at 3355 Gauss that correspond respectively to positive polaron $PTB7^{\cdot +}$ (P^{+}) and negative polaron $PC_{61}BM^{\cdot -}$ (P^{-}) as LEPR measurements outlined. In Figure 4.30 a slice of each TREPR surface is shown after 1000 ns from laser pulse. For thin films we performed experiment orienting the sample surface parallel and perpendicular to magnetic field but no change has been detected.

Simulation of thin PTB7/$PC_{61}BM$ film spectrum is just the weighted sum of two non-interacting S=1/2 polarized species corresponding to P^{-} and P^{+}, as LEPR spectra.

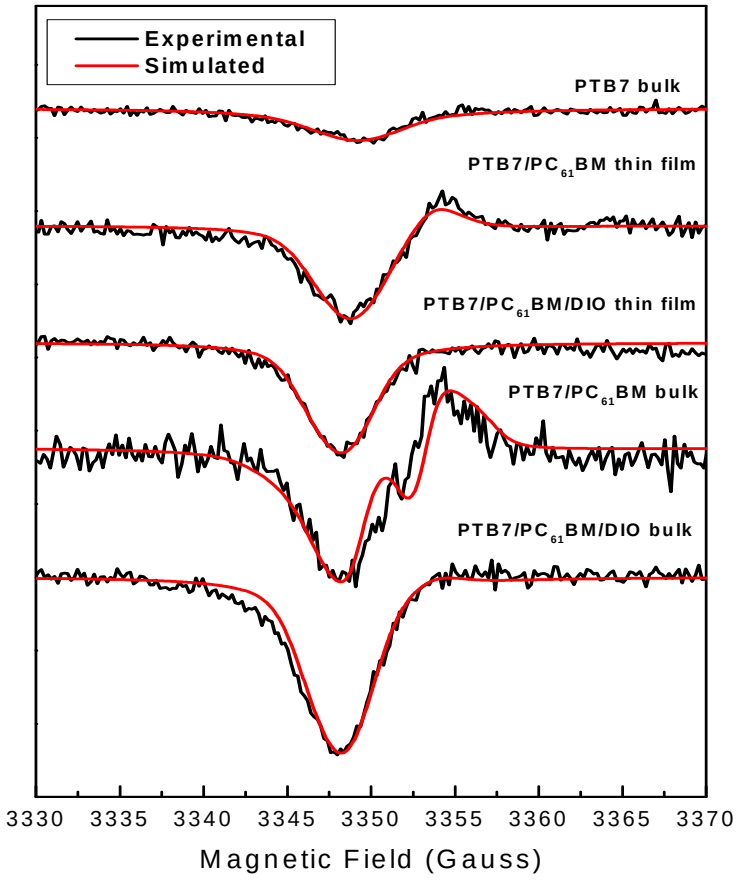

Figure 4.30 TREPR spectra of pristine PTB7 bulk film and PTB7/$PCB_{61}BM$ samples. Simulations were taken as weighted sum of polarized species except for PTB7/$PC_{61}BM$ bulk were SCRP was considered. Spectra are shown in 1000 ns delay after laser pulse.

Bulk evaporated PTB7/$PC_{61}BM$ spectrum shows a little shoulder at 3351 Gauss, which can be quite well simulated summing a SCRP contribution to a stable P^+ generated by self-ionization of polymer, which exhibits an emission at 3350 Gauss signal even if not blended with a fullerene counterpart. Looking at spectra for: 0.3µs , 0.4µs, 1µs delay after laser pulse, an increasing asymmetry of spectral features is observed (figure 4.31). The weight coefficients ratio P^+/SCRP: 0, 0.03, 0.1 show an increasing formation of stable P^+ species during time. Anyway self-ionization of polymer isn't, as expected, a favorite process particularly when a fullerene derivative is present.

The reason why SCRP specie was detected only for bulk evaporated film is still under analysis.

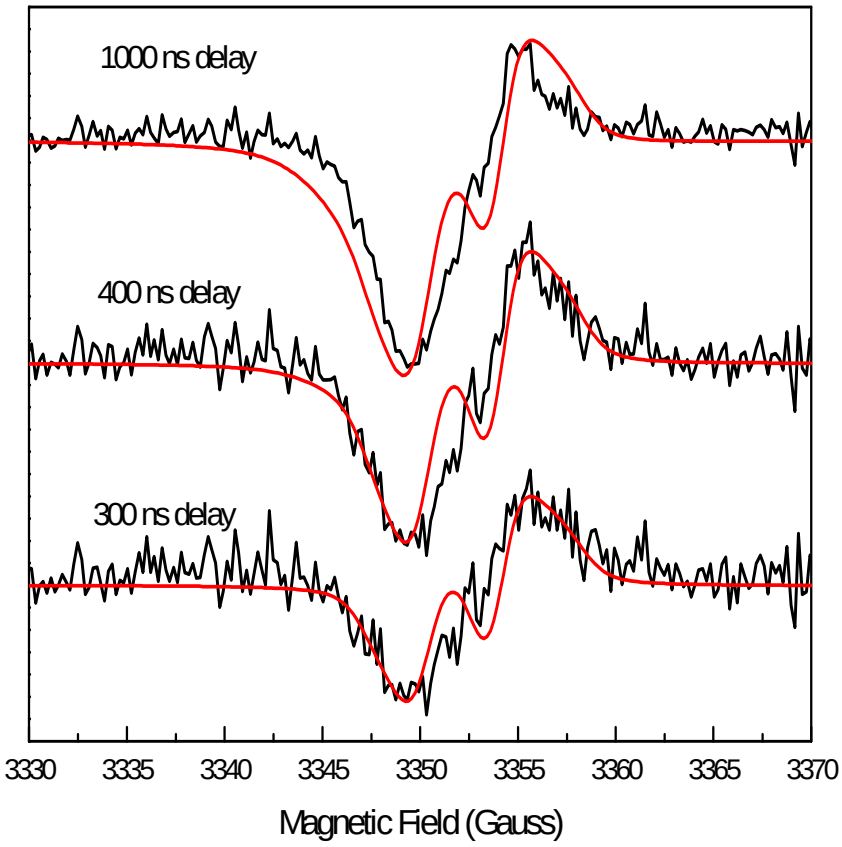

Figure 4.31 TREPR spectra of bulk PTB7/$PC_{61}BM$ taken at different delays after laser pulse. SCPR is observed at 300 ns. As delay time increases, the contribution of the sole polymer cation P^+ causes a progressive asymmetry of spectra.

Anyway these kind of materials have generally a high degree of intrinsic disordered mainly in amorphous regions, which implies some limits to morphology reproducibly. Generally long living SCRPs form, whenever charge mobility and recombination are both inhibited i.e. in amorphous region. PTB7/$PC_{61}BM$/DIO (figure 4.30) spectra show very little high field contribution (P^-). As discussed in LEPR paragraph. From dipolar parameter D (~5 Gauss) it was possible to estimate a distance of about 2nm between the two polarons just after electron transfer. TREPR spectra in polaron region confirm LEPR observation.

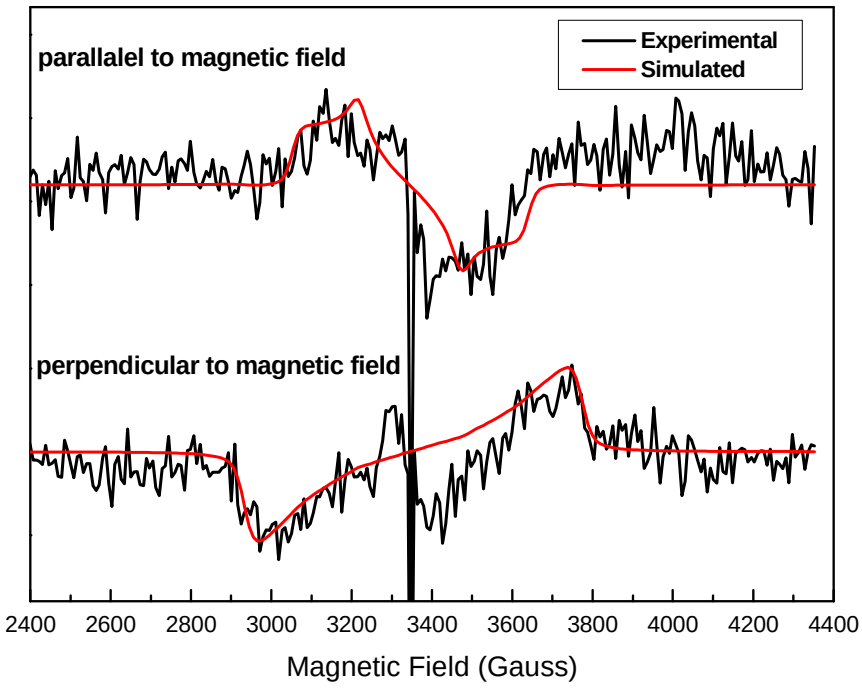

Figure 4.32 TREPR triplet spectra of PTB7 in spin coated PTB7/$PC_{61}BM$/DIO. Simulation outlines that triplets of PTB7 is partially oriented and populated by recombination of SCRP species. The same behavior is observed for all spin-coated samples. Spectra were recorded after 1000 ns after laser pulse.

TREPR 2000 gauss sweep spectra show for all four films a typical pattern of triplet state generated by recombination from polarized SCRP states in the first 1000 ns after laser pulse, (see Jablonski diagram in figure 1.5). Signals invert their polarization for longer time with a maximum at 4000ns. Furthermore thin PTB7/$PC_{61}BM$ and PTB7/$PC_{61}BM$/DIO films show orientation dependent spectral features which outlines a partial orientation of chains of polymer on the surface of deposition. In figures 4.32 and 4.33 we display an example of oriented triplet spectral shape of PTB7 found in thin samples, for parallel and perpendicular direction of magnetic field with respect to plane of deposition.

Simulations of spectra at 1000 ns and 4000ns were carried out, for spin coated films, considering an uniaxial orienting potential (see section 4.4.2): $p(\vartheta) = exp\left(-\varepsilon_{2,0}/2(1-3cos^2\vartheta)\right)$ and taking as axis of preferential orientation the dipolar Z direction of the triplet tensor and a positive orienting parameter $\varepsilon_{2,0}$.

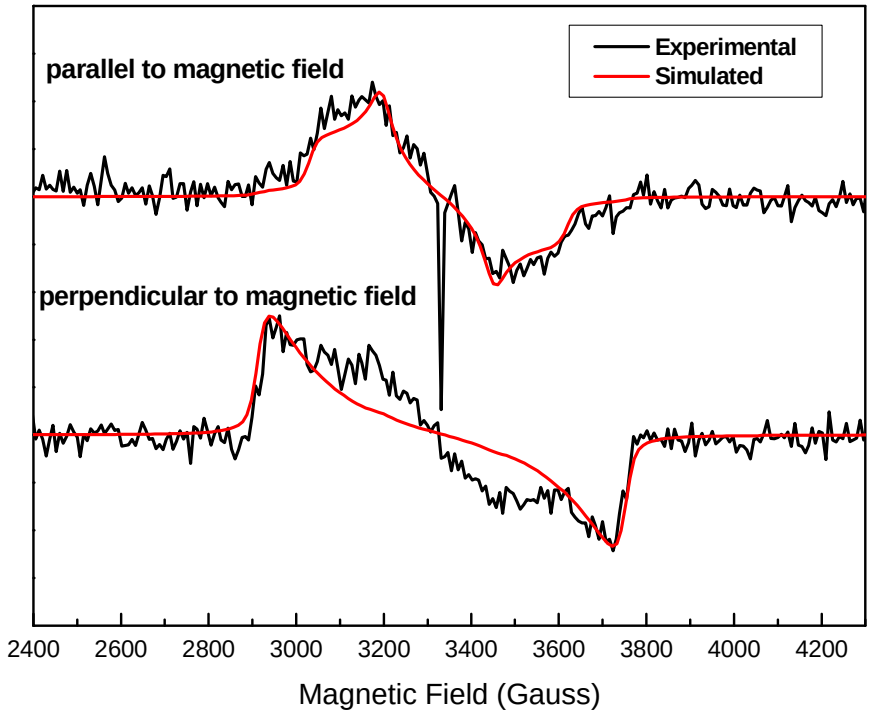

Figure 4.33 TREPR triplet spectra of PTB7 in spin coated PTB7/$PC_{61}BM$/DIO. Simulation outlines that triplets of PTB7 is partially oriented and populated by ISC process. The same behavior is observed for all spin-coated samples. Spectra were recorded after 4000 ns after laser pulse.

For bulk evaporated substrates simulation, no need of orientation dependence is required so isotropic phase was considered (not shown).

For 1000 ns delay spectra, we found a ZFS parameters (Table 4.11) of D=-420 Gauss , E=55 Gauss and fields population of p_1=0.14 p_2=0.72 p_3=0.14 denoting T_0 is the most populated level as expected by a recombination triplet pattern. We simulated 4000 ns delay spectra as ISC triplets (Figure 4.33). This is quite natural considering that decay constants of triplets excited sublevels are determined by the spin-selective ISC process which results in a different variation of T_{+1},T_0,T_{-1} populations with time.

We found the same ZFS parameters and ISC populations: p_x =0.40 p_y= 0.44 p_z=0.16 .

Spin-coating deposition is considered the main responsible of polymer chains orientation.

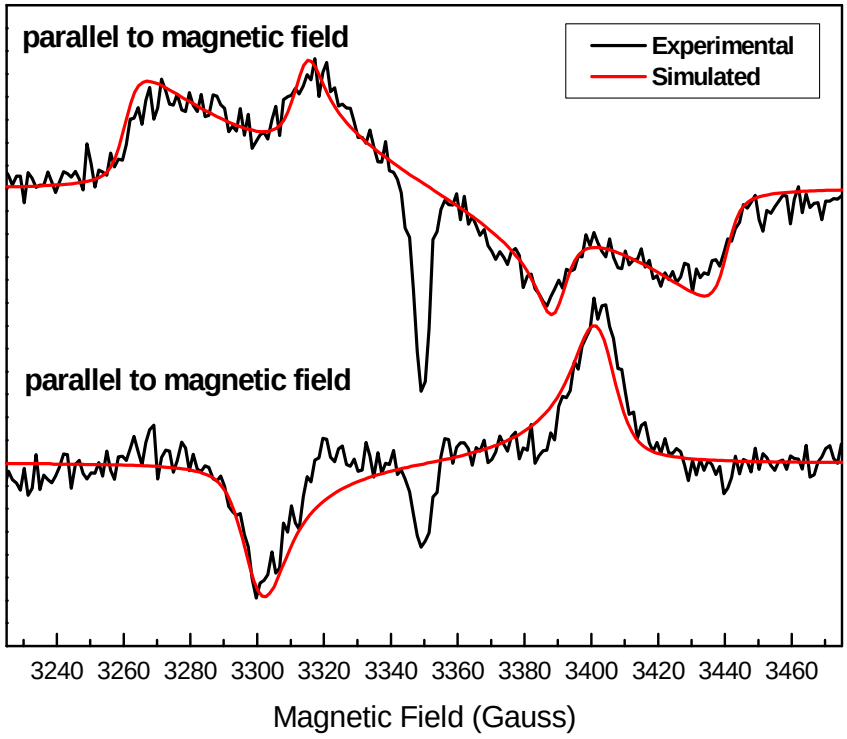

Figure 4.34 TREPR triplet spectra of $PC_{61}BM$ in spin coated PTB7/$PC_{61}BM$/DIO. Simulation outlines that triplets of $PC_{61}BM$ is partially oriented when DIO is present. ISC population were required. Spectra were recorded after 1000 ns after laser pulse.

As shown for P3HT in (77), chains of polymer spread over the surface of deposition and not perpendicular to it. This is a general behavior that can be assigned to long-chain polymers. PTB7 simulation shows that the dipolar *Z* axis of polymer lies perpendicular to plane deposition, moreover we considered *Z* direction parallel to g_z which is evaluated perpendicular to aromatic plane of polymer (18). Thus we can conclude that experiments confirm the polymer to lie preferentially facing aromatic ring up to substrate of deposition.

Spin coated PTB7/$PC_{61}BM$/DIO shows an orientation dependence of $PC_{61}BM$ triplet features (figure 4.34) while the other samples show a powder-like behavior. Simulations of oriented triplet spectra were performed assuming ISC mechanism, analogous uniaxial orienting potential as PTB7 triplet and taking *X* dipolar axis of $PC_{61}BM$ tensor as axis of preferential order.

ZFS parameters and ISC populations found are respectively D=-90 Gauss , E=5 Gauss, p_x=0.23 , p_y=0.77, p_z=0 and they are in good agreement with literature (78).

In order to understand the relation between the dipolar tensor orientation with respect to some molecular symmetry axes, we compared PTB7/$PC_{61}BM$ with a fulleropyrrolidine (79), a C_{60} mono-adduct. Neglecting the substituent to propan-ring of $PC_{61}BM$, the two molecules both belong to the C_{2v} symmetry point group, independently from the symmetry of the addends.

In figure 4.35 the two molecules with C_{2v} axis lying in the substituent plane are shown. Fulleropyrrolidine has *X* dipolar axis parallel to C_{2v} molecular axis (*Z*-molecular axis) thus we can conclude that $PC_{61}BM$, when DIO is present, is oriented facing up the substituent group. In figure 4.36 a graphical representation of molecular order found for these samples.

PTB7/$PC_{71}BM$/DIO films (Figure 4.37) spectra show only an emission contributes relatives to P^+. The increasing asymmetry of the two spectral features with time (not shown), analogous to PTB7/$PC_{61}BM$/DIO films, is due to the contribution of polymer self-ionitation. Bulk and thin films PTB7/$PC_{71}BM$ show the emission contribution of polymer and absorption for fullerene.

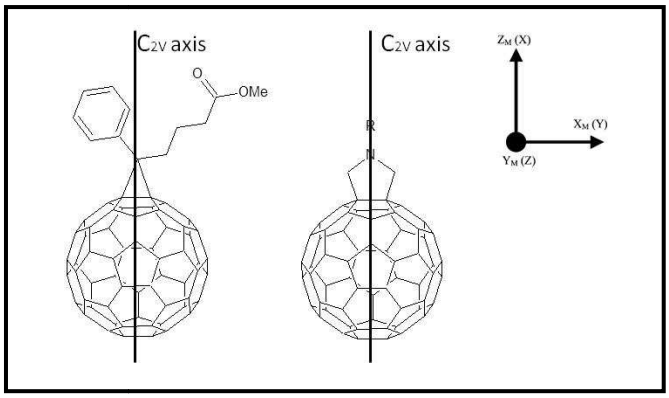

Figure 4.35 $PC_{61}BM$ and fulleropyrrolidine and relative C_{2v} axes are shown respectively on the left and right side. Neglecting substituent groups, it's possible to assign molecule to the same symmetry point group and consequently assume a similar mutual orientation of dipolar tensore principal frame with a molecular frame (shown up-right).

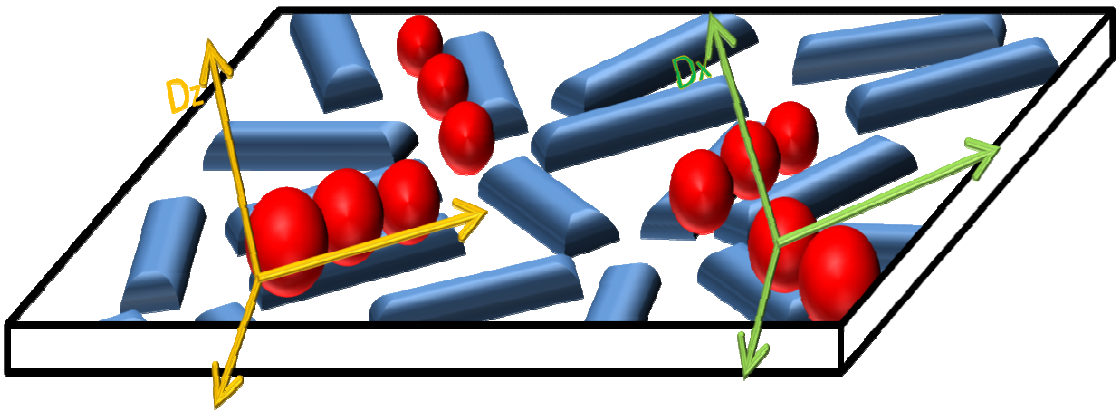

Figure 4.36 thin film PTB7/$PC_{61}BM$/DIO graphical representation of molecular ordering. The yellow reference frame refers to triplet dipolar tensor principal axes and green one refers to $PC_{61}BM$ one dipolar tensor principal axes. From simulation it's possible to find out that the z direction of polymer tensor is parallel to x direction of fullerene tensor.

Simulations were carried out by adding two weighted non-interacting S=1/2 polarized contributes. No SCRP species were observed. Similar *g*-factors make simulations more difficult to interpret without a kind of arbitrariness, anyway P^- contribution, when present, is generally a little shoulder on the emission P^+ signal.

TREPR data confirm LEPR stating that additive DIO strongly effects the charge mobility of fullerene. TREPR 2000 gauss sweep spectra show, as in $PC_{61}BM$ films, the typical features of PTB7 triplet. For thin films we found the same partial orientation of chains polymer as PTB7/$PC_{61}BM$ films and simulations of spectra were carried out assuming recombination triplet populations for signal shorter than 1000 ns and ISC triplet population for signals arising in longer time. For thin PTB7/$PC_{71}BM$/DIO samples, a partial orientation of fullerene triplet features is found. As for $PC_{61}BM$, we simulated it using uniaxial orienting potential and taking an axis lying in *XZ* plane of dipolar tensor directions as axis of preferential orientation. Finally we used a positive orienting parameter $\varepsilon_{2,0}$.

From simulations, figure 4.39 we get D=-92 Gauss E=5 Gauss and ISC populations p_x =0.21 p_y= 0.50 p_z=0.29. We can invoke symmetry similarity with (80), comparing C_{70} mono-adduct with $PC_{71}BM$. Derivatives of C_{70} have generally a minor degree of symmetry so assumptions are less strong. Anyway comparing the two systems, it can be seen that one the axes of order of C_{70} mono-adduct lies in a symmetry plane rather than a symmetry axis (figure 4.38). This somehow reproduces the $PC_{71}BM$ case, where the axis of preferential order is found to be along the *XZ* dipolar plane. In figure 4.40 a graphical representation of molecular order found for these samples. The order parameter S of the two blends were calculated by (4.10): $S_{PTB7} = 0.84 \div 0.87$, $S_{PC_{61}BM} = 0.90 \div 0.93$ and $S_{PC_{71}BM} = 0.90 \div 0.93$.

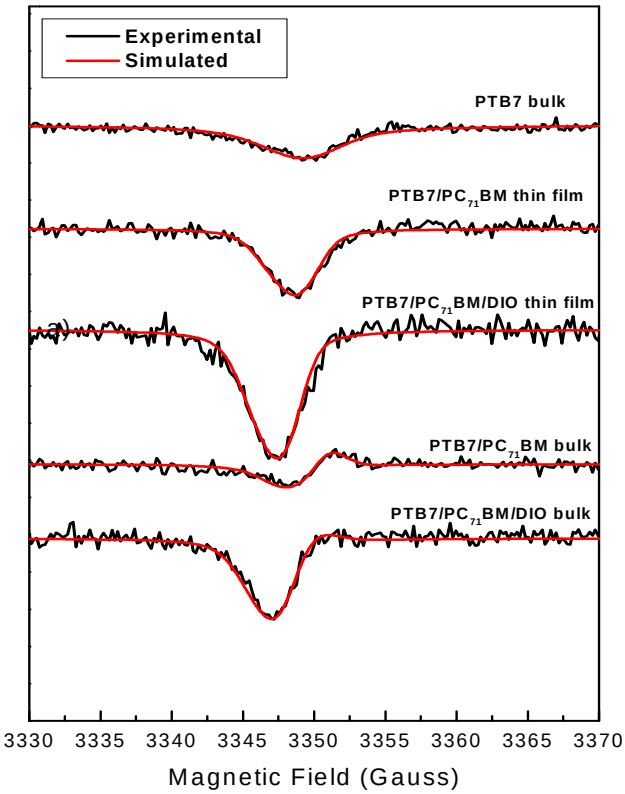

Figure 4.37 TREPR spectra of pristine PTB7, spin-coated PTB7/$PC_{71}BM$,spin-coated PTB7/$PC_{71}BM$/DIO bulk PTB7/$PC_{71}BM$,bulk PTB7/$PC_{71}BM$/DIO. Spectra are shown in 1000 ns delay after laser pulse.

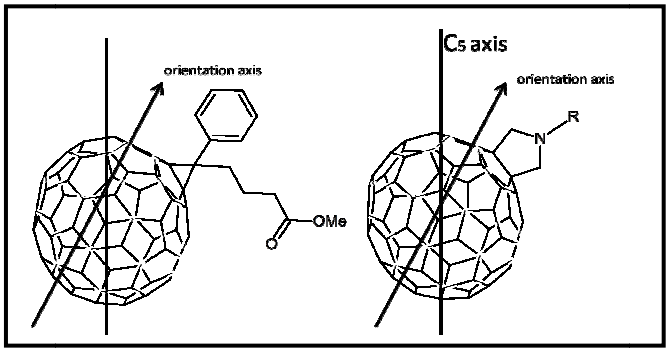

Figure 4.38 One axis of preferential orientation of both molecules lies in a symmetry plane and not in symmetry axis reflecting the less degree of simmetry of $PC_{71}BM$ with respect to $PC_{61}BM$

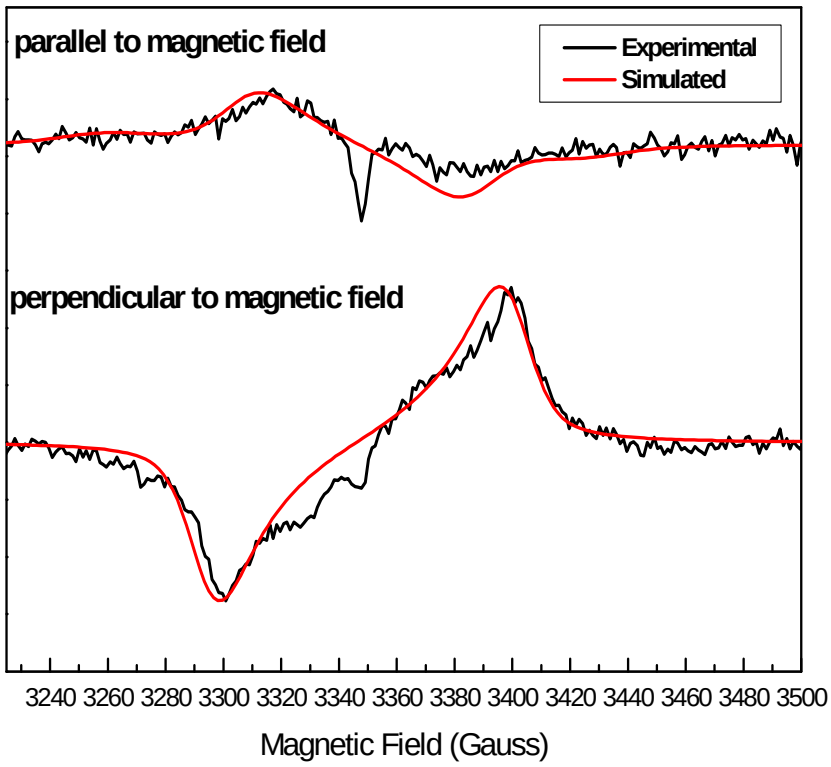

Figure 4.39 TREPR triplet spectra of $PC_{71}BM$ in spin coated PTB7/$PC_{71}BM$/DIO. Simulation outlines that triplets of $PC_{71}BM$ is partially oriented when DIO is present. ISC population were required. Spectra were recorded after 1000 ns after laser pulse.

Table 4.11

PTB7, $PC_{61}BM$ and $PC_{71}BM$ triplets simulations parameters. $\varepsilon_{2,0}$ is the parameter of order as is taken to be positive for both species. Populations are given from lowest energy level to highest.

	D (Gauss)	E (Gauss)	ISC populations	Ric. populations	$\varepsilon_{2,0}$
PTB7	-420	55	0.40:0.44:0.16	0.14:0.72:0.14	8
$PC_{61}BM$	-90	5	0.23:0.77:0	\	15
$PC_{71}BM$	-92	5	0.21: 0.50:0.29	\	15

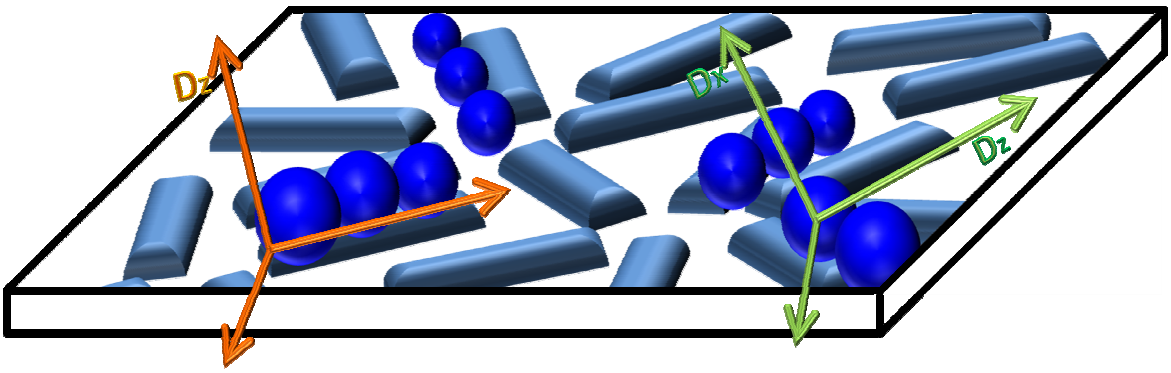

Figure 4.40 thin film PTB7/$PC_{71}BM$/DIO graphical representation of molecular ordering. The yellow reference frame refers to triplet dipolar tensor principal axes and green one refers to $PC_{71}BM$ one dipolar tensor principal axes. From simulation it's possible to find out that the z direction of polymer tensor is tilted to some direction in the XZ plane of fullerene dipolar tensor axes.

In the end we can conclude that oriented polymer phase is present, given by spin-coating deposition, acts ad template for fullerene molecules dissolved in DIO. This results in two highly oriented phases that can be responsible for the high efficiency of solar cells processed with DIO.

Eco-detected Spectra

ED spectra were performed under illumination (EDlightON) in order to have signals of both P^+ and P^-. Spectra were recorded only for sample without additive for the greatest signal/noise ratio especially for fullerene derivatives contributes that almost disappear when DIO is present. Spectra, shown in figure 4.41, display the two signals attributed in the low field to P^+ and to P^- at high field. For relaxation times measurements, we limited for the case of blends without DIO. Results are displayed in Table 4.12. PTB7 cation has a greater T_1 than $PC_{61}BM$ and this causes the LEPR signal of polymer to saturate at low microwave power. The LEPR signals ratio confirms the T_1 measurements and a lower intensity PTB7 signal is

Table 4.12

Relaxation T_1 and T_2 constants of P^+ and P^- on samples are listed. Respectively a:spin coated PTB7/PC_{61}BM, b: bulk evaporated PTB7/PC_{61}BM, c: spin coated PTB7/PC_{71}BM d: bulk evaporated PTB7/PC_{71}BM. Relaxation times were recorded under continuous white light illumination at 80K.

	T_1(ns)		T_2(ns)	
SAMPLES	**fullerene**	**PTB7**	**fullerene**	**PTB7**
Thin film PTB7/PC_{61}BM	$(3.03 \pm 1.70) \cdot 10^3$	$(1.01 \pm 0.34) \cdot 10^5$	$(3.14 \pm 0.74) \cdot 10^3$	$(2.89 \pm 0.30) \cdot 10^3$
Bulk PTB7/PC_{61}BM	$(1.23 \pm 0.20) \cdot 10^4$	$(1.57 \pm 0.20) \cdot 10^5$	$(2.90 \pm 0.50) \cdot 10^3$	$(3.65 \pm 1.50) \cdot 10^3$
Thin film PTB7/PC_{71}BM	$(1.00 \pm 0.10) \cdot 10^6$	$(8.93 \pm 1.87) \cdot 10^5$	$(6.33 \pm 1.00) \cdot 10^3$	$(4.22 \pm 3.00) \cdot 10^3$
Bulk PTB7/PC_{71}BM	$(2.68 \pm 0.40) \cdot 10^5$	$(5.44 \pm 4.00) \cdot 10^4$	$(3.74 \pm 0.70) \cdot 10^3$	$(4.34 \pm 2.00) \cdot 10^3$

recorded with respect to fullerene. PC_{71}BM showed a T_1 enhance of about two orders of magnitude and this can be attributed to the low degree of symmetry of C_{70} cage. The high degree of degeneration of C_{60} levels allows a very efficient coupling with electronic and vibrational degrees of freedom causing an increasing of relaxation processes. PC_{71}BM T_1 is greater than PTB7 anyway it was not possible to detect a direct effect on the LEPR spectra due to the overlap between EPR lines. T_2 measurements have a great level of uncertainty for PTB7/PC_{71}BM samples but generally the same order of magnitude was observed for all samples. Even if EDlightON signal of polarons should depends only on T_2 no correspondence was found in spectra. This can be explained by a different efficiency in polarons recombination for each samples that decrease the intensity of the T_2 signal.

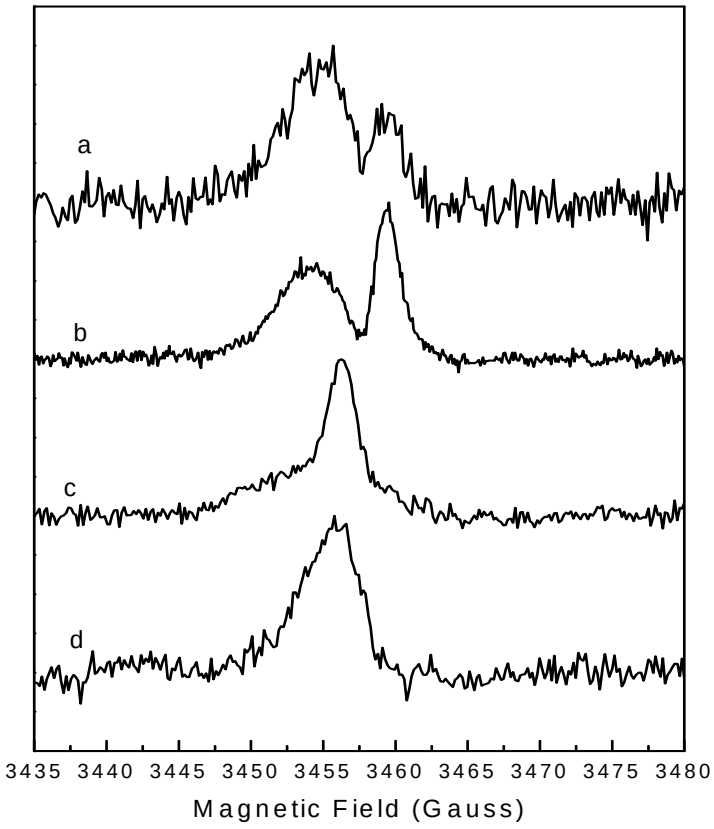

Figure 4.41 EDlightON spectra of respectively a: a: thin film PTB7/$PC_{61}BM$, b: bulk evaporated PTB7/$PC_{61}BM$, c: thin film PTB7/$PC_{71}BM$ d: bulk evaporated PTB7/$PC_{71}BM$. Low field signals belong to P^+ signal and high field signals belong to P^-.

Chapter 5 - Conclusions

Different photovoltaic conjugated polymer/fullerene based blends have been studied by various EPR spectroscopy techniques. For density of localized states inside mobility edge we applied LMEPR which is able to discriminate EPR signal of positive and negative polarons with different lifetimes of trapping by using modulated white light excitation. Distribution of lifetime was not found univocally but apparent lifetimes constants were found for P3HT blended with different fullerene: PC60PhOMe, C60MM12, $PC_{61}BM$, C60H12, C60Ph2,1-4 and $PC_{61}BM$ blended with different polymers: P3HT,MDMOPPV,PCDTBT,PTB7. By Cole-Cole model for dielectric relaxation, it was outlined that apparent lifetime is dependent manly on polymer counterpart and thus is considered the responsible for shape of localized states density. Cole-Cole model was found to not fit perfectly data and this discordance was attributed to high cut-off constant in EPR signal recording. Moreover it was found that signal decay of localized sate cannot generally be considered a single-exponential decay.

The same samples were thus studied by exciting blends at different wavelengths from 400 nm to 900 nm. We found that despite expectation, EPR signal does not follow the absorption spectra of blends but have a maximum shifted at high wavelengths. For P3HT blended with different fullerene: PC60PhOMe, C60MM12, $PC_{61}BM$, C60H12, C60Ph2,1-4 we found an almost regular shift of maximum of about 100 nm while for $PC_{61}BM$ blended with different polymers: P3HT,MDMOPPV,PCDTBT,PTB7 we found a wider shifted concluding that the λ-dependent photophysics is strictly dependent on polymers. The shifted EPR maximum was attributed to long living energy states populated at wavelengths under the mobility edge, while for hot states, populated above the mobility edge, a minimum is observed due to high mobility. A comparison with apparent lifetimes by LMEPR outlined that for samples with a rich low-energy states distribution, a greater shift between absorption and EPR intensity is observed.

Thin films of P3HT/$PC_{61}BM$ by spin-coating showed an orientation dependent LEPR signal denoting presence of a macroscopic order with respect an axis perpendicular to plane of deposition taken as director. Order was attributed to polymer chains

tendency to spread over the substrate of deposition during casting. Nematic phase-like ordering potential was assumed in order to perform simulations and get an order parameter S on a range between -4 and -6. For $PC_{61}BM$ and for SPRC state no orientation dependence was found. Moreover by SCRP simulations it was possible to find the average distance between polymer and fullerene of about 2nm.

Effect of additive DIO was studied for bulk and thin films of PTB7/$PC_{61}BM$ and PTB7/$PC_{71}BM$. LEPR showed that bulk and thin films PTB7/$PC_{61}BM$ and PTB7/$PC_{71}BM$ films show typical behavior of photovoltaic blends displaying radical cation and anion formation under irradiation. TREPR measurement around single radicals resonance fields confirms presence of polarized radicals coming from SCRP state. We confirm *g* tensors principal values found in literature. From SCRP simulations it was possible to find a dipolar parameter D of about 5 Gauss, leading to 2nm distance between polymer and fullerene at the interface. Presence of DIO gives rise to an increase in charge mobility and consequently in recombination of fullerene denoting the disappearance of anion signals in all kind of samples.

TREPR spectra outline presence of PTB7 recombination triplet for all films stating that energy of triplet state of polymer lies lower than change transfer state. Particularly for thin films we found that PTB7 triplet features have orientation dependent and allows us to determine that *Z* direction of dipolar tensor of polymer lies perpendicularly to pi-rings and to plane deposition and principal values of D=-420 Gauss and E=55 Gauss. Populations of PTB7 triplet states were attributed to recombination triplet for the first 1000 ns after triplet generation and to ISC triplet for longer time. This is said to come from the different decay coupling constants between the three triplet sublevels with single ground state. Comparing TREPR spectra of pristine PTB7 and PTB7/fullerene samples it was moreover possible to find the self-ionization contribution of polymer. Spin-coated PCB7/fullerene/DIO samples shown a partially DIO-induced orientation of fullerene phase. Specifically we found that triplet *X* axis tensor of $PC_{61}BM$ is the axis of partial orientation and by a symmetry analogy with a fulleropyrrolidine we found that the *X* axis coincides with the Z_M molecular axis parallel to C_{2V} axis. ZFS parameter of D=-90 E=5 were in good agreement with literature. For $PC_{71}BM$ we found that the axis

of preferential orientation lies in *XZ* dipolar plane and this agree with study carried out in C_{70} mono-adduct that , with a good degree of approximation, can be considered an analogous system. ZFS parameters found were of D=-92 Gauss and E=5 Gauss..

References

1. Lewis NS, Crabtree G. Basic research needs for solar energy utilization: Report of the basic energy sciences workshop on solar energy utilization, april 18-21, 2005. . 2005.

2. Cartlidge E. Bright outlook for solar cells. Physics world. 2007;20(7):20-4.

3. Kaur N, Singh M, Pathak D, Wagner T, Nunzi J. Organic materials for photovoltaic applications: Review and mechanism. Synth Met. 2014;190:20-6.

4. Thompson BC, Fréchet JM. Polymer–fullerene composite solar cells. Angewandte Chemie International Edition. 2008;47(1):58-77.

5. Brabec CJ, Sariciftci NS, Hummelen JC. Plastic solar cells. Advanced Functional Materials. 2001;11(1):15-26.

6. Dennler G, Scharber MC, Brabec CJ. Polymer-Fullerene Bulk-Heterojunction solar cells. Adv Mater. 2009;21(13):1323-38.

7. Nelson J. Organic photovoltaic films. Current Opinion in Solid State and Materials Science. 2002;6(1):87-95.

8. Zhang Y, Basel TP, Gautam BR, Yang X, Mascaro DJ, Liu F, et al. Spin-enhanced organic bulk heterojunction photovoltaic solar cells. Nature communications. 2012;3:1043.

9. Foertig A, Kniepert J, Gluecker M, Brenner T, Dyakonov V, Neher D, et al. Nongeminate and geminate recombination in PTB7: PCBM solar cells. Advanced Functional Materials. 2014 MAR;24(9):1306-11.

10. Krinichnyi V. Dynamics of charge carriers photoinduced in poly (3-dodecylthiophene)/fullerene bulk heterojunction. Solar Energy Mater Solar Cells. 2008;92(8):942-8.

11. Nunzi J. Organic photovoltaic materials and devices. Comptes Rendus Physique. 2002;3(4):523-42.

12. Yang C, Lee JK, Heeger AJ, Wudl F. Well-defined donor–acceptor rod–coil diblock copolymers based on P3HT containing C 60: The morphology and role as a surfactant in bulk-heterojunction solar cells. Journal of Materials Chemistry. 2009;19(30):5416-23.

13. Chang L, Lademann HW, Bonekamp J, Meerholz K, Moulé AJ. Effect of trace solvent on the morphology of P3HT: PCBM bulk heterojunction solar cells. Advanced Functional Materials. 2011;21(10):1779-87.

14. Groves C, Reid OG, Ginger DS. Heterogeneity in polymer solar cells: Local morphology and performance in organic photovoltaics studied with scanning probe microscopy. Acc Chem Res. 2010;43(5):612-20.

15. Moulé AJ, Meerholz K. Controlling morphology in polymer–fullerene mixtures. Adv Mater. 2008;20(2):240-5.

16. Pivrikas A, Neugebauer H, Sariciftci NS. Influence of processing additives to nano-morphology and efficiency of bulk-heterojunction solar cells: A comparative review. Solar Energy. 2011;85(6):1226-37.

17. Haugeneder A, Neges M, Kallinger C, Spirkl W, Lemmer U, Feldmann J, et al. Exciton diffusion and dissociation in conjugated polymer/fullerene blends and heterostructures. Physical Review B. 1999;59(23):15346.

18. Niklas J, Mardis KL, Banks BP, Grooms GM, Sperlich A, Dyakonov V, et al. Highly-efficient charge separation and polaron delocalization in polymer-fullerene bulk-heterojunctions: A comparative multi-frequency EPR and DFT study. Physical Chemistry Chemical Physics. 2013;15(24):9562-74.

19. Cunningham PD, Hayden LM. Carrier dynamics resulting from above and below gap excitation of P3HT and P3HT/PCBM investigated by optical-pump terahertz-probe spectroscopy†. The Journal of Physical Chemistry C. 2008;112(21):7928-35.

20. Hwang I, Moses D, Heeger AJ. Photoinduced carrier generation in P3HT/PCBM bulk heterojunction materials. The Journal of Physical Chemistry C. 2008;112(11):4350-4.

21. Piris J, Dykstra TE, Bakulin AA, Loosdrecht PHv, Knulst W, Trinh MT, et al. Photogeneration and ultrafast dynamics of excitons and charges in P3HT/PCBM blends. The Journal of Physical Chemistry C. 2009;113(32):14500-6.

22. Roncali J. Molecular engineering of the band gap of p-conjugated systems: Facing technological applications. Macromolecular Rapid Communications. 2007;28(17):1761-75.

23. FACCHETTI A, ORTIZ RP, MARKS TJ. Self-assembled mono-and multilayers for functional opto-electronic devices. Supramolecular Materials for Opto-Electronics:119.

24. Janssen G, Aguirre A, Goovaerts E, Vanlaeke P, Poortmans J, Manca J. Optimization of morphology of P3HT/PCBM films for organic solar cells: Effects of thermal treatments and spin coating solvents. The European Physical Journal Applied Physics. 2007;37(03):287-90.

25. Voigt MM, Guite A, Chung D, Khan RU, Campbell AJ, Bradley DD, et al. Polymer Field-Effect transistors fabricated by the sequential gravure printing of polythiophene,

two insulator layers, and a metal ink gate. Advanced Functional Materials. 2010;20(2):239-46.

26. Li G, Shrotriya V, Huang J, Yao Y, Moriarty T, Emery K, et al. High-efficiency solution processable polymer photovoltaic cells by self-organization of polymer blends. Nature materials. 2005;4(11):864-8.

27. Hoth CN, Schilinsky P, Choulis SA, Brabec CJ. Printing highly efficient organic solar cells. Nano letters. 2008;8(9):2806-13.

28. Etzold F, Howard IA, Mauer R, Meister M, Kim T, Lee K, et al. Ultrafast exciton dissociation followed by nongeminate charge recombination in PCDTBT: PCBM photovoltaic blends. J Am Chem Soc. 2011;133(24):9469-79.

29. Moon JS, Jo J, Heeger AJ. Nanomorphology of PCDTBT: PC70BM bulk heterojunction solar cells. Advanced Energy Materials. 2012;2(3):304-8.

30. Nevil N, Ling Y, Van Mierloo S, Kesters J, Piersimoni F, Adriaensens P, et al. Charge transfer in the weak driving force limit in blends of MDMO-PPV and dithienylthiazolo [5, 4-d] thiazoles towards organic photovoltaics with high V OC. Physical Chemistry Chemical Physics. 2012;14(45):15774-84.

31. Liang Y, Xu Z, Xia J, Tsai S, Wu Y, Li G, et al. For the bright future-bulk heterojunction polymer solar cells with power conversion efficiency of 7.4%. Adv Mater. 2010 MAY 25;22(20):E135.

32. He Y, Zhou Y, Zhao G, Min J, Guo X, Zhang B, et al. Poly (4, 8-bis (2-ethylhexyloxy) benzo [1, 2-b: 4, 5-b'] dithiophene vinylene): Synthesis, optical and photovoltaic properties. Journal of Polymer Science Part A: Polymer Chemistry. 2010;48(8):1822-9.

33. Negri F, Orlandi G, Zerbetto F. Quantum-chemical investigation of franck-condon and jahn-teller activity in the electronic spectra of buckminsterfullerene. Chemical physics letters. 1988;144(1):31-7.

34. Buckley C, Hunter D, Hore P, McLauchlan K. Electron spin resonance of spin-correlated radical pairs. Chemical physics letters. 1987;135(3):307-12.

35. Haufler R, Conceicao J, Chibante L, Chai Y, Byrne N, Flanagan S, et al. Efficient production of C60 (buckminsterfullerene), C60H36, and the solvated buckide ion. J Phys Chem. 1990;94(24):8634-6.

36. Yu G, Gao J, Hummelen J, Wudl F, Heeger A. Polymer photovoltaic cells: Enhanced efficiencies via a network of internal donor-acceptor heterojunctions. Science-AAAS-Weekly Paper Edition. 1995;270(5243):1789-90.

37. Sariciftci N, Hebger A. Reversible, metastable, ultrafast photoinduced electron transfer from semiconducting polymers to buckminsterfullerene and in the corresponding donor/acceptor heterojunctions. International Journal of Modern Physics B. 1994;8(03):237-74.

38. Kooistra FB, Knol J, Kastenberg F, Popescu LM, Verhees WJ, Kroon JM, et al. Increasing the open circuit voltage of bulk-heterojunction solar cells by raising the LUMO level of the acceptor. Org Lett. 2007;9(4):551-4.

39. Po R, Maggini M, Camaioni N. Polymer solar cells: Recent approaches and achievements. The Journal of Physical Chemistry C. 2009;114(2):695-706.

40. Varotto A, Treat ND, Jo J, Shuttle CG, Batara NA, Brunetti FG, et al. 1, 4-Fullerene derivatives: Tuning the properties of the electron transporting layer in Bulk-Heterojunction solar cells. Angewandte Chemie International Edition. 2011;50(22):5166-9.

41. Boyd R, Smith G. Polymer dynamics and relaxation. Cambridge University Press; 2007.

42. Dimitrov SD, Bakulin AA, Nielsen CB, Schroeder BC, Du J, Bronstein H, et al. On the energetic dependence of charge separation in low-band-gap polymer/fullerene blends. J Am Chem Soc. 2012;134(44):18189-92.

43. Aguirre A, Gast P, Orlinskii S, Akimoto I, Groenen EJ, El Mkami H, et al. Multifrequency EPR analysis of the positive polaron in I 2-doped poly (3-hexylthiophene) and in poly [2-methoxy-5-(3, 7-dimethyloctyloxy)]-1, 4-phenylenevinylene. Physical Chemistry Chemical Physics. 2008;10(47):7129-38.

44. Collins BA, Li Z, Tumbleston JR, Gann E, McNeill CR, Ade H. Absolute measurement of domain composition and nanoscale size distribution explains performance in PTB7:PC71BM solar cells. Advanced Energy Materials. 2013 JAN;3(1):65-74.

45. Guo S, Herzig EM, Naumann A, Tainter G, Perlich J, Mueller-Buschbaum P. Influence of solvent and solvent additive on the morphology of PTB7 films probed via X-ray scattering. J Phys Chem B. 2014 JAN 9;118(1):344-50.

46. Atherton NM. Principles of electron spin resonance. Ellis Horwood ed. ; 1993.

47. Weil JA, Bolton JR. Electron paramagnetic resonance: Elementary theory and practical applications. John Wiley & Sons; 2007.

48. Hoff AJ. Advanced EPR: Applications in biology and biochemistry. Elsevier; 1989.

49. Hoff AJ. Electron spin polarization of photosynthetic reactants. Q Rev Biophys. 1984;17(02):153-282.

50. Tan J, Thurnauer MC, Norris JR. Electron spin echo envelope modulation due to exchange and dipolar interactions in a spin-correlated radical pair. Chemical physics letters. 1994;219(3):283-90.

51. Schafferhans J, Baumann A, Deibel C, Dyakonov V. Trap distribution and the impact of oxygen-induced traps on the charge transport in poly (3-hexylthiophene). Appl Phys Lett. 2008;93(9):093303.

52. Schafferhans J, Baumann A, Wagenpfahl A, Deibel C, Dyakonov V. Oxygen doping of P3HT: PCBM blends: Influence on trap states, charge carrier mobility and solar cell performance. Organic Electronics. 2010;11(10):1693-700.

53. Steiger J, Schmechel R, Von Seggern H. Energetic trap distributions in organic semiconductors. Synth Met. 2002;129(1):1-7.

54. Garcia-Belmonte G, Munar A, Barea EM, Bisquert J, Ugarte I, Pacios R. Charge carrier mobility and lifetime of organic bulk heterojunctions analyzed by impedance spectroscopy. Organic Electronics. 2008;9(5):847-51.

55. Deledalle F, Tuladhar PS, Nelson J, Durrant JR, Kirchartz T. Understanding the apparent charge density dependence of mobility and lifetime in organic bulk heterojunction solar cells. Journal of Physical Chemistry C. 2014 MAY 1 2014;118(17):8837-42.

56. Baranovski S. Charge transport in disordered solids with applications in electronics. John Wiley & Sons; 2006.

57. Carati C, Bonoldi L, Po R. Density of trap states in organic photovoltaic materials from LESR studies of carrier recombination kinetics. Physical Review B. 2011;84(24):245205.

58. Lakowiz J. Principles of fluorescence spectroscopy. 3^ nd ed. . 2006.

59. Evaristo Riande RD. Electrical properties of polymers. ; 2004.

60. Cole KS, Cole RH. Dispersion and absorption in dielectrics I. alternating current characteristics. J Chem Phys. 1941;9(4):341-51.

61. Noone KM, Subramaniyan S, Zhang Q, Cao G, Jenekhe SA, Ginger DS. Photoinduced charge transfer and polaron dynamics in polymer and hybrid photovoltaic thin films: Organic vs inorganic acceptors. The Journal of Physical Chemistry C. 2011;115(49):24403-10.

62. Epshtein O, Nakhmanovich G, Eichen Y, Ehrenfreund E. Dispersive dynamics of photoexcitations in conjugated polymers measured by photomodulation spectroscopy. Physical Review B. 2001;63(12):125206.

63. Krinichnyi V, Yudanova E, Denisov N. Light-induced EPR study of charge transfer in poly (3-hexylthiophene)/fullerene bulk heterojunction. J Chem Phys. 2009;131(4):044515.

64. Krinichnyi V, Yudanova E. Light-induced EPR spectroscopy of charge carriers photoinduced in polymer/fullerene bulk heterojunctions. Journal of Renewable and Sustainable Energy. 2009;1(4):043110.

65. Marumoto K, Muramatsu Y, Kuroda S. Quadrimolecular recombination kinetics of photogenerated charge carriers in regioregular poly (3-alkylthiophene)/fullerene composites. Appl Phys Lett. 2004;84(8):1317-9.

66. Nelson J. Diffusion-limited recombination in polymer-fullerene blends and its influence on photocurrent collection. Physical Review B. 2003;67(15):155209.

67. Nogueira AF, Montanari I, Nelson J, Durrant JR, Winder C, Sariciftci NS, et al. Charge recombination in conjugated polymer/fullerene blended films studied by transient absorption spectroscopy. The Journal of Physical Chemistry B. 2003;107(7):1567-73.

68. Bakulin AA, Rao A, Pavelyev VG, van Loosdrecht PH, Pshenichnikov MS, Niedzialek D, et al. The role of driving energy and delocalized states for charge separation in organic semiconductors. Science. 2012 Mar 16;335(6074):1340-4.

69. Lee J, Vandewal K, Yost SR, Bahlke ME, Goris L, Baldo MA, et al. Charge transfer state versus hot exciton dissociation in polymer− fullerene blended solar cells. J Am Chem Soc. 2010;132(34):11878-80.

70. Bakulin AA, Rao A, Pavelyev VG, van Loosdrecht PH, Pshenichnikov MS, Niedzialek D, et al. The role of driving energy and delocalized states for charge separation in organic semiconductors. Science. 2012 Mar 16;335(6074):1340-4.

71. Kobori Y, Noji R, Tsuganezawa S. Initial molecular photocurrent: Nanostructure and motion of weakly bound charge-separated state in organic photovoltaic interface. The Journal of Physical Chemistry C. 2013;117(4):1589-99.

72. Watanabe S, Tanaka H, Ito H, Kuroda S, Mori T, Marumoto K, et al. Direct determination of interfacial molecular orientations in field-effect devices of P3HT/PCBM composites by electron spin resonance. Organic Electronics. 2011;12(4):716-23.

73. Liu F, Zhao W, Tumbleston JR, Wang C, Gu Y, Wang D, et al. Understanding the morphology of PTB7: PCBM blends in organic photovoltaics. Advanced Energy Materialsr. 2014 APR;4(5):1301377.

74. Chen W, Xu T, He F, Wang W, Wang C, Strzalka J, et al. Hierarchical nanomorphologies promote exciton dissociation in polymer/fullerene bulk heterojunction solar cells. Nano Letters. 2011 SEP;11(9):3707-13.

75. Ito M, Palanisamy K, Kumar A, Murugesan VS, Shin P, Tsuda N, et al. Characterization of the organic thin film solar cells with active layers of PTB7/PC71BM prepared by using solvent mixtures with different additives. International Journal of Photoenergy. 2014:694541.

76. Lou SJ, Szarko JM, Xu T, Yu L, Marks TJ, Chen LX. Effects of additives on the morphology of solution phase aggregates formed by active layer components of high-efficiency organic solar cells. J Am Chem Soc. 2011 DEC 28;133(51):20661-3.

77. Aguirre A, Gast P, Orlinskii S, Akimoto I, Groenen EJJ, El Mkami H, et al. Multifrequency EPR analysis of the positive polaron in I-2-doped poly(3-hexylthiophene) and in poly[2-methoxy-5-(3,7-dimethyloctyloxy)]-1,4-phenylenevinylene. Physical Chemistry Chemical Physics. 2008;10(47):7129-38.

78. Franco L, Toffoletti A, Ruzzi M, Montanari L, Carati C, Bonoldi L, et al. Time-resolved EPR of photoinduced excited states in a semiconducting polymer/PCBM blend. Journal of Physical Chemistry C. 2013 JAN 31;117(4):1554-60.

79. Ceola S, Franco L, Maggini M, Corvaja C. Optical spectrum of C 60 mono-adducts: Assignment of transition bands using time-resolved EPR magneto-photo-selection. Photochemical & Photobiological Sciences. 2006;5(12):1177-82.

80. Franco L, Toffoletti A, Maggini M. Time resolved EPR of [70]fullerene monoadducts in the photoexcited triplet state. Physical Chemistry Chemical Physics. 2012;14(41):14358-64.